12-2010

DEVELOPMENT OF A CARBOHYDRATE MICROARRAY SYSTEM AND A MICROCANTILEVER-BASED BIOSENSOR FOR DETECTION OF TARGET BACTERIA

Yunyan Cheng
Clemson University, chyunyan@gmail.com

DEVELOPMENT OF A CARBOHYDRATE MICROARRAY SYSTEM AND A MICROCANTILEVER-BASED BIOSENSOR FOR DETECTION OF TARGET BACTERIA

A Thesis
Presented to
the Graduate School of
Clemson University

In Partial Fulfillment
of the Requirements for the Degree
Master of Science
Microbiology

---

by
Yunyan Cheng
December 2010

Accepted by:
Tzuen-Rong Jeremy Tzeng, Committee Chair
Tamara McNealy
Nader Jalili

ABSTRACT

The increasing number of disease outbreaks results in a demand for novel pathogen detectors. Carbohydrates serving as receptors for pathogen lectins have become the focus of such research. Two primary sugars, α-D-mannose and α-L-fucose, as receptors for *Escherichia coli* and *Pseudomonas aeruginosa*, respectively, are of great interest to researchers due to their high affinity. These interactions can be studied using carbohydrate microarrays, which are also suitable platforms for detecting bacterial pathogens. In addition, carbohydrates have the potential to act as sensing molecules in microcantilever-based biosensors. The goal of this research was to design a carbohydrate microarray system to study the interactions between bacteria and their carbohydrate receptors, and to apply these results to development of a microcantilever-based biosensor.

First, a carbohydrate microarray system was developed and evaluated utilizing the recognition specificity between α-D-mannose and type-1 fimbriae of *E. coli* ORN178. Chemically synthesized polysaccharides were immobilized non-covalently onto nitrocellulose membrane-coated glass slides using a contact printer. This microarray system was used to establish the optimized conditions of bacterial cultivation and hybridization for the expression of lectins. It specifically detects *E. coli* ORN178 with a detection limit of 10^4-10^5 cells/membrane. This binding interaction is absent when using *E. coli* ORN208 (a mutant of ORN178 strain expressing abnormal type-1 fimbriae), or *E. coli* O157:H7 as the targets. In addition, this binding interaction is abolished when pre-exposing *E. coli* ORN178 to free mannose. Then, the feasibility of utilizing this

carbohydrate microarray system for profiling of bacteria by their carbohydrate binding specificity was investigated using eight carbohydrates and six bacterial strains. Each bacterial strain was cultivated and allowed to hybridize to the carbohydrate microarray under its optimal conditions for cell growth and lectin expression.

Second, a gold-coated microcantilever-based biosensor was covalently functionalized with carbohydrates, which served as the sensing molecules, followed by hybridization with 10^6cells/mL or 10^9cells/mL *E. coli* strains expressing green fluorescent proteins. Fluorescence emitted from *E. coli* ORN178/pGREEN or *E. coli* ORN208/pGREEN cells of both concentrations was observed under an epi-fluorescent microscope. Statistical analysis of the resonance frequencies, measured using Polytec Micro System Analyzer (MSA)-400, of both uncoated microcantilevers and microcantilevers functionalized with carbohydrates indicated that carbohydrate molecules were uniformly coated on the surface of functionalized microcantilevers. However, there was no statistically significant evidence to conclude that these two bacterial strains bound specifically to these fabricated microcantilever surfaces, a result different from our expectation, probably due to the non-uniform binding of bacterial cells.

This research represents the first step into the development of a carbohydrate microarray system for the evaluation of bacterial binding specificity to host cell surface carbohydrates and a microcantilever biosensor based on the interactions between bacterial adhesins and host cell receptors. By exploring the use of adhesin-carbohydrate binding specificities for bacteria classification, identification, and detection, this research opens the door for more investigations in the bacteria-carbohydrate interactions and in the

development of diagnostic tools and biosensors that are more stable, easier to fabricate, and ones that do not require sample pre-enrichment, cell lysis, or cell staining typically required for current antibody- or nucleic acid-based bioassays.

ACKNOWLEDGEMENTS

First of all, I would like to express my sincere thanks to Dr. Jeremy Tzeng for his continuous support, guidance and encouragement from the experimental design to the data analyses in this research. Without him I could not have grown so much academically. I also want to thank Dr. Tamara McNealy and Dr. Nader Jalili, who served on my committee. Dr. Tamara McNealy helped me revise my proposal for this research and conduct experiments for fluorescent dye studies. Dr. Jalili introduced the field of microcantilever-based biosensors to me and guided me when I used the Polytec Micro System Analyzer in his lab measuring microcantilever resonance frequencies. I thank both of them for their invaluable assistance, time and effort, and for being so patient with me.

I would like to recognize my fellow labmates for their kindness in sharing experimental equipment and material, especially John Abercrombie, Donna Weinbrenner and Pallavi Vedantam. In addition, my peers, Reza Saeidpourazar, Siddharth Aphale, and Parikshit Mehta from the Department of Mechanical Engineering, and Tugba Demir from the Department of Materials Science and Engineering, helped me to become familiar with the microcantilever measurements and always answered my microcantilever related questions. I would also like to thank three undergraduate students, Lauren Hayes, Yekaterina Demchenko, and Jessica Tzeng, who assisted me in investigating the feasibility of a biotinylated carbohydrate as a visualizing agent, in studying the

appropriateness of the carbohydrate microarray system in bacteria profiling, and in revising this thesis, respectively.

During the writing of this thesis, Ms. Barbara Ramirez from the Department of English graciously put in a great deal of time and effort in helping me revise the draft of this thesis. I was totally clueless on how to write my thesis and how much I needed to improve my written English before this process. She taught me how to write each chapter, how to transit from one topic to the next, and how to lead my readers through my research. She polished my writing. I thank her for her precious time and invaluable comments.

The materials presented here are based upon work supported by the CSREES/USDA under Project No. SC-1700344 and by the National Science Foundation under MRI Program Grant No. CMMI-0619739. Any opinions, findings, conclusions, and recommendations expressed in this material are those of the author and do not necessarily reflect the views of the National Science Foundation.

TABLE OF CONTENTS

Table of Contents (continued) **Page**

Table of Contents (continued) **Page**

LIST OF FIGURES

List of Figures (continued)

Figure **Page**

LIST OF TABLES

CHAPTER 1

INTRODUCTION

In the last two decades, the spread of foodborne and environmental pathogens across the globe has increased significantly because of strain variation and emerging antibiotic resistance, as well as the increase in the international travel of people and the shipment of livestock, plants, and vegetables. The number of foodborne illness per year estimated by the U.S. Government is approximately 76 million; as a result, 325,000 hospitalizations and 5,000 death have been documented annually, meaning foodborne diseases cause the death of approximately 13 people per day although the food supply in the United States is safer than most of the places in the world [1]. These foodborne illnesses cost $357 billion to $1.4 trillion per year, as calculated by Roberts using data obtained from the Center for Disease Control and Prevention [2]. In addition, environmental pathogens in natural recreational waters such as beaches and lakes were responsible for 84 reported disease outbreaks and 5,300 patients from 1986 to 1998 in the United States [3]. To address these problems, pathogen detection techniques which are fast, accurate, specific and sensitive are in great need in the areas of food safety, clinic diagnosis and environmental protection.

Established conventional detection methods such as culture method [4], polymerase chain reaction (PCR) [5], and enzyme immunoassay [6] are commonly used for pathogen detection. Although culture method is the most popular detection method, the growth of bacteria cells in selective media is time-consuming, and typically requires

days of cultivation. In addition, this method does not work well in distinguishing related bacterial strains. PCR, which involves DNA amplification followed by gel electrophoresis, requires less time and is more accurate than the culture method. Recently, real-time PCR has been designed for even faster analysis. However, it still requires an enrichment step for low concentrated samples, which may cause false positives. Antibody-based pathogen detection offers the potential of rapid analysis, but the production of specific antibodies is expensive, difficult and time-consuming.

Recently, two new techniques utilizing carbohydrate microarray and biosensors have been used separately to detect pathogens [7,8]. One **long term goal** of research in this area is to combine these two technologies to design a novel biosensor for the detection of intact pathogen cells effectively and without requiring the use of labels. To address this goal, the **hypotheses** of this research are: (1) polyacrylamide-conjugated carbohydrates can be immobilized on nitrocellulose-coated Whatman FAST slides and the carbohydrate moieties are available for bacterial adherence and (2) carbohydrates can be functionalized on microcantilevers serving as sensing molecules in biosensors for specific and sensitive bacteria detection by measuring the shifts in resonance frequency induced by bound bacteria.

The **specific aims** of this research are to:

1. Develop a carbohydrate microarray system for the evaluation of the binding characteristics of two selected bacterial strains to their specific carbohydrate receptor. The specific tasks are:
    a. Bacterial strain validation

b. Carbohydrate microarray development

c. *Escherichia coli* ORN178 and α-D-mannose binding validation using carbohydrate microarray

d. *Pseudomonas aeruginosa* PAO1 and α-L-fucose binding validation using carbohydrate microarray

2. Utilize a microcantilever-based biosensor for the detection of target bacteria. The specific tasks are:

    a. Carbohydrate functionalization method investigation

    b. The measurements of resonance frequency shifts of gold-coated microcantilevers in the absence and presence of target bacteria

The completion of this study will provide fuller and more detailed information about the conditions required for bacterial adherence to carbohydrate receptors and, as a result, a better understanding of the feasibility of using carbohydrate microarrays and carbohydrate functionalized biosensors for pathogen detection.

CHAPTER 2

LITERATURE REVIEW

Although carbohydrates are one of the primary macromolecules in organisms, research mainly focused on dietary and structural sugars before the 1990s. Then, a new area of carbohydrate characteristics was suggested by several research groups. In 1999, Apweiler *et al.* reported that more than 60% of the proteins in the SWISS-PROT protein sequence data bank are linked with carbohydrates either through the amino acid asparagine (*N*-linked) or through the amino acids threonine and serine (*O*-linked), a phenomenon known as glycosylation [9,10]. In addition, all eukaryotic cell surfaces were found to be coated with glycoconjugates, complex carbohydrates linked to proteins and lipids, as reported by Roseman in 2001 [11].

As a result of these findings, complex carbohydrates with diverse components and structures were hypothesized to play a role in cell communications, both between internal cells such as in cell apoptosis and cancer metastasis, and between internal cells and external cells and molecules such as in the adherence of viruses, toxins and bacteria. For example, in 1995, Perillo *et al.* reported that carbohydrates can either speed up cell apoptosis by lengthening the *N*-linked carbohydrate side chain in protein galectin-1 expressed by endothelial cells or slow it down or by blocking the *O*-linked carbohydrate side chain synthesis in this protein [12]. Two years later, Kannagi reported that glycocojugates sialyl lewis A and X located on liver, stomach, lung, and ovary cancer cell surfaces mediate cancer metastasis by adhering to vascular endothelial cell surface

protein E-selectin [13]. At the same time, researchers also reported the role of carbohydrates in mediating external molecule recognition of viruses and toxins. As Conner *et al.* reported, intestinal glycoproteins with α2-3 sialic acids are receptors for avian influenza viruses as are α2-6 configurated sialic acids located in the upper respiratory tract and lungs for human influenza viruses [14]. In addition, Abrami *et al.* found that glycosylated proteins linked with carbohydrate phosphatidilinositol on intestinal epithelial cell surfaces function as binding sites of aerolysin, a protoxin generated by a human pathogen *Aeromonas hydrophila* [15].

In the last decade, carbohydrate mediated bacterial adherence has attracted much attention, as it is an important prerequisite for bacterial colonization on host cell surfaces, helping the pathogen to obtain nutrients, become internalized in host tissue, deliver toxins, and survive the host's defending processes such as urination and respiration [16].

2.1 Carbohydrates as Receptors for Bacterial Adherence

2.1.1 Overview

Most bacterial adherence is mediated by cell surface components or appendages, namely adhesins, which recognize **three types** of molecules on host cell surfaces. The **first type**, proteins, have been the focus of a significant number of studies including the one conducted by Kuusela *et al.*, who found that the CadF adhesin on *Campylobacter jejuni* cell surfaces mediated a strong attachment to type I, III and V collagens isolated from extracellular matrix [17]. The **second type** involves lipids on host cell surfaces. Although they have received less attention, Sylvester *et al.* found an S-like protein on the

cell surface of another *Campylobacter* species, *C. upsaliensis*, acted as an adhesin, binding to phospholipids phosphatidylethanolamin on human small intestine epithelial cell surfaces [18]. The majority of bacterial adhesins are lectins, which interact with the **third type** of carbohydrates conjugated with proteins or lipids on host cell surfaces. In gram-positive bacteria, lectins are located in the peptidoglycan layer or anchored on the cytoplasmic membrane extending out of the cell wall. In gram-negative cells, they are often found as amorphous components on cell surfaces or as parts of fimbriae or pili, two names sometimes used interchangeably [19].

The expression of lectins switches frequently between ON and OFF, influenced by growth conditions, a phenomenon known as phase variation [19]. For example, Henderson *et al.* reported that uropathogenic *E. coli* changes periodically from the fimbriated stage to the non-fimbriated one and then back at 37℃ while its fimbriae expression is completely shut off at 26℃ [20]. These phase variations play a role in helping bacterial populations adapt to different environments since they generate a mixture of fimbriated and non-fimbriated cells, increasing the survival rate of the population. While the former is equipped for adherence to colonization sites, the latter can detach from a surface, transferring to another host and escaping the host immune system attack before colonization by hiding the strong immunogen of fimbriae [20]. When the conditions are favorable, the surviving non-fimbriated cells are subjected to phase variation again, expressing fimbriae and binding to carbohydrates to initiate colonization.

During this binding process, lectins exhibit different specificities related to their carbohydrate receptors. These specificities, which are determined by the capability of the free carbohydrate molecules to inhibit the binding of bacterial cells to host surfaces, can be categorized into two groups, i.e., primary sugar specificity and fine sugar specificity [21]. The former refers to the simplest carbohydrate structures inhibiting adherence, which are usually shared by several bacteria, while the latter describes more specific bacterial adherence to different oligosaccharides [21]. For example, both *E. coli* and *Klebsiella pneumonia* bind to mannoside, while they exhibit different affinity for *p*-nitrophenyl-mannoside [22]. These two specificities can also occur within species, demonstrated by the different carbohydrate recognition pattern of three uropathogenic *E. coli* isolates mediated by the PapG adhesin subclasses G1, G2 and G3 located on their P fimbriae [23]. All three lectins bind to the simplest structure of Galα4Gal, while each subclass recognizes this structure in different glycolipids, GbO3, GbO4, and GbO5, resulting in their different colonization sites of human bladder, human kidney, and dog kidney, respectively [23]. The fine sugar specificity is often delicate, demonstrated by the binding of *E. coli* K99 to *N*-glycolylneuraminic acid but not to *N*-acetylneuraminic acid with only a hydroxyl group difference from the former [24].

Despite the high specificity, the adherence of lectin to both primary and fine sugars usually has a dissociation constant K_a in the range of millimolar, meaning a low affinity, since K_a inversely reflects the adherence affinity of lectins to carbohydrates. A higher affinity is desired for research on lectin-carbohydrate interactions, and, therefore, several methods for improving this affinity have been studied, including chemical

derivatization and lectin or receptor multivalency. Firon *et al.* found the inhibitory effect of α-mannoside derivatized using two chemical agents methylumbelliferyl and *p*-nitro-o-chlorophenyl was two to three orders larger than that of natural methyl α-mannoside on the adherence of *E. coli* to yeasts or to rabbit epithelial cells [25]. Simon *et al.* studied the inhibitory effect of human serum albumin possessing 20% (mol/mol) 3'-sialyllactose (NeuAcα2-3Galβ1-4Glc) on the adherence of *Helicobacter pylori* to epithelial cells, concluding that it was approximately 100 times more effective than the carbohydrate itself [26]. In addition to chemical artifacts and natural polymers, two lectin-monosaccharide interactions, type-1 fimbriae--mannose and PA-II lectin--fucose recognition, attract much research attention because of their naturally high affinities [27,28].

2.1.2 Mannose as a Receptor for *Escherichia coli* ORN178 Type-1 Fimbriae

E. coli ORN178, which is found in the lower intestines, causes infection only when it colonizes other tissues or immune-suppressed hosts [29]. This strain expresses 100 to 400 type-1 fimbriae [30], uniformly distributed on cell surfaces. Each fimbria consists of four protein subunits, FimA, FimF, FimG and FimH [31]. FimA, the major component, helically forms a fiber from 1μm to 2μm in length and 7nm in width [32]. This fiber has a hollow axial core in its center with a diameter of 20Å to 25Å [33]. The other three subunits are located at the end of this fiber. Among them, FimH is the adhesin, recognizing the carbohydrate receptor α-D-mannose. Specifically, FimH consists of two domains, the pilin domain (160-273 a.a.) and the lectin domain (1-156 a.a.) [31,34].

While the former is responsible for fimbria incorporation, the latter is a β-barrel exhibiting a single mannose binding site at its distal end, binding to the non-reducing end of one α-mannose molecule but not β-mannose [34]. A crystal structure generated by Hung *et al.* indicated that all mannose hydroxyl groups link with FimH protein residues, and, therefore, the mannose molecule is deeply buried at the end of the β-barrel [35].

The dissociation constant K_a for the interrelationship between type-1 fimbriae and mannose is in the micromolar range, meaning that their affinity is almost 1000 times higher than the average, which is in the millimolar range [27]. This affinity can be increased when a chain of mannose residues at least 20nm long is attached to a relatively rigid backbone [36]. For example, Sharon reported that glycoproteins with a chain of mannose moieties, such as trisaccharide Manα3Manα4GlcNAc, exhibited a higher affinity for type-1 fimbriae than did mannose monomers [30], suggesting the multivalency of this lectin-carbohydrate recognition. In addition, this affinity can also be increased when the mannose is in an aromatic ring or linked with an aliphatic chain, indicating a hydrophobic binding site next to the FimH mannose binding site [30], a hypothesis supported by Nagahori *et al.*, who found that an aromatic polymer covalently attached to multiple mannose residues was 1000 times more inhibitory than monomers in the binding of type-1 *E. coli* to horse red blood cells [36].

2.1.3 Fucose as a Receptor for *Pseudomonas aeruginosa* PA-II Lectins

In addition to the first type of fimbriae-related lectin-carbohydrate interactions, the second type involves the binding of an afimbrial lectin PA-II of *P. aeruginosa* to α-L-

fucose. As an opportunistic pathogen, *P. aeruginosa* colonizes in inflamed and damaged tissues such as cystic fibrotic lungs and burn wounds, causing both acute and chronic infections [37,38]. A soluble PA-II lectin assists this colonization as reported by Chemani *et al.*, who found that the number of adhered mutant *P. aeruginosa* cells with abnormal PA-II lectin to lung epithelial cell cultures was half of that of the wild type cells, resulting in a faster bacteria clearance time and a smaller infected lung area *in vivo* [39]. In addition, Adam *et al.* observed a decrease in the waving frequency of cell cilia in respiratory track epithelial cell cultures after exposure to purified lectin PA-II, indicating that this lectin affected this important host's self-cleansing mechanism [40].

Glick and Garber first purified this soluble lectin primarily from the cytoplasm of an ear infection isolate, with minor amounts from the periplasm, the cytoplasmic and outer membranes [41,42]. This localization is different from other lectins which are found on outer membranes, making it difficult to explain the role of PA-II lectin in assisting bacterial adherence in the airway. To research further their expression, Tielker *et al.* compared planktonic *P. aeruginosa* cells with sessile ones harvested from a biofilm for the expression of PA-II lectins in their cytoplasm and outer membranes [43]. They found that while both cellular fractions exhibited PA-II lectins, the majority of the lectins were located in the cytoplasm in the planktonic cells but on the outer membranes in the sessile ones [43]. In addition to these cell types, lectin expression is also influenced by growth conditions and quorum sensing. Gilboa-Garber reported that cells incubated at 28 ℃ in nutrient broth for 1 day expressed more lectins with higher activity than those incubated in modified Grelet's medium for 2 or 3 days [44], probably due to the high protein

concentration in the former. Winzer *et al.* found that PA-II lectin (gene *lecB*) synthesis was initiated by a quorum sensing regulator RhlR, which regulates a *lux* box-like element located 42bp upstream of the *lecB* gene's transcriptional starting site [45]. The RhlR regulator was positively regulated by another transcriptional quorum sensing regulator LasR [45]. Abnormal LasR regulators delayed the synthesis of PA-II lectin [45]. The PA-II lectins expressed on the outer membranes specifically recognize L-fucose, a phenomenon supported by the findings of Chemani *et al.* that methyl-L-fucoside inhibited the binding of *P. aeruginosa* to human lung epithelium [39]. This strain has a high dissociation constant K_a of 0.625 μM for α-L-fucose and an even higher affinity for *p*-nitrophenyl-α-L-fucose [46]. This specificity to L-fucose requires Ca^{2+} cations, as reported by Mitchell *et al.*, who crystallized PA-II lectin, finding that it is a β-sandwich consisting of nine anti-parallel strands with four subunits, each of which bind to one fucose molecule in the presence of two Ca^{2+} cations [47]. In addition, Imberty *et al.* reported that Mg^{2+} and Zn^{2+} are also prerequisites for the binding to occur [48].

2.2 Carbohydrate Microarray Systems

To study these lectin-carbohydrate interactions, such traditional approaches as enzyme-linked lectin assay [49], isothermal titration calorimetry [50], surface plasmon resonance [51], hemagglutination inhibition assay [52], and X-ray crystallographic technique [53] have been used. Although these approaches successfully detailed lectin-carbohydrate recognition, they require intensive labor and large amounts of carbohydrates. Therefore, they are not suitable for rapid high-throughput analysis. To

address this issue, in 2002 several research groups simultaneously developed carbohydrate microarrays on surfaces ranging from multiwell plates [54] to modified glass slides [55,56,57]. In such a carbohydrate microarray system, nanoliters of hundreds of carbohydrates can be effectively printed using a manual or robotic printer. Microliters of protein suspensions are usually added to this system to study their interactions with these carbohydrates.

2.2.1 Obtaining Carbohydrate Molecules: Isolation from Nature vs. Chemical Synthesis

The first step in designing carbohydrate microarrays is to obtain pure carbohydrate molecules of desired structures through either isolation from nature or chemical synthesis. For the **first method**, oligosaccharides are usually obtained from bacterial and plant polysaccharides as well as mammalian milk and urine through degradation, acid/alkaline hydrolysis, and enzymatic reactions [58]. For the **second method**, different techniques such as the one-pot approach [59], enzyme-catalyzed reaction [60], and solid-phase synthesis [61] have been reported. Chemical synthesis has advantages over natural isolation in obtaining carbohydrates. First, relatively large quantities of pure carbohydrates can be produced easily through chemical synthesis, while the yield of the first method is usually low and impure due to the heterogeneity of carbohydrates [62]. Second, a spacer and a functional group, both of which are usually required for immobilization on carbohydrate microarray surfaces, can be easily added to the particular carbohydrate molecules through chemical synthesis [62]. However, this

method is challenged by the complexity of the carbohydrates due to their branches, their spatial atom arrangements, and their requirement of a large variety of monosaccharides as building blocks. Because of these disadvantages, chemical synthesis currently is limited to a small number of specialized laboratories, a situation comparable to the synthesis of nucleotides and peptides in the 1960s [63]. To address this issue, Plante *et al.* designed an automatic oligosaccharide synthesis system in which building blocks were linked to a solid surface reacting with monosaccharides in solution as a potential platform for non-specialists [64].

2.2.2 Carbohydrate Microarray Fabrication

Both isolated and synthesized carbohydrates can be attached to microarray surfaces through covalent or non-covalent bonds. Covalent attachment, which is used more frequently than the other, involves coupling a functional group on the carbohydrates and a reactive group on the surface through various reactions [62]. For example, Houseman and Mrksich synthesized ten functionalized monosaccharides as potential receptors for five plant lectins and covalently attached them to self-assembled monolayers of alkanethiols on gold-coated coverslips through the Diels–Alder cycloaddition reaction [65]. In addition, Park and Shin conjugated one monosaccharide *N*-acetylglucosamine and three glycosylamine disaccharides with maleimide groups for covalent binding to thiol-modified glass slides through the hetero-Michael addition reaction, followed by hybridization with three plant lectins [66]. Other examples of

covalent bonds are the cyan chloride coupling of amines, the squarate bond, and the [3+2] Huisgen-cycloaddition bond [62].

Covalent attachment enables high immobilization stability due to the chemical reactions between the carbohydrates and the surfaces, while non-covalent attachment is easier to achieve, allowing for free physical adsorption of carbohydrates to certain surfaces such as multi-well microplates and nitrocellulose membranes. For non-covalent attachment, simple carbohydrates require chemical derivatization to increase their size, while naturally purified complex molecules of polysaccharides and glycoconjugates can be directly used [67]. For example, Bryan *et al.* derivatized monosaccharide galactose and seven oligosaccharides by linking them to aliphatic hydrocarbons followed by non-covalent attachment to the plastic surfaces of 96-well plates for interactions with three plant lectins [54]. Another research group, Wang *et al.*, printed 48 polysaccharides and glycoproteins isolated from microbes and host cells on nitrocellulose membrane-coated glass slides, followed by hybridization with human sera, screening for antibodies [55].

This carbohydrate attachment is achieved through printing dense and uniform arrays of carbohydrate dots, with diameter ranging from 75μm to 500μm depending on the surface energy of the slide, the printer and the carbohydrate solution [68]. The transferred carbohydrate solution volume is typically in the range of 50pL to 100nL, minimizing reagent cost [69]. The two methods for carbohydrate printing are the contact and the non-contact methods. The **first** involves solid pins, split pins, nano-tips, or microstamps [69], delivering carbohydrate solutions through physical contact with the array surfaces. Although these contact printing tools are easy to handle and used

frequently in industry and laboratories, they have several disadvantages, including pin clogging, lack of droplet uniformity, tip deformation and low speed [69]. The **second** type, the non-contact printing, such as ink-jet printing, electrospray deposition, and laser writing has advantages including reduced contamination and high throughput [69]. However, Nishioka *et al.* reported that an enzyme of peroxidase lost its activity after being printed on a 96-well microplate using a piezoceramic actuated inkjet printer [70]. In addition, Barbulovic-Nad *et al.* reported a second disadvantage of this method: irregular spot sizes and satellite droplets due to splashing [69]. Since both contact and non-contact methods have advantages and disadvantages, their application largely depends on the experimental design.

2.2.3 Carbohydrate Microarray Signal Detection

The binding of molecules to these printed carbohydrates is usually detected based on surface plasmon resonance (SPR), biotin-avidin interaction, or fluorescence. The **first** analyzes light reflected from a prism made from gold film on which the binding activities occur [71]. This method is able to quantify binding affinities and constants, and to perform real-time measurements without requiring labels [71]. However, its high cost and complexity make its wide-spread application impractical. The **second** one relies on substrate color formation mediated by avidin or streptavidin, which binds to the biotin tags in biotinylated molecules. The third is the most prevalent method, using a fluorescent signal scanner or microscope to measure or observe the signals emitted from the fluorophores attached to the binding molecules [62]. Fluorescence generation is a

three-stage process [72]. The **first** stage is excitation resulting in an excited electronic singlet when the fluorophores absorb energy from an external source such as a laser beam or a mercury lamp. In the **second** stage, which lasts typically 1-10 nanoseconds, the fluorophores partially dissipate their excited energy. The **third** stage is fluorescence emission, when the fluorophores emit energy photons at a lower intensity and longer wavelength than that absorbed in the first stage as a result of energy dissipation in the second stage. Photobleaching may occur during the second stage, irreversibly destroying the fluorophores; otherwise, they may be excited again, meaning the three states are cyclical [72].

2.2.4 Carbohydrate Microarray Applications

After the protocols of carbohydrate obtaining, surface fabrication and signal detection have been investigated, researchers began to focus on the application of this system in, for example, the field of microbiology. In 2004, a carbohydrate microarray screening for potential drug targets of antibiotics was designed by Disney and Seeberger, who covalently arrayed a group of carbohydrates of aminoglycoside antibiotics, for hybridization with synthesized fluorescent-labeled RNA which mimics bacterial ribosome RNA [73]. However, the majority of carbohydrate microarrays are designed to study the relationship between carbohydrates and proteins, primarily antibodies. For example, in 2006, Parthasarathy *et al.* used a *Burkholderia pseudomallei* polysaccharides microarray to screen for potential antibodies in rabbit and human sera [74]. At the same time, limited direct hybridization of microorganisms, such as intact viruses and whole

bacterial cells, using carbohydrate microarrays have been reported. For example, Blixt *et al.* printed 200 natural and synthetic carbohydrates on amine-reactive glass slides and added a variety of carbohydrate binding agents for hybridization, including influenza virus A/Puerto Rico/8/34 (H1N1), which recognized NeuAcα2–3Gal and NeuAcα2–6Gal containing sialosides [75]. Similarly, Disney and Seeberger subjected fluorescence-labeled *E. coli* to a carbohydrate microarray consisting of synthesized monosaccharides and oligosaccharides covalently immobilized on modified glass slides, confirming the recognition of mannosides by this bacterial strain [76]. The glycomics center at the University of Emory School of Medicine maintains a glycan library of approximately 230 synthetic and derivatized carbohydrates for microarray printing on *N*-hydroxysuccinimide (NHS)-activated glass slides, screening for glycan specific antibodies and glycosyltransferases as well as for pathogens such as influenza virus field isolates [77]. As these studies indicate, the use of carbohydrate microarrays in detecting and profiling of target bacteria is feasible.

2.3 Microcantilever-Based Biosensors

2.3.1 Overview

These carbohydrate-bacteria binding profiles obtained from carbohydrate microarrays can be applied to biosensors for the detection of target bacteria. Typically, a biosensor consists of three parts, sensing molecules, a transducer and a signal processor [78]. The immobilized sensing molecules determine the specificity of the microcantilever-based biosensors, since the beam itself exhibits no selectivity in binding

biological molecules. The transducer translates the interactions between the sensing molecules and the target into optical, mechanical or electronic signals, which are then displayed as outcomes using a signal processor [79]. Depending on the transduction mechanism involved, biosensors can be classified as **optical**, such as fluorescence resonance energy transfer (FRET) biosensors [80] and surface plasmon resonance (SPR) biosensors [81], or **electrochemical** ones, such as electrochemical impedance spectroscopic (EIS) biosensors [82] and amperometric biosensors [8,83]. One type of optical biosensor, a microcantilever-based biosensor, was first introduced in 1986 by Binnig *et al.* in their demonstration of the innovative scanning atomic force microscopy technology [84]. Structurally, microcantilevers have a relatively large base with a beam or several beams anchored at one or both ends, resembling a miniature diving board [79]. Most of the beams are rectangles, with a few being triangles. The length, width and thickness of the rectangular ones are typically 100 μm-500 μm, 20 μm-50 μm, and 0.5 μm-2 μm, respectively [79]. In the last twenty years, these microcantilevers have attracted much attention due to their ability to serve as specific, sensitive, real-time, and multifunctional detectors.

The use of microcantilevers as biosensors has many advantages. **First**, their ultra small size decreases the amount of sample required for detection. **Second**, detection using microcantilevers does not require fluorescent or chemiluminescent labels and, therefore, saves time and expense as well as avoids possible binding site interference [85]. **Third**, mass production of microcantilevers using conventional micromachining techniques enables the parallel microcantilever fabrication of sensing molecules [79].

2.3.2 Fabrication of Sensing Molecules

Most sensing molecules used in biosensors, including those for bacteria detection, are DNA and proteins. For the first type, thiol groups are commonly used to modify oligonucleotides, resulting in a self-assembled monolayer on gold surfaces. In one such study, Marie *et al.* modified the 5' end of an oligonucleotide with a thiol group, followed by immobilization on gold-coated microcantilevers [86]. Similarly, protein thiol modification is also a widely used strategy as exemplified by Karyakin *et al.*, who split the antibody immunoglobulin G into half, exposing the thiol groups for antibody immobilization on gold surfaces [87]. Carbohydrates, a third biomacromolecule, are used less frequently than the other two as sensing molecules on biosensors and, therefore, have received limited research attention.

2.3.3 Signal Transduction

The immobilization of sensing molecules and their binding to target molecules change the characteristics of the microcantilever beams, including their surface stress and mass. These changes are reflected in the deflection of the beams and the shift in their resonance frequencies [88,89]. The deflection, which is detected in the static mode, requires asymmetrical functionalization on the two sides of a microcantilever beam so that adsorbents bind to only one side, generating a surface stress forcing the beam to bend [90]. In contrast, the shift in resonance frequency, which is detected in the dynamic mode, is used in both one- and two-sided functionalized microcantilevers; however, they must be actuated to measure this frequency. Cost-effective actuation can be induced using

ambient conditions such as room temperature and acoustic noise; however, these conditions do not possess enough energy to vibrate microcantilevers with high resonance frequencies [91]. In addition, this operation requires a precisely controlled environment. As a result, external energy sources are frequently used. In 1994, Florin *et al.* designed a scanning stylus atomic force microscope involving microcantilevers with magnetic tips actuated by a magnetic field [92,93]. In 2002, Stephan, *et al.* used alpha particle ionization to create an electrostatic field for microcantilever sensor actuation [94], and in 2008, Shin *et al.* constructed an array of five microcantilevers driven by a piezoelectric holder made from $Pb(Zr_{0.52}Ti_{0.48})O_3$ connected to an AC source [95]. During this actuation process, the piezoelectric material contracts and expands based on the excitation frequency induced by an electric charge, deforming the adjacent non-piezoelectric layer [96]. When this frequency is the same as the natural resonance frequency of the non-piezoelectric layer, the impedance of the piezoelectric layer changes sharply and is then detected by a signal processor [96].

2.3.4 Signal Processing and Output

The deflection and resonance frequencies of microcantilevers are monitored by several signal processing techniques such as piezoresistivity [97], capacitive readout [98] and optical readout [99]. The first one measures the resistivity change of piezoresistive materials induced by the change in microcantilever surface stress using a sensitive Wheatstone's bridge [97]. The second one involves a transducer plate consisting of a microcantilever and a parallel capacitor, the capacitance of which changes based on the

motion of the microcantilever and is detected by a sensitive bridge network [98]. Although the read-out electronics required by these two methods are integrated on the microcantilever saving equipment and space, their high intrinsic noise level impacts their sensitivity and their electrical connections require a waterless environment for output [100]. Therefore, optical read-out, which measures the position of a laser beam reflecting the movement of the microcantilever, is more often used than the other two, For example, in the study conducted by Mahmoodi and Jalili generating a non-linear equation for non-homogenous microcantilever beams, the laser beam pointed on the microcantilever was reflected to a laser-Doppler vibrometry in the Micro System Analyzer 400, accurately representing the vibration of the microcantilever [101].

2.3.5 Application in Pathogen Detection

Since the design of microcantilever-based biosensors has improved over the last ten years, it is practical for them to serve as pathogen detectors, answering the need for food safety and national biological security. Most of these detectors reported thus far use antibody-antigen interactions, with a few using DNA complementary recognition. The first type is exemplified by Weeks *et al.*, who functionalized a gold-coated silicon nitride microcantilever with a thiol-linked bacterial antibody capable of detecting 25 adsorbed *Salmonella enteric* cells through optical deflection representing surface stress changes [102]. A study of the second type was reported by Cha *et al.*, who immobilized thiol-functionalized cDNA obtained from polymerase chain reactions on gold-coated microcantilevers, detecting a 243-mer nucleotide from the Hepatitis B virus precore/core

region using an impedance analyzer measuring resonance frequencies [103]. However, the preparation of specific antibodies for a particular bacterial strain is tedious and expensive, while the DNA-based detection requires DNA extraction from pathogens, rather than detecting the intact cells.

In the last decade, carbohydrate-lectin interactions investigated using carbohydrate microarrays have suggested the capability of carbohydrates to serve as sensing molecules in microcantilever-based biosensors, detecting entire bacterial cells in liquid samples. However, very few biosensors based on this interaction have been reported thus far, probably due to the novelty of this field.

CHAPTER 3

MATERIALS AND METHODS

A flow chart summarizing the methods used in this research is shown in Fig. 1. Specifically, after bacterial cultivation, the *Escherichia coli* strains were validated for their recognition of mannose, followed by carbohydrate microarray design, optimization, and evaluation. Then, the optimized conditions obtained from carbohydrate microarrays were applied to microcantilever-based biosensors and the shifts in their resonance frequencies were measured.

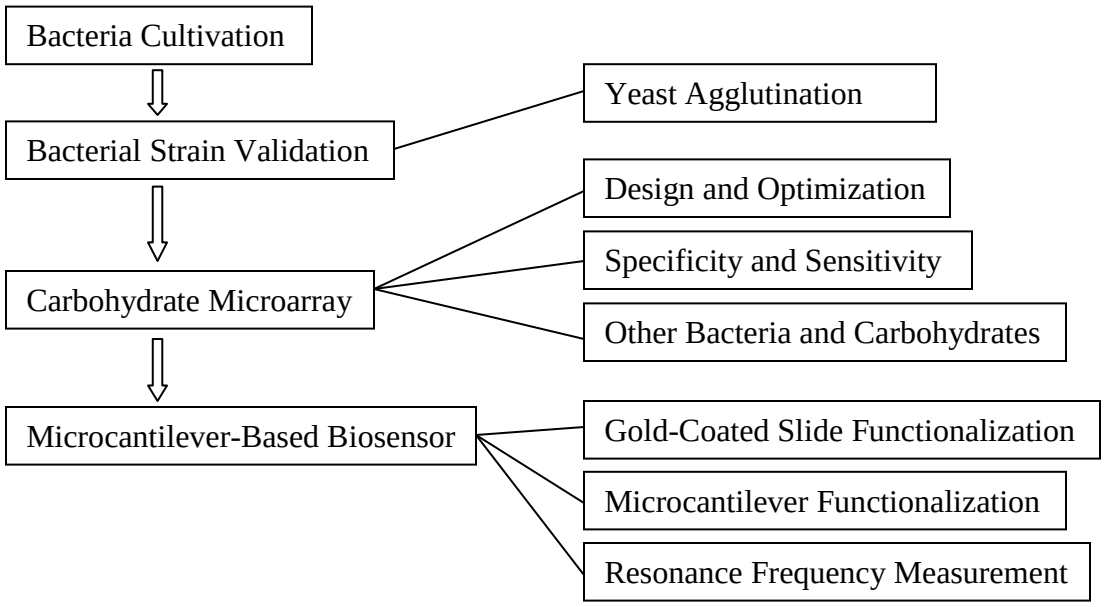

Figure 1: Method Flow Chart.

3.1 Bacterial Strains and Plasmids

Table 1: Bacterial Strains Used in this Research.

Bacterial Strains	Description	Source
E. coli ORN178	*E. coli* K12 derivative, tetracycline resistant	[104]
E. coli ORN178/pGREEN	*E. coli* ORN178 transformed with pGREEN plasmid, ampicillin resistant	[106]
E. coli ORN208	*E. coli* K12 derivative, kanamycin resistant	[104]
E. coli ORN208/pGREEN	*E. coli* ORN208 transformed with pGREEN plasmid, ampicillin resistant	[106]
E. coli O157:H7	Wild-type	[107]
E. coli O157:H7/pWM1007	Fluorescent and kanamycin resistant	[107]
Pseudomonas aeruginosa PAO1	Wild-type	[108]
P. aeruginosa PAO1/pMRP9-1	Fluorescent and carbenicillin resistant	[108]
P. aeruginosa PAO1*lecB*::T^r	Insertional transposon *lecB* gene mutant	[109]
Klebsiella pneumonia	Wild-type	ATCC[a] 13883
Salmonella typhimurium	Wild-type	ATCC 13311

a: American Type Culture Collection

As shown in Table 1, a total of 11 bacterial strains were used in this research. The wild type *E. coli* ORN178 and its *fimH* gene mutant strain *E. coli* ORN208 were graciously provided by Dr. Chu-Cheng Lin from the National Taiwan Normal University (Taiwan) [104]. They are both derivatives of *E. coli* K12. *E. coli* ORN178 has the *tetR* gene inserted serving as a selective marker for the adjacent *fimH* gene [32], and the *fimH* allele *fimH*304 in *E. coli* ORN208 has a partial deletion created by a *kan* gene inserted in the XhoI site [105]. As a result, *E. coli* ORN178 expresses type-1 fimbriae with functional FimH adhesin, while *E. coli* ORN208 expresses abnormal type-1 fimbriae with mutated FimH. These two strains were previously transformed with pGREEN plasmids in Dr. Jeremy Tzeng's lab at Clemson University [106]. This plasmid, purchased from the Carolina Biological Supply Company (Burlington, NC), carries an ampicillin resistant gene *ampR* and encodes green fluorescent proteins (GFP), which contributes to the fluorescence of the two transformants, *E. coli* ORN178/pGREEN and *E. coli* ORN208/pGREEN.

E. coli O157:H7 and *E. coli* O157:H7/pWM1007 was kindly provided by Dr. Xiuping Jiang in the Department of Food Science and Human Nutrition at Clemson University [107]. The plasmid pWM1007 possesses kanamycin resistance and expresses GFP. *Pseudomonas aeruginosa* PAO1 and *P. aeruginosa* PAO1/pMRP9-1 were kindly provided by Dr. Matt Parsek in the Department of Microbiology at the University of Washington in Seattle, WA [108]. The plasmid pMRP9-1 carries genes for fluorescence and carbenicillin resistance. An insertional transposon mutant *P. aeruginosa* PAO1*lecB*::T^r without functional *lecB* gene was purchased from the *P. aeruginosa* PAO1

transposon mutant library at the University of Washington in Seattle, WA [109]. The transposon was located at nucleotide position 204 [39]. Non-fluorescent strains of *Klebsiella pneumonia* and *Salmonella typhimurium* were purchased from American Type Culture Collection (ATCC) (Manassas, VA, USA) and the ATCC numbers are 13883 and 13311, respectively.

3.2 Cultivation Methods

These bacterial strains were then cultivated in sterilized tryptic soy agar (TSA) and tryptic soy broth (TSB), both purchased from EMD Chemicals, Inc. (Darmstadt, Germany). To maintain the copies of the fluorescent plasmids, 100 μg/mL kanamycin (Sigma Aldrich, St. Louis, MO) was sterilized using a 0.45 μm Syrfil-MF Syringe filter (Corning Incorporated, Corning, NY) and added to the media of *E. coli* O157:H7/pWM1007. Similarly, 300 μg/mL carbenicillin (Cellgro® Mediatech, Inc., Manassas, VA) was sterilized and added to the media of *P. aeruginosa* PAO1/pMRP9-1. The media of *E. coli* ORN178/pGREEN and *E. coli* ORN208/pGREEN contained 50 μg/mL sterilized ampicillin (Sigma Aldrich, St. Louis, MO). The agar media was then poured into 100 × 15mm polystyrene Petri dishes. Both media were refrigerated at 4 ℃ until ready to use.

All six bacterial strains were streaked on TSA plates and inoculated in TSB tubes using sterile techniques, and incubated (Fisher Scientific 30D Econotemp Incubator) at 37 ℃ for 24 hours. The bacterial colonies on the agar plates were then suspended in phosphate buffer saline (PBS) (ICN Biomedical Inc. Aurora, OH).

With the purpose to facilitate the expression of PA-II lectin, *P. aeruginosa* PAO1/pMRP9-1 and its *lecB* mutant *P. aeruginosa* PAO1*lecB*::T^r was also inoculated in a nutrient broth (Difco Laboratories, Detroit, MI) and a Grelet's modified medium with 0.2% (w/v) choline added daily as described by Gilboa-Garber [44]. It was then incubated at 28 ℃ for 1 day, 2 days, or 3 days before harvest.

3.3 Bacterial Growth Phase Determination

It has been demonstrated that expression of bacterial adhesins are regulated and growth-phase dependent [43,110]. A growth curve was generated to determine how long the bacteria strain of *E. coli* ORN178/pGREEN should be incubated to obtain a culture at a particular growth phase, with the purpose to study the effect of growth phase on bacterial binding activity. A colony grown on a TSA plate was inoculated into a 50mL tube of TSB containing 50 μg/mL ampicillin. An optical density value was immediately measured at 600nm (OD_{600}) using a spectrophotometer (Bio-Rad SmartSpec^{TM} 3000) with the medium serving as the blank solution. Then, the bacteria suspension was placed in a shaking-incubator (New Brunswick Scientific) at 37 ℃. Twenty-four OD_{600} readings were taken over 27 hours. With OD_{600} as the y axis and hour as the x axis, a growth curve was plotted in the software Microsoft Excel.

3.4 The Relationship between Population Concentration and Optical Density

Optical density measurement is an easy way to obtain information about bacterial population concentrations. The relationship between the two was investigated so that the

number of cells in a suspension can be calculated given an optical density value. *E. coli* ORN178 colonies were suspended in PBS to obtain an OD_{600} of 1.5. Seven tubes of bacterial suspension two-fold serially diluted with PBS was made, and their OD_{600} values were measured using the spectrophotometer. Then, a ten-fold serial dilution was generated for each of the seven tubes. For each ten-fold dilution, 100 µL of the suspension was spread on a TSA plate using a glass spreader followed by incubation at 37 ℃ for 24 hours. The number of colonies was counted using plates with 25-250 colonies on them. The population concentration was calculated based on the equation below and plotted as the y axis and OD_{600} as the x axis in Microsoft Excel:

Population concentration = (number of colonies)/ (dilution factor) (1)

where the dilution factor is the number indicating the ten-fold dilution such as 10^{-1} or 10^{-8}.

3.5 Yeast Agglutination Assay

Yeast cells exhibit mannan, a polymer of mannose, on the cell surfaces [25] and was used to verify the binding of *E. coli* ORN178/pGREEN and the non-binding of *E. coli* ORN208/pGREEN to α-D-mannose. Individual overnight culture was suspended in PBS (OD_{600}=1) and mixed separately with a yeast suspension at ratios from 1:9 to 9:1 based on volume. The yeast suspension was made by dissolving a commercially available baker's yeast (RedStar Instant Yeast) in PBS (OD_{600}=1). Wet mount slides were immediately observed under a Motic AE31 inverted phase-contrast/epi-fluorescence microscope (Ted Pella, Inc., Redding, CA) with a filter for GFP.

3.6 Non-Viable Cell Preparation

Both target and non-target microorganisms in field samples could be viable, non-viable, and of unknown biosafety level. Therefore, it is beneficial to inactivate the samples prior to testing. To study the effect of bacterial viability on adhesin-receptor specificity, *E. coli* ORN178/pGREEN cells were incubated with 25mg/mL formaldehyde (Sigma-Aldrich, St. Louis, MO) for 40min, followed by three washes with PBS. The cells were then suspended in PBS (OD_{600}=1) and spread on TSA plates containing 50 μg/mL ampicillin to confirm their viability. Yeast agglutination assay was conducted as described in Section 3.5.

3.7 Carbohydrate Microarray System Setup

E. coli ORN178/pGREEN and *E. coli* ORN208/pGREEN were used to validate the carbohydrate microarray system, which was then applied to the non-viable cells and the remaining bacteria introduced in Section 3.1. This microarray system was developed using a Whatman MicroCaster^{TM} Manual Microarraying System purchased from Whatman, GmhB, with an eight-pin hand tool; an indexing system; a washing station; Whatman FAST slides with 16 nitrocellulose membranes; and a Whatman FAST PAK 16 Protein Array Kit including bottles of protein arraying buffer (2×), protein array blocking buffer (1×), and protein array wash buffer (10×). Initially, 10 μg/μL α-D-mannose (Sigma-Aldrich, St. Louis, MO) dissolved in PBS was mixed with the arraying buffer and printed onto a Whatman FAST slide. To improve immobilization, polyacrylamide (PAA)-conjugated carbohydrates purchased from GlycoTech (Gaithersburg, MD) were

dissolved in PBS at the following concentrations: 10μg/μL, 5μg/μL, 2.5μg/μL, 1μg/μL, and 0.1μg/μL. After being mixed with the arraying buffer (2×), 3μL of each concentration was added to the wells of a PCR microplate (Axygen Inc., Union City, CA). Approximately 50nL carbohydrate solution was transferred from the microplate to a Whatman FAST slide held by the indexing system using the hand tool [111].

After printing, the slide was air-dried at room temperature, followed by carbohydrate immobilization by baking the slide at 80℃ for 30 min (Black & Decker Toast-R-Oven) or leaving it at room temperature overnight. Blocking and bacteria hybridization were conducted following the manufacturer's recommended procedures. Specifically, 80μL blocking buffer was added to each membrane, and the slide was shaken using a microtiter plate shaker (IKA MS3 digital) at 250rpm for 30 min at room temperature. For bacteria hybridization, an 80μL bacterial suspension was added to each membrane, followed by shaking using the same shaker. For the experiment studying the effect of growth phase on bacterial adherence, bacteria cells were incubated for 12 hours, 24 hours, and 48 hours. All of the three samples were adjusted to the same population concentration (OD=1). After hybridization, the slides were washed three times, 5 min each, by being gently shaken in the wash buffer. After they were air-dried, the epi-fluorescence microscope with a GFP filter was used to observe the results, and a ProgRes C5 Camera (Jenoptik Laser, Optik, Systeme GmbH, Germany) connected to the microscope was utilized to take pictures of the field of view.

3.8 Specificity and Sensitivity Tests

To investigate the specificity of the carbohydrate microarray system, 80 μL suspensions of *E. coli* ORN178/pGREEN, *E. coli* ORN178/pGREEN pre-exposed with α-D-mannose, *E. coli* ORN208/pGREEN, and *E. coli* O157:H7/pWM1007 were added to a Whatman FAST slide printed with α-D-mannose-PAA. To prepare the pre-exposed *E. coli* ORN178/pGREEN culture, colonies on a TSA plate were mixed with 10μg/μL α-D-mannose dissolved in PBS (OD_{600}=2). The mixture was then shaken using the microtiter plate shaker at 250rpm for 30 min at room temperature. The bacterial cells were centrifuged at 5,000rpm for 3 min in a microcentrifuge (Eppendorf Centrifuge, Model 5417R), washed with PBS, spun down three times, and finally suspended in PBS (OD_{600}=1, i.e., ~10^9cells/mL).

For the sensitivity test, *E. coli* ORN178/pGREEN cells were suspended in PBS and TSB, followed by a ten-fold serial dilution to obtain suspensions with concentrations from 10^9cells/mL to 10^4cells/mL. Then, 80 μL of each suspension was hybridized with printed α-D-mannose-PAA on a Whatman FAST slide. The corresponding cell number on each membrane was 10^8, 10^7, 10^6, 10^5, 10^4, and 10^3.

3.9 Visualization Methods

To visualize non-fluorescent bacterial strains in the carbohydrate microarray system, four protocols using fluorescent protein dyes, a fluorescent nucleic acid dye, a fluorescent carbohydrate, and a biotinylated carbohydrate were evaluated. First, two fluorescent protein dyes of fluorescein isothiocyanate (FITC) (Acros Organics, NJ)

labeling the amino acid of lysine and Alexa fluor 488 C_5 maleimide (Invitrogen, Eugene, OR) binding to cysteine residues were dissolved in PBS at concentrations of 25μg/mL and 4μg/mL, in preparation for the two staining methods used here [112]. For the first method, 25μg/mL fluorescent dye was mixed with 1mL bacterial cell suspension (OD_{600}=1) in a 1.5mL tube and incubated for 1 hour at room temperature in the dark, followed by three washes with PBS. After being re-suspended in PBS, the cells were ready for hybridization. For the second method, after bacterial hybridization with carbohydrates on Whatman FAST slides, 80μL fluorescent dye (4μg/mL) was added to each membrane and incubated for 1 hour at room temperature in the dark, followed by three washes, 5 min each, by being gently shaken in the wash buffer.

Next, a permeable fluorescent nucleic acid dye, SYTO 9 (3.34mM) (Invitrogen, Eugene, OR) was diluted in 0.85% NaCl (Sigma-Aldrich, St. Louis, MO) solution until a working concentration of 0.83μM was reached. The dye concentration was then decreased to 0.42μM, 0.21μM, 0.10μM, 50nM, and 25nM through two-fold serial dilution to determine the optimum concentration. The staining approaches were the same as for the fluorescent protein dyes.

Third, serially diluted *E. coli* ORN178 and *E. coli* ORN208 suspensions with OD_{600} readings equal to 1, 0.5, 0.25, 0.12, and 0.06 were immobilized on a Whatman FAST slide using the same technique for carbohydrate printing as described in Section 3.7. A column of PBS was also printed on the slide as a negative control. After being baked and blocked, the slide was hybridized for 3 hours with 10μg/μL α-D-mannose-PAA-fluor (GlycoTech, Gaithersburg, MD), a fluorescent derivative of PAA-conjugated

mannose, expecting the fluorescent carbohydrate could visualize the printed bacterial cells. Images were taken under the epi-fluorescence microscope both before and after hybridization.

Fourth, PAA-conjugated mannose linked with a biotin group, specifically α-D-mannose-PAA-biotin, was purchased from GlycoTech (Gaithersburg, MD) and printed on a Whatman FAST slide as described in Section 3.7, followed by hybridization with *E. coli* ORN178 (OD_{600}=100), *E. coli* ORN208 (OD_{600}=100), and PBS. After three washes with the wash buffer, 80μL of 0.2units/mL alkaline phosphatase conjugated avidin (Thermo Scientific, Rockford, IL) diluted in a buffer (pH 7.5) containing 20mM HEPES (Sigma-Aldrich, St. Louis, MO.), 0.5M NaCl, and 0.1mg/mL crystalline bovine serum albumin (MP Biomedicals, LLC., Solon, OH) was added to each membrane and incubated on a microtiter plate shaker (IKA MS3 digital) at 250rpm for 1 hour at room temperature. Then, a substrate solution made from a Vector® Black Alkaline Phosphatase Substrate Kit II (Vector Laboratories, Inc., Burlingame, CA) was added to each membrane; its reaction with alkaline phosphatase linked to avidin during one-hour incubation at room temperature resulted in black dots at the positions where α-D-mannose-PAA-biotin was printed. After three washes with the washing buffer, the slide was scanned using a printer/scanner/fax machine.

3.10 Other Carbohydrates and Bacteria

The carbohydrate microarray was extended to other carbohydrates and bacteria. One of the visualizing protocols utilizing FITC (25μg/mL) was used to stain the six wild

type strains (OD_{600}=10) of *E. coli* ORN178, *E. coli* ORN208, *K. pneumonia*, *E. coli* O157:H7, *P. aeruginosa*, and *S. typhimurium* for one hour followed by three washes with PBS as described in Section 3.9. Wet mount slides of each bacteria were observed under the epi-fluorescence microscope. Then, 80 μL of each bacteria suspension (OD_{600}=100) was added to membranes printed with eight PAA-conjugated carbohydrates (GlycoTech, Gaithersburg, MD) of α-D-mannose-PAA, α-D-galactose-PAA, β-D-galactose-PAA, α-L-fucose-PAA, β-GalNAc-PAA, α-Neu5Ac-PAA, GlcNAcGlcNAc-PAA, and GalGlcNAcGalGlc-PAA. The concentrations of these carbohydrates were 2.5 μg/μL, 1 μg/μL, and 0.1 μg/μL. PAA at the same concentrations (GlycoTech, Gaithersburg, MD) and PBS were printed on the membranes as negative controls. FITC (25 μg/mL) was also printed as a marker locating particular carbohydrate dots.

Gilboa-Garber reported that large expression of PA-II lectins was achieved through incubation in nutrient broth and Grelet's modified medium at 28 ℃ for 1 day, 2 days, and 3 days [44]. To facilitate the expression of lectins, a fluorescent derivative of one of the six wild type strains, *P. aeruginosa* PAO1/pMRP9-1, and its mutant *P. aeruginosa* PAO1*lecB*::Tc^r were incubated as described by Gilboa-Garber [44]. Bacterial cells were harvested through centrifuge at 5,000rpm for 3 min in a microcentrifuge (Eppendorf Centrifuge, Model 5417R) and washed three times with PBS. The mutant was stained with FITC using the protocol described in Section 3.9. Then, both strains were suspended in PBS with 10mM $MgCl_2$, 10mM $CaCl_2$, and 10mM $ZnSO_4$, followed by hybridization with immobilized α-L-fucose-PAA on Whatman FAST slides.

3.11 Gold-Coated Slide Functionalization

For gold-coated microcantilever biosensors, carbohydrate molecules need to be immobilized covalently onto the gold surface. The functionalization protocol was first investigated on gold-coated slide surfaces. Monosaccharides cannot bind directly to gold surfaces just as they cannot be immobilized directly on nitrocellulose membranes. The best way to achieve long-term stability for carbohydrate immobilization is to chemically functionalize the gold surfaces, so that carbohydrate molecules covalently and densely bind to them with enough space between each other [113]. Carbohydrate immobilization on gold-coated slides (Erie Scientific Company, Portsmouth, NH) was investigated using a strategy adopted from Zhi, *et al.* [114]. Specifically, gold-coated slides were soaked in 0.1mM 16-mercaptohexadecanoic acid (MHDA) (Asemblon Inc., Bedmond, WA) dissolved in isobutonal (J. T. Baker, Phillipsburg, NJ) in a glass Petri dish sealed with parafilm (Pechiney Plastic Packaging Company, Chicago, IL) for 24-48 hours to obtain a hydrazide-derivatized self-assembled monolayer (SAM). After being washed three times with 100% ethanol on the microtiter plate shaker at 250rpm, the slides were soaked in a mixture of 2mg/ml 1-ethyl-3-(3-dimethylaminopropyl) carbodiimide (TCI America, Portland, OR) and 1mg/mL adipic dihydrazide (TCI America, Portland, OR) in DMSO (Sigma Aldrich, St. Louis, MO) overnight in a glass Petri dish sealed with parafilm to prevent evaporation. The mixture reacted with the SAM, generating an amine group at the free end of the monolayer. After three washes with ethanol, the slides were air-dried and ready for carbohydrate immobilization.

Then, mannose, α-D-mannose-PAA, α-D-mannose-PAA-fluor, and mannan with concentrations of 10 μg/μL, 5 μg/μL, 2.5 μg/μL, 1 μg/μL, and 0.1 μg/μL were mixed with 1M betaine (TCI America, Portland, OR) to reduce evaporation and then printed on the functionalized gold-coated slides using the Whatman MicroCaster™ Manual Microarraying System. These slides were sealed in a Petri dish with parafilm and incubated at room temperature overnight. During the incubation, aldehyde groups of reducing sugar molecules reacted with the amine groups at the free end of the SAM through a condensation reaction to form imine linkages, thus immobilizing the carbohydrate on the gold surface [114]. At the end of incubation, this slide was washed twice with distilled water to remove unbound carbohydrates. The slide printed with α-D-mannose-PAA-fluor was observed using the epi-fluorescence microscope to verify the coating of carbohydrate molecules.

The blocking, the bacteria hybridization, the washing, and the imaging steps were the same as described previously in Section 3.7. The OD_{600} readings of the suspensions of *E. coli* ORN178/pGREEN and *E. coli* ORN208/pGREEN hybridized with mannose, α-D-mannose-PAA, and α-D-mannose-PAA-fluor were 1, while those hybridized with mannan were 100 to ensure that the bacterial cells were sufficient for the mannan receptors.

3.12 Microcantilever Functionalization and Resonance Frequency Measurements

This carbohydrate immobilization strategy was then applied to gold-coated microcantilevers purchased from BudgetSensors (Innovative Solutions Bulgaria Ltd.,

Bulgaria) [115]. They were coated with 70nm gold on the detector side and rotated monolithic silicon on the other [115]. A symmetric beam ($450 \times 50 \times 2\,\mu m$) was anchored at one end of the large base ($3.4 \times 1.6 \times 0.3mm$) of the cantilever [115]. This beam has a resonant frequency of 13kHz and a force constant of 0.2N/m [115]. Because the microcantilever beams are too fragile, $10\,\mu g/\mu L$ α-D-mannose-PAA and mannan mixed with 1M betaine were dropped until the entire gold surfaces were covered instead of being printed. These cantilevers were then incubated overnight at room temperature. After being washed, the microcantilevers were hybridized with 0.5mL *E. coli* ORN178/pGREEN (OD_{600}=1), *E. coli* ORN178/pGREEN (OD_{600}=0.001), and *E. coli* ORN208/pGREEN (OD_{600}=1) in a 24-well plate (Costar Corning Inc., Corning, NY) for three hours at room temperature. These microcantilevers were observed under the epi-fluorescence microscope.

Finally, uncoated, α-D-mannose-PAA functionalized and bacteria-bound microcantilevers were measured for their resonant frequencies of the first flexural mode in both non-contact and dynamic modes using the Polytec Micro System Analyzer 400 (MSA-400), which has a stroboscopic video microscope, a scanning laser Doppler vibrometer, and a white light interferometer. After being actuated by the real time interface dSPACE 1103 (dSPACE Inc., Wixom, MI), these microcantilever beams generated a position feedback, which was sensed by the built-in vibrometer and transferred to a desktop computer.

3.13 Statistical Analysis

Data obtained from the resonance frequency measurements were expressed as mean ± standard deviation for a particular group size (n). Probability values (p-values) were calculated using a paired one-tailed student's t-test in Microsoft Excel. P-values less than 0.05 were considered to be statistically significant.

CHAPTER 4

RESULTS

Using the methods described in Chapter 3, the results were obtained and categorized into two groups. **First**, after the verification of the recognition of mannose by *E. coli* ORN178/pGREEN, a carbohydrate microarray system based on the Whatman MicroCaster™ manual microarraying system was developed and optimized. In addition, the interactions between other bacteria and carbohydrates including *Pseudomonas aeruginosa* and α-L-fucose were studied using this carbohydrate microarray system. **Second**, the recognition of *E. coli* ORN178 to α-D-mannose was applied to a microcantilever-based biosensor, which was then tested for its detection of *E. coli* ORN178.

4.1 Carbohydrate Microarray System

First, the recognition of mannose by *E. coli* ORN178/pGREEN and non-recognition by *E. coli* ORN208/pGREEN were verified using a yeast agglutination assay. Then, a carbohydrate microarray system was designed and optimized on Whatman FAST slides, followed by specificity and sensitivity tests. Next, bacteria visualization methods were studied to extend the application of this system to field samples. Finally, this carbohydrate microarray system was applied to other carbohydrates and bacteria strains.

4.1.1 Yeast Agglutination Assay

E. coli ORN178/pGREEN cells seen as green rods in Fig. 2 mediated the agglutination of yeast cells seen as transparent ovals (Fig. 2A), but *E. coli* ORN208/pGREEN did not (Fig. 2B). While the volume ratio of bacteria to yeast of 1 to 1 yielded the best agglutination result, the remaining ratios from 1:9 to 9:1 all resulted in agglutination. Given that polymers of mannose are located on yeast cell surfaces [116], this assay suggested that the mannose binding activities were maintained in the two transformants and the volume ratio did not play an important role in yeast agglutination.

A **B**

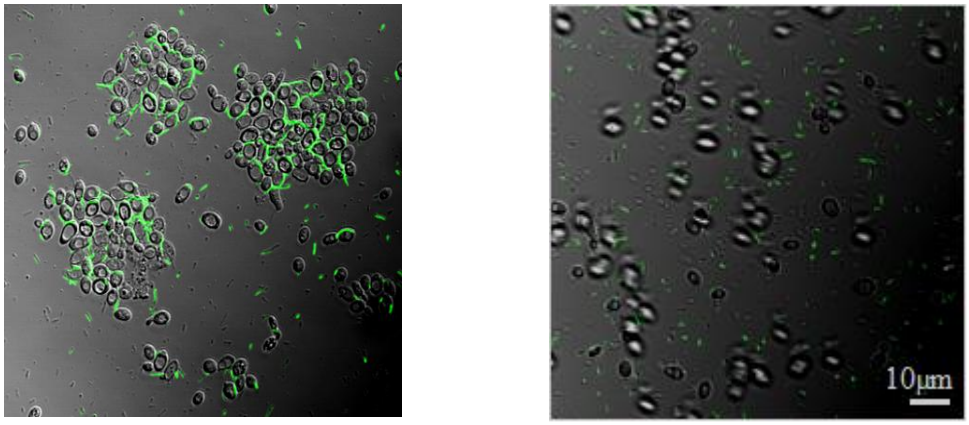

Figure 2: Yeast Agglutination Assay of *Escherichia coli* ORN178/pGREEN and *Escherichia coli* ORN208/pGREEN. Superimposed images obtained using a phase contrast/fluorescence microscope demonstrated (A) yeast agglutination mediated by *E. coli* ORN178/pGREEN and (B) the absence of yeast cell agglutination with *E. coli* ORN208/pGREEN. The magnification was 100×.

4.1.2 Carbohydrate Immobilization Method

Utilizing the mannose binding ability of *E. coli* ORN178/pGREEN, five parts of the system were optimized including carbohydrate immobilization, bacteria hybridization time, bacteria hybridization temperature, bacteria growth phase, and bacteria viability.

For carbohydrate immobilization, the monomer α-D-mannose was first printed on a Whatman FAST slide. However, the hybridization of *E. coli* ORN178/pGREEN did not exhibit fluorescent signals under an epi-fluorescence microscope (data not shown). Then, α-D-mannose-PAA, a polyacrylamide (PAA)-conjugated polysaccharide displaying multivalent sugar moieties, was printed on a slide, which was then left overnight at room temperature (Fig. 3A). The fluorescent signals were similar to those seen after baking the slide at 80℃ for half an hour (Fig. 3B). These results suggested that while monosaccharides bound poorly on the slide, PAA-conjugated carbohydrates were well immobilized. In addition, the multivalent mannose groups in α-D-mannose-PAA were readily available to *E. coli* ORN178/pGREEN cells. Since the result from the baking method was similar to that from the other, the former was applied for subsequent experiments as it was less time-consuming than the latter.

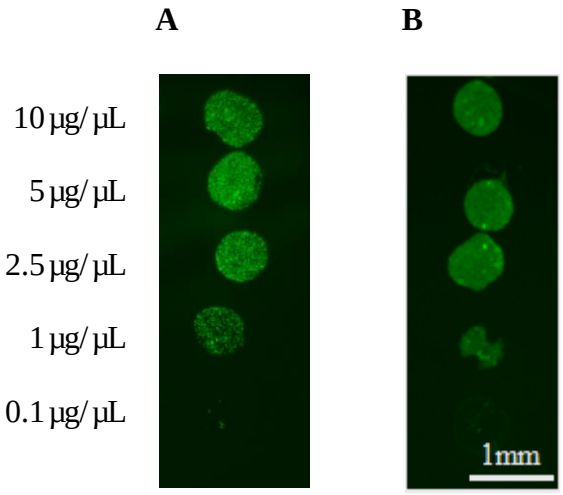

Figure 3: Comparison of Two Carbohydrate Immobilization Methods. Images obtained using an epi-fluorescence microscope demonstrated fluorescent signals emitted from *E. coli* ORN178/pGREEN bound to α-D-mannose-PAA immobilized on Whatman FAST slides after (A) baking the slides at 80 ℃ for 30 min and (B) leaving the slides at room temperature for overnight. The magnification was 25×. The carbohydrate concentration of each dot is shown on the left.

4.1.3 Bacteria Hybridization Time

After carbohydrate immobilization, 80µL *E. coli* ORN178/pGREEN suspensions were hybridized with α-D-mannose-PAA for three hours or overnight on Whatman FAST slides. As these slides indicated that although the signals generated after overnight hybridization (Fig. 4A) were stronger than those after three-hour hybridization (Fig. 4B), the latter were sufficient to demonstrate the binding activity. In addition, the bacterial suspension dried out in several of the overnight samples due to the length of time. In

contrast, there was little evaporation during three-hour hybridization since it took much less time. Because the three-hour hybridization was more effective than overnight, it was applied in subsequent experiments.

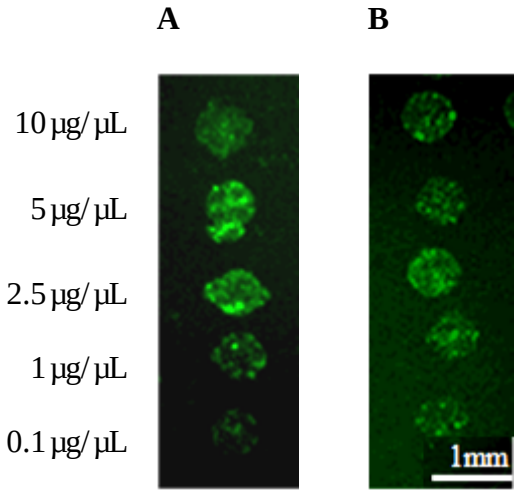

Figure 4: Comparison of Overnight and Three-Hour Bacteria Hybridizations. Images obtained using an epi-fluorescence microscope demonstrated fluorescent signals emitted from *E. coli* ORN178/pGREEN bound to α-D-mannose-PAA immobilized on Whatman FAST slides after (A) overnight hybridization and (B) three-hour hybridization. The magnification was 25×. The carbohydrate concentration of each dot is shown on the left.

4.1.4 Bacteria Hybridization Temperature

Three temperatures were investigated to determine their effect on the hybridization of *E. coli* ORN178/pGREEN with α-D-mannose-PAA: 37 ℃ (Fig. 5A), room temperature (Fig. 5B) and 4 ℃ (Fig. 5C). Intense fluorescent signals were observed from all three samples as seen in Fig. 5. This experiment suggested that temperature did

not affect the binding ability of *E. coli* ORN178/pGREEN to mannose. For convenience, all subsequent experiments were conducted at room temperature since no extra equipment was required.

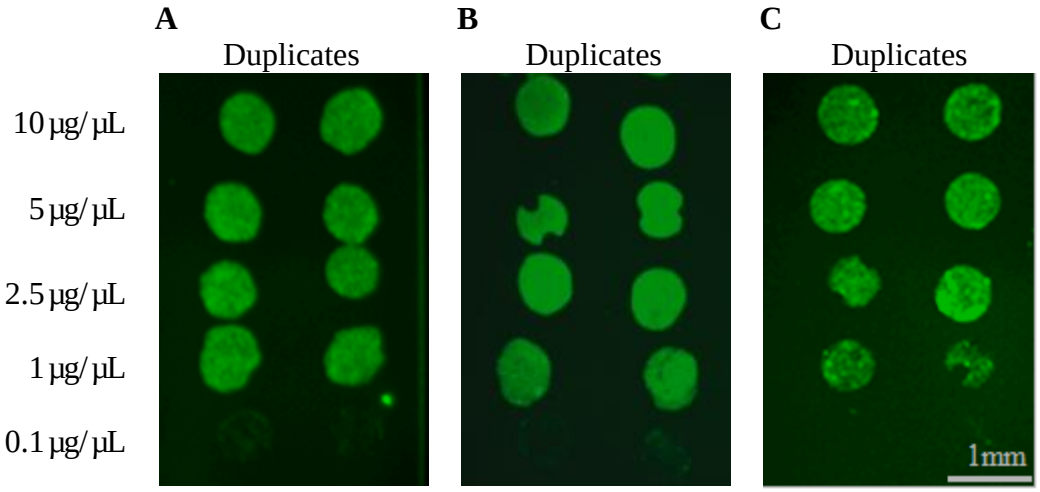

Figure 5: Comparison of Three Bacteria Hybridization Temperatures. Images obtained using an epi-fluorescent microscope demonstrated fluorescent signals emitted from *E. coli* ORN178/pGREEN bound to α-D-mannose-PAA immobilized on Whatman FAST slides after hybridization at (A) 37 ℃, (B) room temperature, or (C) 4 ℃. The magnification was 25×. The carbohydrate concentration of each dot is shown on the left.

4.1.5 Bacteria Growth Phase

The *E. coli* ORN178/pGREEN cells incubated for 12 hours generated a weak signal after their hybridization with α-D-mannose-PAA (Fig. 6A), while cells incubated for 24 hours emitted a strong fluorescent signal (Fig. 6B). Based on the growth curve in Fig. 7, the cells were in the exponential and stationary phases, respectively. After being

incubated for 48 hours, the cells maintained their binding ability (Fig. 6C). These results suggested that the strong affinity to mannose was developed in the stationary phase and maintained thereafter. In the subsequent experiments, bacterial cells were incubated approximately 24 hours before hybridization.

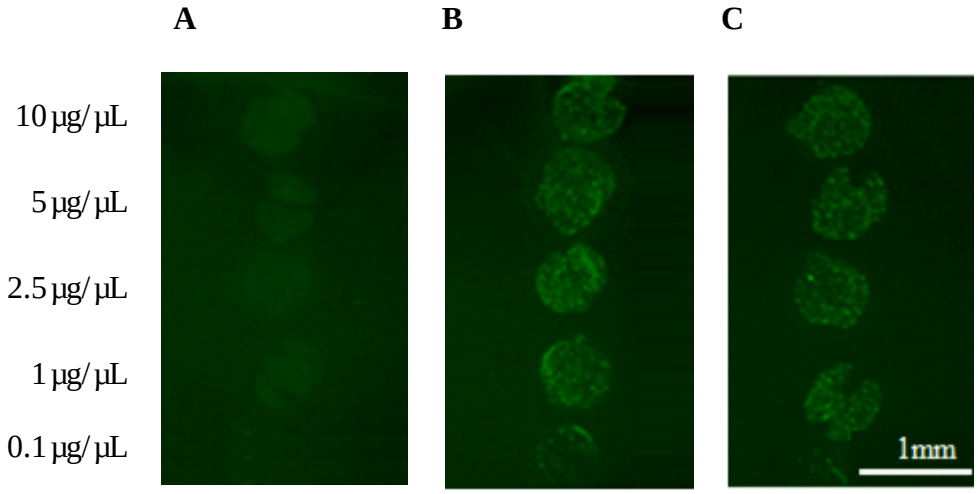

Figure 6: Comparison of Three Bacteria Growth Phases. Images obtained using an epi-fluorescence microscope demonstrated fluorescent signals emitted from *E. coli* ORN178/pGREEN bound to α-D-mannose-PAA immobilized on a Whatman FAST slide harvested at (A) 12 hours, (B) 24 hours, and (C) 48 hours. The magnification was 25×. The carbohydrate concentration of each dot is shown on the left.

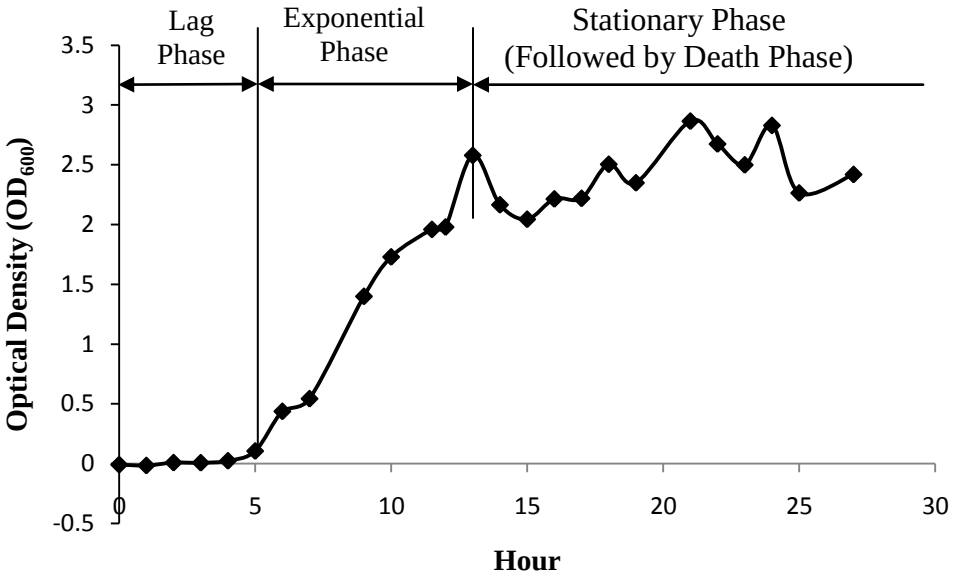

Figure 7: Growth Curve of *Escherichia coli* ORN178/pGREEN. The lag, exponential, and stationary phases are labeled in the graph.

4.1.6 Bacteria Viability

Formaldehyde treated *E. coli* ORN178/pGREEN cells did not form colonies on TSA plates after a 24-hour incubation, indicating the bacterial cells were killed by the reagent. These dead cells mediated yeast cells agglutination (Fig. 8A) and bound to α-D-mannose-PAA on a Whatman FAST slide (Fig. 8B). These results indicated that the non-viable cells killed by formaldehyde maintained their mannose binding ability.

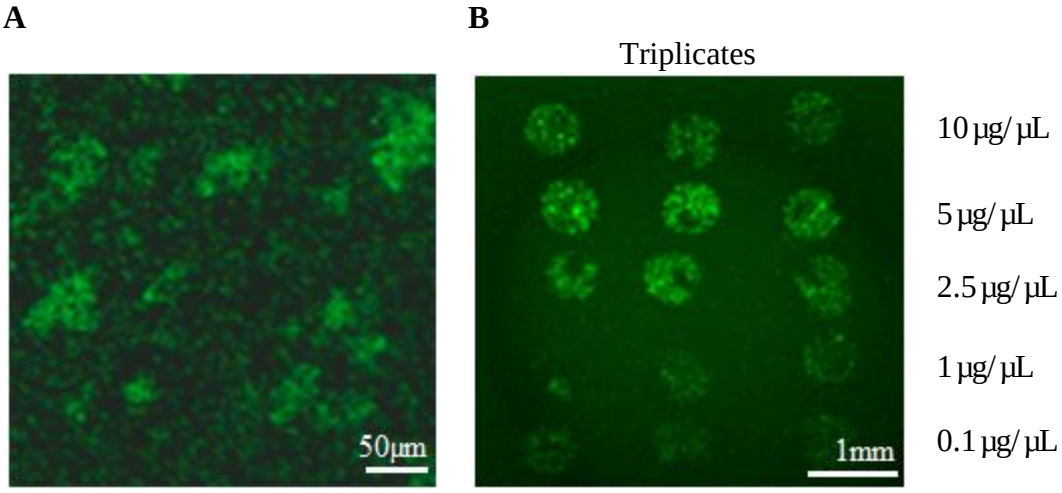

Figure 8: Yeast Agglutination and Carbohydrate Microarray Using Non-Viable Bacterial Cells. Images obtained using an epi-fluorescence microscope demonstrated (A) yeast agglutination mediated by *E. coli* ORN178/pGREEN cells killed by formaldehyde magnified at 100×, and (B) fluorescent signals emitted from these cells bound to α-D-mannose-PAA immobilized on a Whatman FAST slide magnified at 25×. The carbohydrate concentration of each dot is shown on the right.

4.1.7 Specificity Test

After the development and optimization of the carbohydrate microarray system, **three strains** of *E. coli* were hybridized with mannose immobilized on a Whatman FAST slide to determine the binding and the detection specificities. The **first** strain studied was *E. coli* ORN178/pGREEN, its fluorescence decreasing as the α-D-mannose-PAA concentration decreased (Fig. 9A), and its binding ability being completely inhibited by pre-exposure to 10μg/μL free α-D-mannose (Fig. 9B). The **second** and **third** strains

investigated were *E. coli* ORN208/pGREEN with abnormal type-1 fimbriae and *E. coli* O157:H7/pWM1007 (OD_{600}=1) without type-1 fimbriae [117]. The results found that neither bound to α-D-mannose-PAA as shown in Fig. 9C and Fig. 9D, respectively. This specificity test indicated that the binding is α-D-mannose and type-1 fimbriae specific. And there was no non-specific binding to the background. It also demonstrated that the carbohydrate microarray system was able to differentiate among related *E. coli* strains and specifically detect type-1 fimbriae.

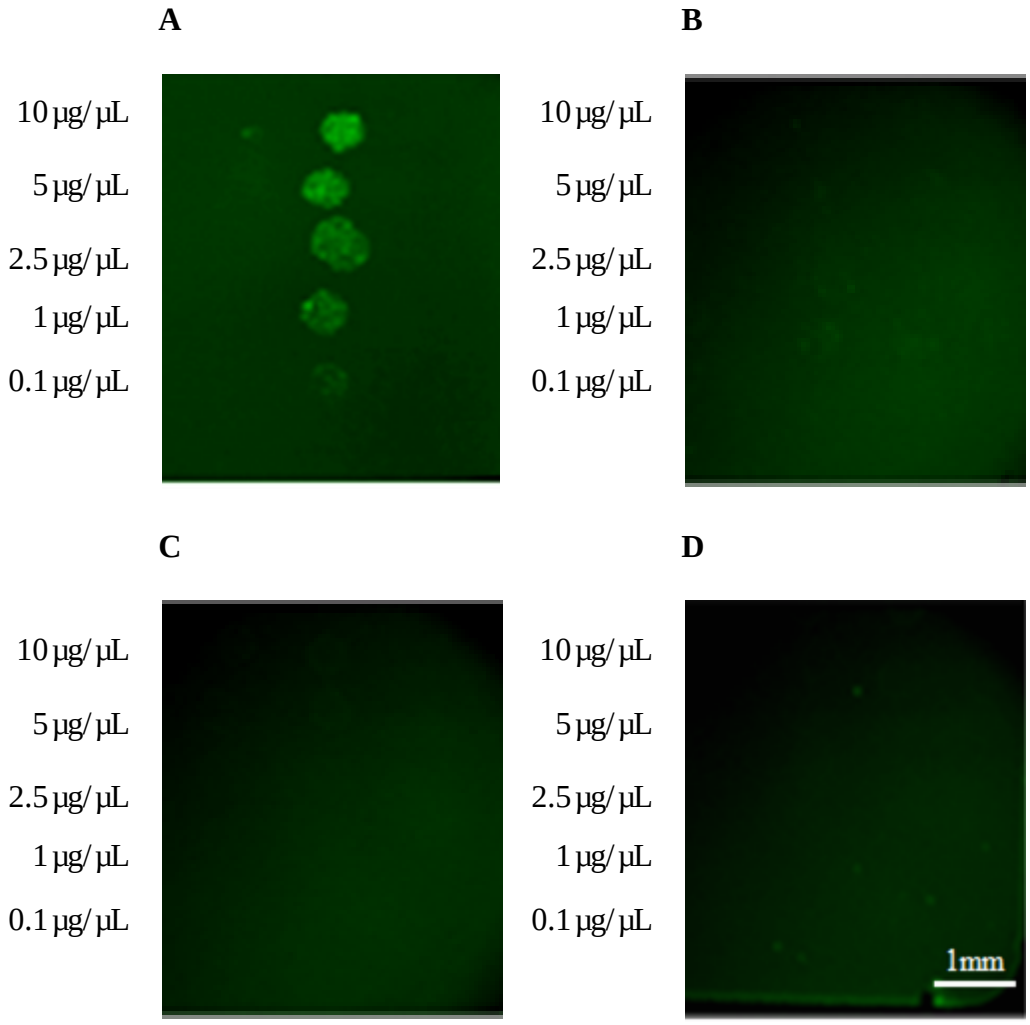

Figure 9: Specificity Test of the Carbohydrate Microarray. Images obtained using an epi-fluorescence microscope demonstrated fluorescent signals emitted from *E. coli* strains bound to α-D-mannose-PAA immobilized on a Whatman FAST slide. The mobile binding agents used in each section were: (A) *E. coli* ORN178/pGREEN, (B) *E. coli* ORN178/pGREEN pre-exposed to 10µg/µL free mannose, (C) *E. coli* ORN208/pGREEN, and (D) *E. coli* O157:H7/pWM1007. The magnification was 25×. The carbohydrate concentration of each dot is shown on the left.

4.1.8 Sensitivity Test

The sensitivity of the carbohydrate microarray system was determined in detecting the lowest number of *E. coli* ORN178/pGREEN cells suspended in phosphate buffere saline (PBS) and in Tryptic Soy Broth (TSB) with 50 µg/mL ampicillin. The number of bacterial cells was estimated using the relationship between optical density and population concentration. A graph demonstrating this relationship was plotted with the population concentration (cfu/mL) as the y axis and the OD_{600} as the x axis using *E. coli* ORN178 (Fig. 10). A straight line described as the equation below was generated through linear regression:

$$y=1.21\times10^{9}x \qquad (1)$$

The coefficient of determination (R^2) was equal to 0.9888, which was close to 1, indicating that the regression line reliably represented the relationship of the two.

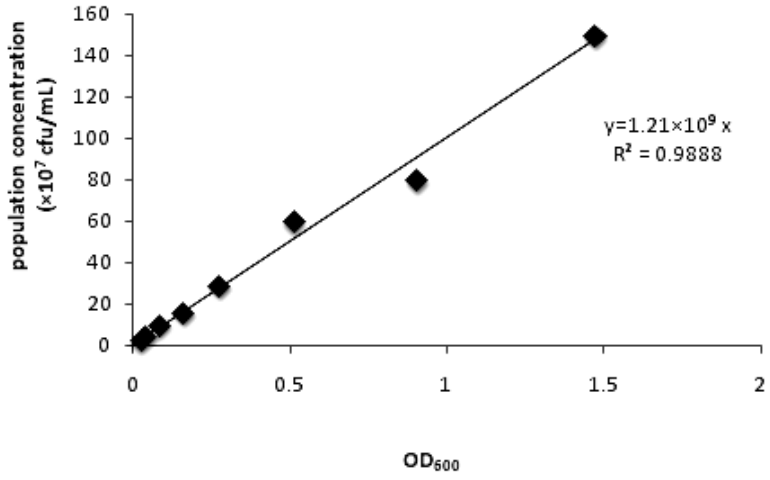

Figure 10: The Relationship between Population Concentration and OD_{600} Reading of *Escherichia coli* ORN178. The equation of the regressed line is $y=1.21\times10^{9}x$, with the coefficient of determination (R^2) equal to 0.9888.

After bacterial hybridization, fluorescence emitted from bacterial cells decreased as the number of bacterial cells on the nitrocellulose membranes decreased. Strong fluorescent signals were observed after the hybridization of 10^8 PBS-buffered cells (Fig. 11A), while the signals were weaker when the cell number was 10^7 (Fig. 11B). The signals decreased even more when the cell number decreased to 10^6 (Fig. 11C) and 10^5 (Fig. 11D). After the hybridization with 10^4 bacterial cells, the signal approached the background, thus defining the detection limit (Fig. 11E). Fluorescent signals were not visually detectable when the cell number was 10^3 (Fig. 11F).

When the cells were suspended in TSB, similar results were observed after the hybridization with 10^8 cells (Fig. 12A), 10^7 cells (Fig. 12B), and 10^6 cells (Fig. 12C) on each membrane, while the signal intensity was weaker than that emitted from PBS buffered cells. Signals generated after the hybridization with 10^5 cells (Fig. 12D) approached the background, while there were no signals observed when the cell number decreased to 10^4 (Fig. 12E). As a negative control, 10^8 *E. coli* ORN208/pGREEN cells suspended in TSB did not bind to α-D-mannose-PAA as shown in Fig. 12F.

These results indicate that the detection limit for *E. coli* ORN178/pGREEN in PBS was 10^4-10^5 cells/membrane. For the cells suspended in TSB, the detection limit was 10-fold higher at 10^5-10^6 cells/membrane.

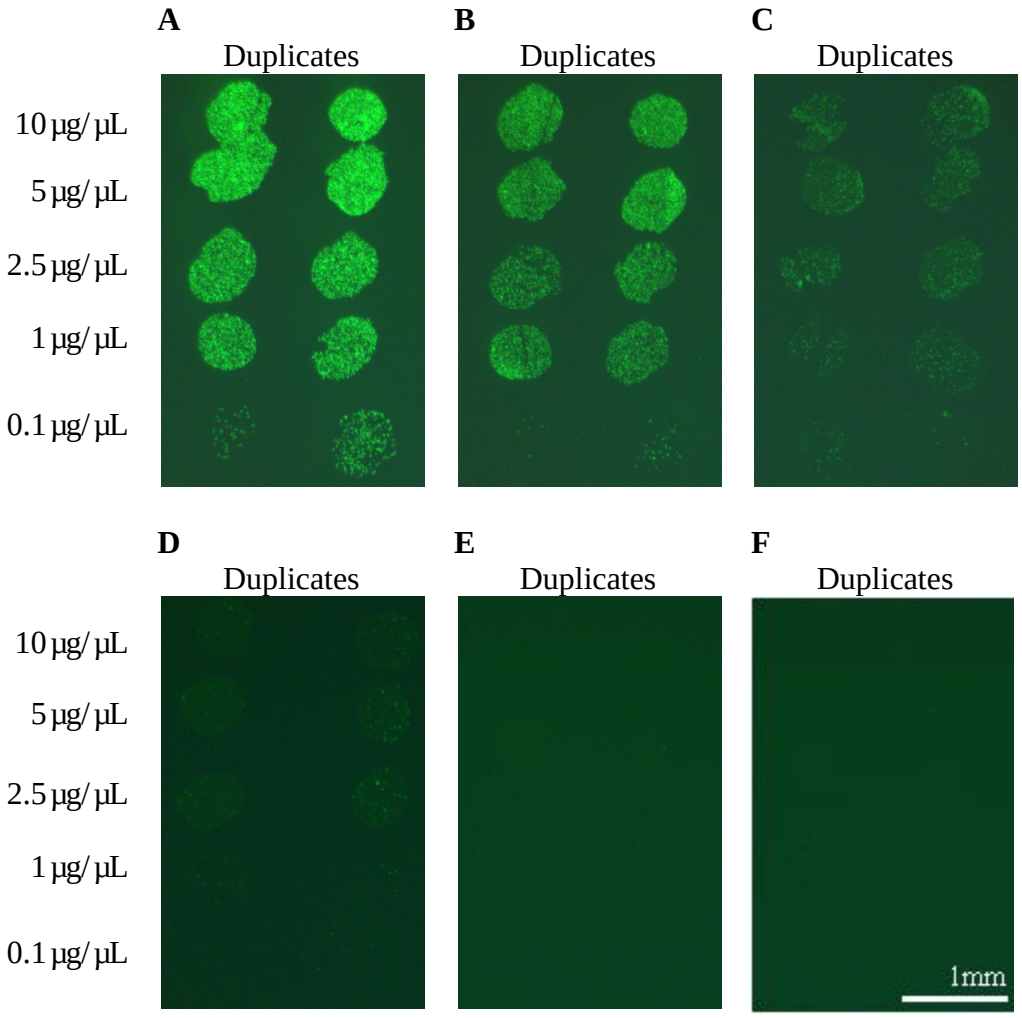

Figure 11: Sensitivity Test of the Carbohydrate Microarray in Detecting *Escherichia coli* ORN178/pGREEN Cells Suspended in Phosphate Buffer Saline. Images obtained using an epi-fluorescence microscope demonstrated fluorescent signals emitted from (A) 10^8 cells, (B) 10^7 cells, (C) 10^6 cells, (D) 10^5 cells, (E) 10^4 cells, and (F) 10^3 cells bound to α-D-mannose-PAA on a Whatman FAST slide. The magnification was 25×. The carbohydrate concentration of each dot is shown on the left.

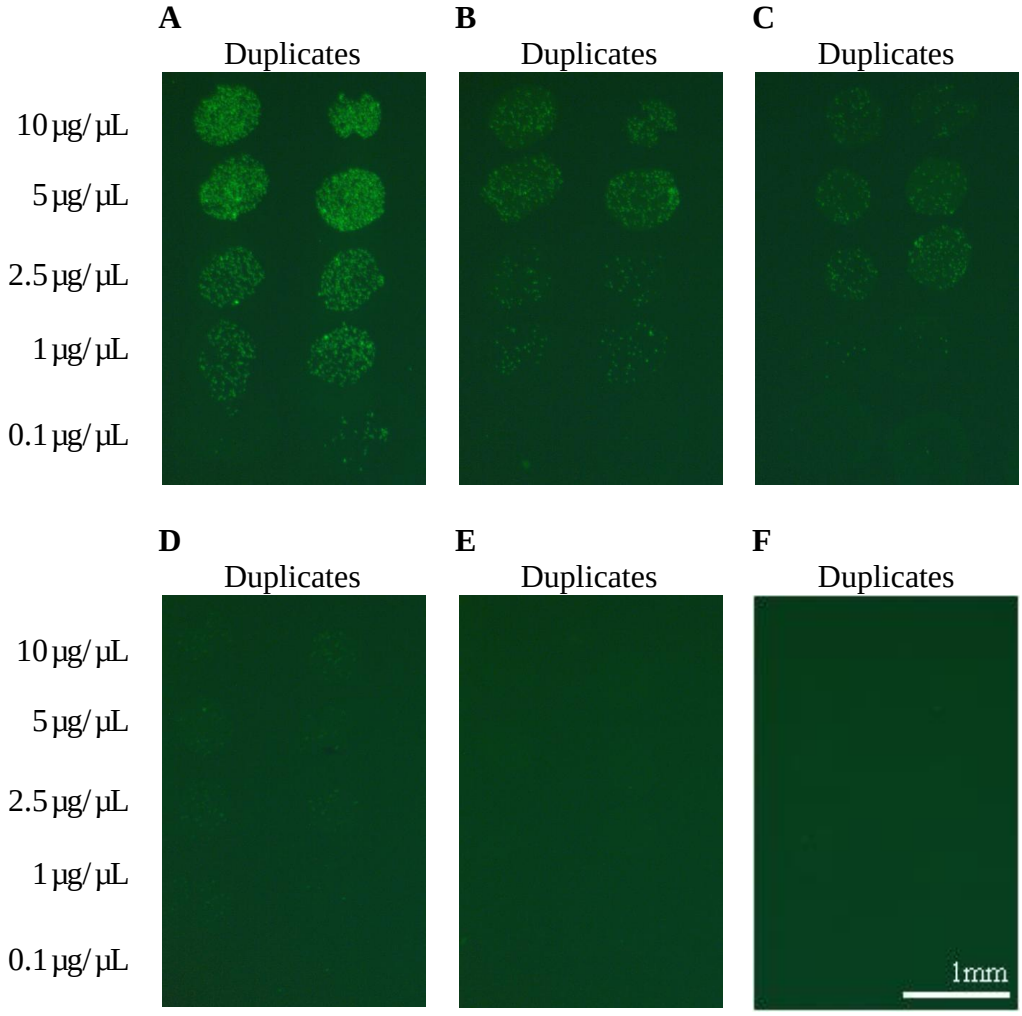

Figure 12: Sensitivity Test of the Carbohydrate Microarray in Detecting *Escherichia coli* ORN178/pGREEN Cells Suspended in Tryptic Soy Broth. Images obtained using an epi-fluorescence microscope demonstrated fluorescent signals emitted from (A) 10^8 cells, (B) 10^7 cells, (C) 10^6 cells, (D) 10^5 cells, and (E) 10^4 cells bound to α-D-mannose-PAA on a Whatman FAST slide. (F) *E. coli* ORN208/pGREEN (10^8 cells) suspended in TSB did not bind, serving as a negative control. The magnification was 25×. The carbohydrate concentration of each dot is shown on the left.

4.1.9 Visualization Method

To design, optimize and evaluate the carbohydrate microarray system, *E. coli* ORN178/pGREEN expressing intracellular fluorescent proteins was used. Utilizing this system, the binding of non-fluorescent *E. coli* ORN178 and *E. coli* ORN208 was subsequently investigated. Visualization protocols utilizing fluorescent protein dyes, a fluorescent nucleic acid dye, a fluorescent carbohydrate, and a biotinylated carbohydrate were developed to demonstrate these bacterial binding activities.

4.1.9.1 Fluorescent Protein Dyes

Two fluorescent protein dyes, fluorescein isothiocyanate (FITC) and Alexa Fluor 488 C_5 maleimide, a FITC substitute with enhanced characteristics, were studied for their visualization feasibility here by staining *E. coli* ORN178 and *E. coli* ORN208 either before or after their hybridization with α-D-mannose-PAA on Whatman FAST slides.

After being suspended in FITC (25μg/mL) for one hour, the fluorescence of individual cells of *E. coli* ORN178 (Fig. 13A) and *E. coli* ORN208 (Fig. 13D) were observed on a regular glass slide under an epi-fluorescence microscope. *E. coli* ORN178 stained with FITC both before (Fig. 13B) and after hybridization (Fig. 13C) resulted in intense fluorescence on a Whatman FAST side. However, *E. coli* ORN208 stained either before (Fig. 13E) or after hybridization (Fig. 13F) did not result in fluorescence with printed α-D-mannose-PAA. These experiments indicate that FITC can be used to stain *E. coli* ORN178 and *E. coli* ORN208 and to visualize the binding of *E. coli* ORN178 to α-D-mannose-PAA on Whatman FAST slides.

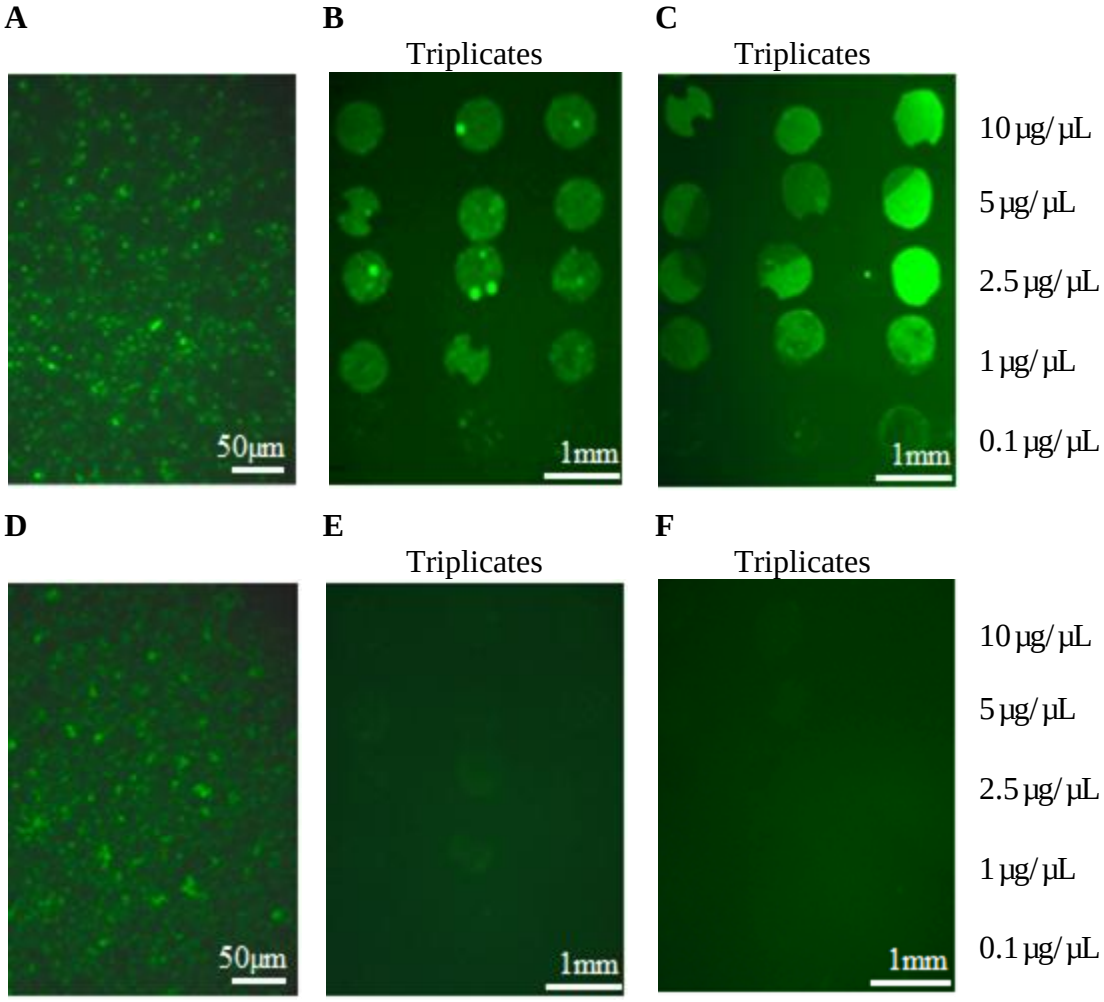

Figure 13: FITC Visualization for Individual Cells of *Escherichia coli* ORN178 and *Escherichia coli* ORN208 and for Carbohydrate Microarrays. Images obtained using an epi-fluorescence microscope demonstrated individual cells of FITC (25µg/mL) stained (A) *E. coli* ORN178 and (D) *E. coli* ORN208 magnified at 100×, and the fluorescent signals emitted from *E. coli* ORN178 stained by FITC (B) before and (C) after hybridization to α-D-mannose-PAA on a Whatman FAST slide magnified at 25×. *E. coli* ORN208 did not emit signals on microarray either stained (E) before or (F) after hybridization. The carbohydrate concentration of each dot is on the right.

After being stained with Alexa Fluor 488 C_5 maleimide both before (Fig. 14A) and after hybridization (Fig. 14B), *E. coli* ORN178 emitted strong fluorescent signals, while *E. coli* ORN208 did not bind to α-D-mannose-PAA as expected (Fig. 14C). These results suggest that Alexa Fluor 488 C_5 maleimide can also be used to visualize the binding of *E. coli* ORN178 to α-D-mannose-PAA on Whatman FAST slides.

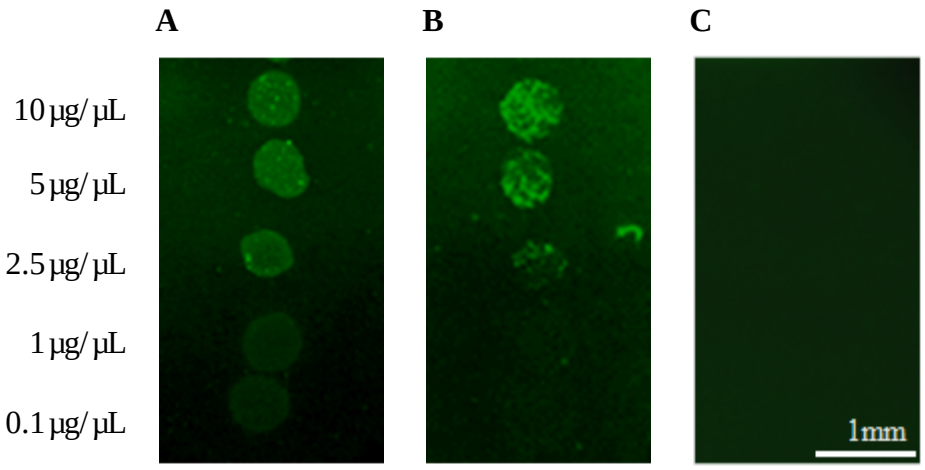

Figure 14: Alexa Fluor 488 C_5 Maleimide Visualization of *Escherichia coli* ORN178 and *Escherichia coli* ORN208. Images obtained using an epi-fluorescent microscope demonstrated fluorescence signals emitted from *E. coli* ORN178 stained by Alexa Fluor (A) before or (B) after hybridization, and (C) *E. coli* ORN208 stained by Alexa Fluor before hybridization to α-D-mannose-PAA on a Whatman FAST slide magnified at 25×. The carbohydrate concentration of each dot is shown on the left.

4.1.9.2 Fluorescent Nucleic Acid Dye

The nucleic acid dye SYTO 9 (0.83µM) was used to stain *E. coli* ORN178 before hybridization, resulting in the fluorescence of individual cells as seen in Fig. 15A (top).

However, as this figure indicates, a bright green background was generated after hybridization with α-D-mannose-PAA on a Whatman FAST slide (Fig. 15A bottom), probably due to the high concentration of SYTO 9. The fluorescence of individual cells could not be observed against this bright background. To address this problem, the concentration was decreased to 0.42μM (Fig. 15B), 0.21μM (Fig. 15C), 0.10μM (Fig. 15D), 50nM (Fig. 15E), and 25nM (Fig. 15F). Even though cells were fluorescent before hybridization when the dye concentration was above 0.21μM, the background remained green after hybridization even when the dye concentration was as low as 25nM (Fig. 15F). Staining with SYTO 9 after hybridization also generated a green background (data not shown). These experiments indicate that SYTO 9 dye is not appropriate as a visualizing dye for the carbohydrate microarray system.

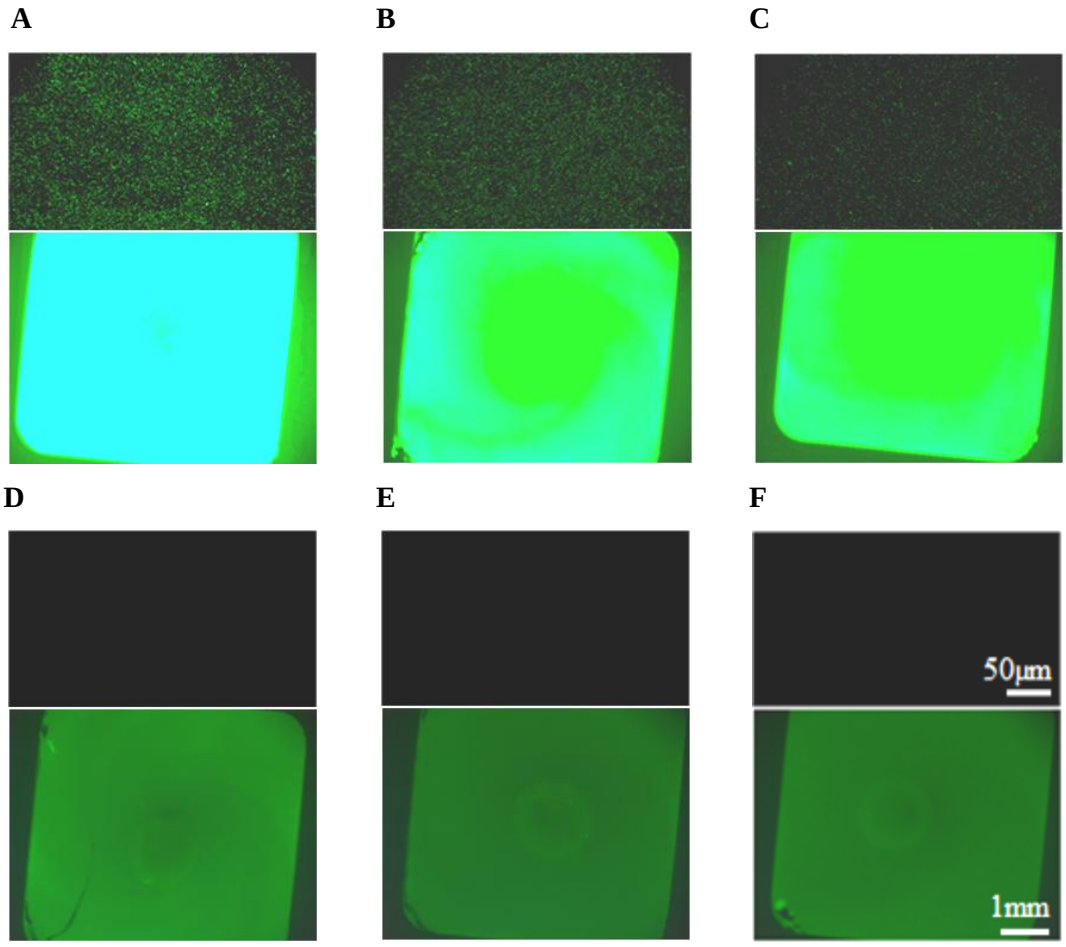

Figure 15: SYTO 9 Visualization for Individual Cells of *Escherichia coli* ORN178 and for Carbohydrate Microarrays. Wet mount pictures of SYTO 9 dye stained *E. coli* ORN178 cells (top) magnified at 100× and the corresponding hybridization results with α-D-mannose-PAA on Whatman FAST slides (bottom) magnified at 25× as observed under an epi-fluorescence microscope. The concentrations of SYTO 9 dye were (A) 0.83µM, (B) 0.42µM, (C) 0.21µM, (D) 0.10µM, (E) 50nM, and (F) 25nM.

4.1.9.3 Fluorescent Carbohydrate

PAA-conjugated mannose linked with a fluorescent group, specifically α-D-mannose-PAA-fluor, was investigated for its appropriateness as a visualizing agent added as an array solution. *E. coli* ORN178 and *E. coli* ORN208 cells were directly printed on a Whatman FAST slide, their auto-fluorescence shown in Fig. 16A and Fig. 16B, respectively. The mobile agent α-D-mannose-PAA-fluor increased the fluorescence intensity of *E. coli* ORN178 (Fig. 16C) and *E. coli* ORN208 (Fig. 16D); however, there was almost no difference in the signals between the two strains. These experiments suggest that fluorescent carbohydrates cannot be used to visualize binding activities.

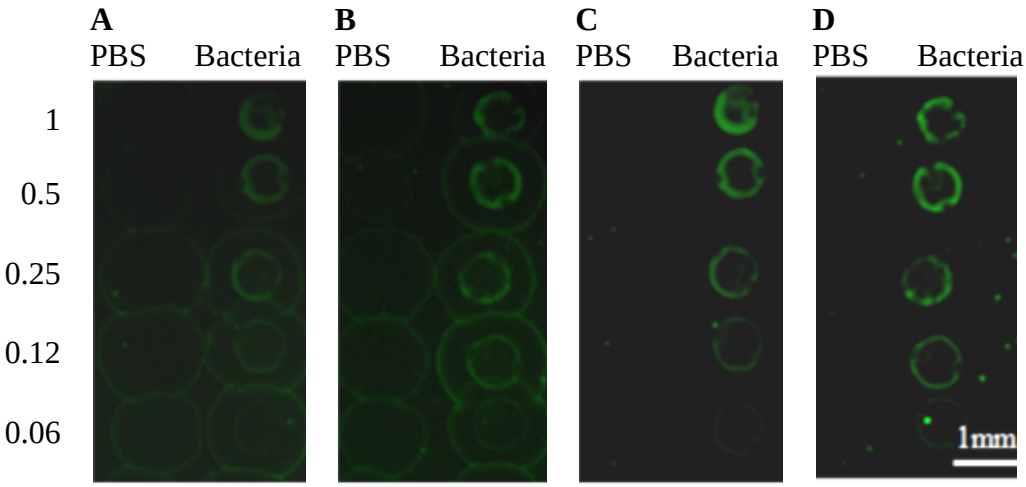

Figure 16: Fluorescent Carbohydrate for Visualizing Carbohydrate Microarrays. Images obtained using an epi-fluorescence microscope demonstrated the auto-fluorescence of directly printed (A) *E. coli* ORN178 and (B) *E. coli* ORN208, as well as the fluorescence from α-D-mannose-PAA-fluor bound to printed (C) *E. coli* ORN178 and (D) *E. coli* ORN208 on a Whatman FAST slide magnified at 25×. The OD_{600} of printed bacteria dots are shown on the left.

4.1.9.4 Biotinylated Carbohydrate

PAA-conjugated mannose linked with a biotin group, specifically α-D-mannose-PAA-biotin, was investigated for its feasibility as a visualizing agent with the addition of color-forming substrates. The images obtained by scanning a Whatman FAST slide using a printer/scanner indicated that after hybridization with *E. coli* ORN178 at a high concentration (OD_{600}=100) (Fig. 17A), the color generated by the biotin substrates was weaker than that after the *E. coli* ORN208 hybridization (Fig. 17B). The color intensity observed on the membrane hybridized with *E. coli* ORN208 was similar to that on the membrane hybridized with PBS (Fig. 17C). These results suggested that *E. coli* ORN178 at a high concentration bound to carbohydrate dots partially blocked the biotin substrate color formation, while *E. coli* ORN208 and PBS did not block it. However, a biotinylated carbohydrate is an inappropriate visualization agent for this research because these phenomena were not consistent and the high bacterial concentration needed to block the color formation is impractical for field samples.

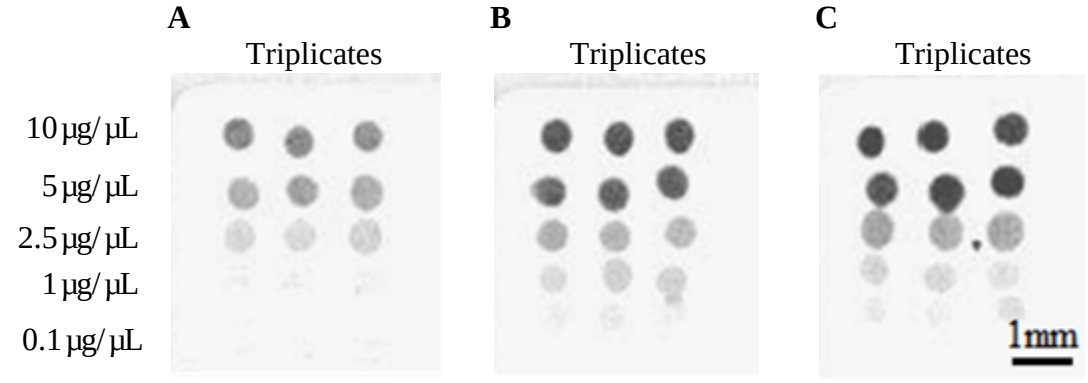

Figure 17: Biotinylated Carbohydrate as the Immobilized Agent for Visualizing Carbohydrate Microarrays. Images obtained from a scanner demonstrated that the substrate color formation was partially blocked by (A) the binding of *E. coli* ORN178 to α-D-mannose-PAA-biotin, but not by (B) *E. coli* ORN 208, or by (C) PBS. The carbohydrate concentration of each dot is shown on the left.

4.1.10 Other Carbohydrates and Bacteria

In addition to *E. coli* ORN178 and α-D-mannose-PAA, the binding activities of other bacterial strains to carbohydrates were studied using the carbohydrate microarray system. The non-fluorescent strains were first stained with FITC and then hybridized with a microarray constructed from the eight carbohydrates of α-D-mannose-PAA, α-D-galactose-PAA, β-D-galactose-PAA, α-L-fucose-PAA, β-GalNAc-PAA, α-Neu5Ac-PAA, GlcNAcGlcNAc-PAA, and GalGlcNAcGalGlc-PAA.

4.1.10.1 FITC Staining

Six wild type strains were stained with 25μg/mL FITC for one hour. Images obtained under an epi-fluorescence microscope demonstrated signals emitted from the individual cells of *E. coli* ORN178 (Fig. 18A), *E. coli* ORN208 (Fig. 18B), *E. coli* O157:H7 (Fig. 18C), *Klebsiella pneumoniae* (Fig. 18D), *Pseudomonas aeruginosa* (Fig. 18E), and *Salmonella typhimurium* (Fig. 18F). These results indicate that FITC is appropriate for staining various bacterial strains.

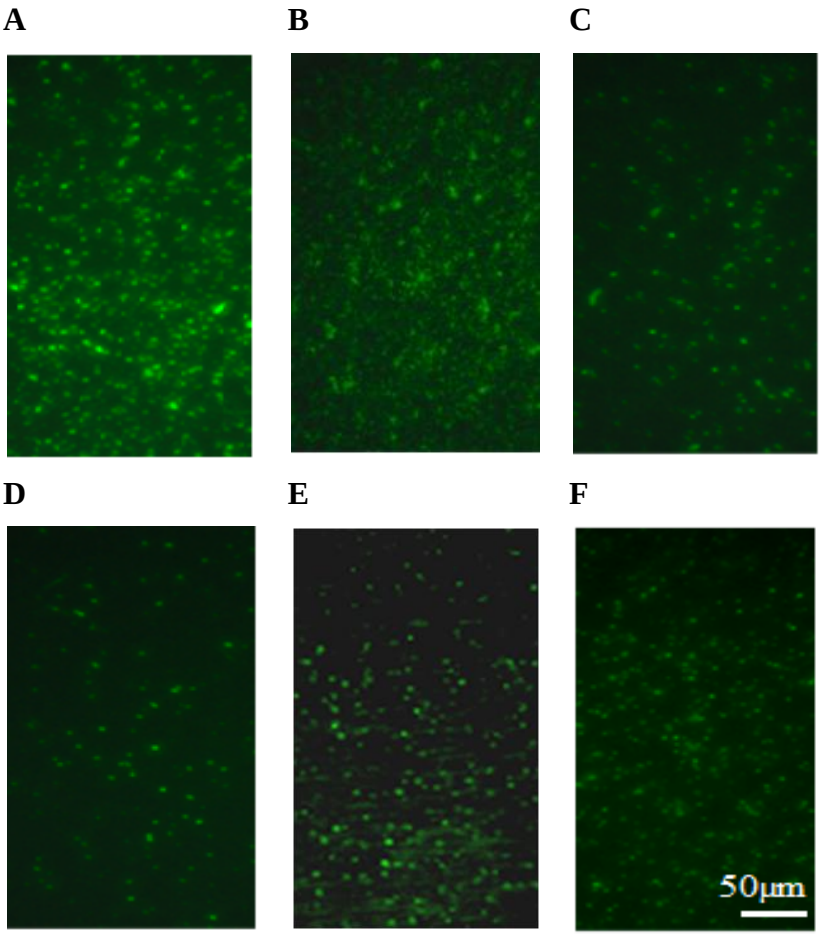

Figure 18: FITC Stained Wild Type Bacteria. Wet mount pictures obtained using an epi-fluorescence microscope demonstrated individual cells of FITC (25μg/mL) stained (A) *E. coli* ORN178, (B) *E. coli* ORN208, (C) *E. coli* O157:H7, (D) *Klebsiella pneumoniae*, (E) *Pseudomonas aeruginosa*, and (F) *Salmonella typhimurium*. The magnification was 100×.

4.1.10.2 Carbohydrate Microarray

These bacteria strains were then investigated using a carbohydrate microarray system constructed with the eight PAA conjugated carbohydrates, with PAA and PBS serving as negative controls and FITC serving as a marker to locate the positions of each carbohydrate dot. The images in Fig. 19 demonstrated fluorescent signals emitted from the FITC dots and from the bound bacterial cells as summarized in Table 2.

Strong signals were emitted from the FITC stained *E. coli* ORN178 cells at positions where α-D-mannose-PAA was printed, and weak signals were observed at the β-GalNAc-PAA and α-Neu5Ac-PAA dots (Fig. 19A). *E. coli* ORN208 weakly bound to α-D-mannose-PAA, β-GalNAc-PAA and α-Neu5Ac-PAA dots (Fig. 19B). Weak signals emitted from *E. coli* O157:H7 were also observed at α-D-galactose-PAA, α-L-fucose-PAA, β-GalNAc-PAA, and α-Neu5Ac-PAA dots (Fig. 19C). *K. pneumoniae* (Fig. 19D), *S. typhimurium* (Fig. 19E), and *P. aeruginosa* (Fig. 19F) all bound to α-D-mannose-PAA, β-GalNAc-PAA, and GlcNAcGlcNAc-PAA, exhibiting weak signals. In addition, *K. pneumonia* also bound to β-D-galactose-PAA and α-L-fucose-PAA. *S. typhimurium* exhibited weak affinity for β-D-galactose-PAA and *P. aeruginosa* for α-L-fucose-PAA. None of the bacteria bound to PAA or PBS as expected. Post-hybridization FITC stain was also investigated, yielding similar results (data not shown). These results suggest that *E. coli* ORN178 not only exhibits a strong affinity for α-D-mannose-PAA but also a weak affinity for other carbohydrates such as α-Neu5Ac-PAA. Under the same conditions, other bacteria also weakly bound to some of the carbohydrates printed.

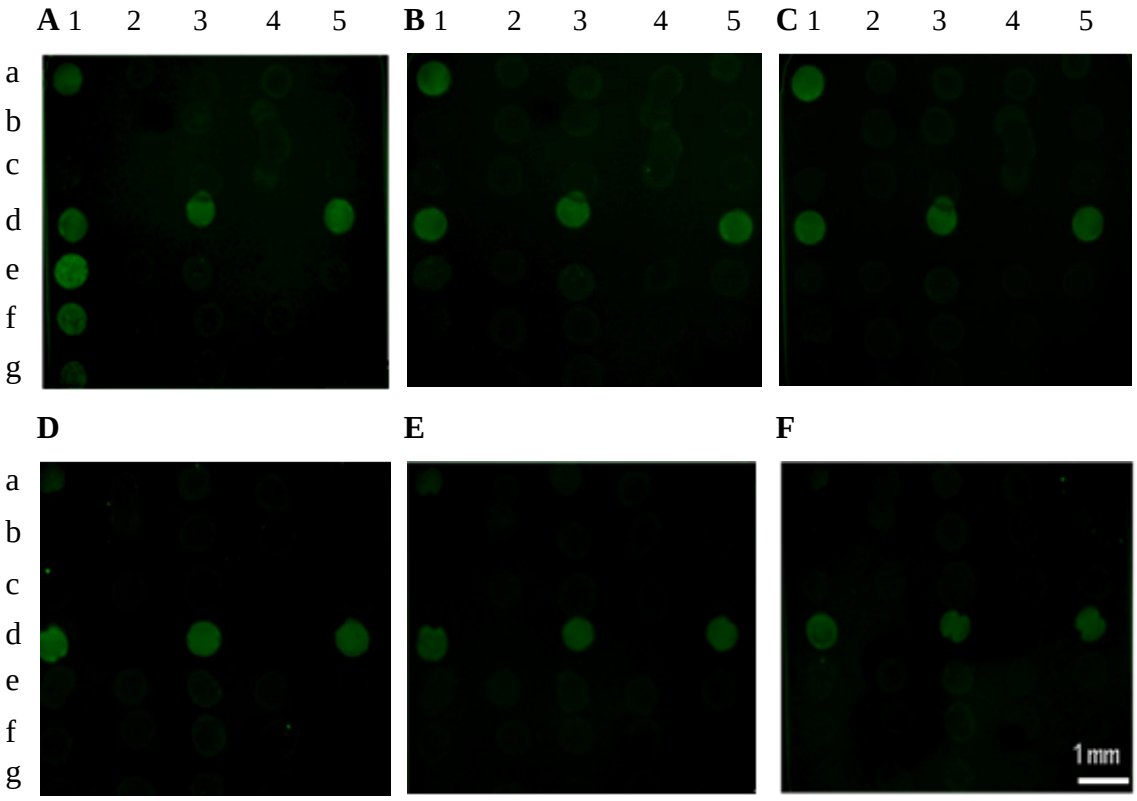

Figure 19: Carbohydrate Microarrays Constructed with Eight Carbohydrates for the Evaluation of their Binding by Six Bacteria. Images obtained using an epi-fluorescence microscope demonstrated the binding profiles of FITC stained (A) *E. coli* ORN178, (B) *E. coli* ORN208, (C) *E. coli* O157:H7, (D) *Klebsiella pneumoniae*, (E) *Salmonella typhimurium*, and (F) *Pseudomonas aeruginosa* magnified at 25X.

a1, **d1**, **d3**, and **d5**: FITC as markers to locate each solution spotted; **b1** and **c1**: buffer solutions; **e1**, **f1**, and **g1**: 2.5μg/μL, 1μg/μL, and 0.5μg/μL α-D-mannose-PAA; **a2**, **b2**, and **c2**: 2.5μg/μL, 1μg/μL, and 0.5μg/μL α-D-galactose-PAA; **e2**, **f2**, and **g2**: 2.5μg/μL, 1μg/μL, and 0.5μg/μL β-D-galactose-PAA; **a3**, **b3**, and **c3**: 2.5μg/μL, 1μg/μL, and 0.5μg/μL α-L-fucose-PAA; **e3**, **f3**, and **g3**: 2.5μg/μL, 1μg/μL, and 0.5μg/μL β-GalNAc-PAA; **a4**, **b4**, and **c4**: 2.5μg/μL, 1μg/μL, and 0.5μg/μL α-Neu5Ac-PAA; **e4**, **f4**, and **g4**: 2.5μg/μL, 1μg/μL, and 0.5μg/μL GlcNAcGlcNAc-PAA; **a5**, **b5**, and **c5**: 2.5μg/μL, 1μg/μL, and 0.5μg/μL GalGlcNAcGalGlc-PAA; **e5**, **f5**, and **g5**: 2.5μg/μL, 1μg/μL, and 0.5μg/μL PAA.

Table 2: The Affinity of Six Bacterial Strains to Eight Carbohydrates.

Sugars	*E. coli* ORN178	*E. coli* ORN208	*E. coli* O157:H7	*Klebsiella pneumoniae*	*Salmonella typhimurium*	*Pseudomonas aeruginosa*
α-D-mannose-PAA[a]	+++[b]	+/-	-	+/-	-/+	+/-
α-D-galactose-PAA	-	-	-/+	-	-	-
β-D-galactose-PAA	-	-	-	+/-	-/+	-
α-L-fucose-PAA	-	-	+/-	-/+	-	-/+
β-GalNAc-PAA	+	+	+/-	+	+	+
α-Neu5Ac-PAA	+	+	+/-	-	-	-
GlcNAcGlcNAc-PAA	-	-	-	-/+	-/+	-/+
GalGlcNAcGalGlc-PAA	-	-	-	-	-	-
PAA	-	-	-	-	-	-
PBS[c]	-	-	-	-	-	-

[a]PAA: polyacrylamide
[b]-, -/+, +/-, +, +++: denote the intensity of fluorescent signals from weak to strong
[c]PBS: phosphate buffered saline

4.1.10.3 *Pseudomonas aeruginosa* and α-L-Fucose

The binding activity of fluorescent *P. aeruginosa* PAO1/pMRP9-1 to α-L-fucose-PAA was further studied using new media and hybridization buffers, times and temperatures, with the purpose to facilitate the expression of PA-II lectins. The images obtained using an epi-fluorescence microscope showed that high concentrated cells (OD_{600}=100) incubated for one day in Grelet's modified medium bound to α-L-fucose emitted fluorescent signals (Fig. 20A), although they were not as intense as those emitted from *E. coli* ORN178 cells bound to α-D-mannose (Fig. 19A). But the cells incubated for two days (Fig. 20B) or three days (Fig. 20C) did not bind. Cells cultivated in nutrient broth did not bind after being incubated for one day (Fig. 20D), two days (Fig. 20E), or three days (Fig. 20F). The mutant *P. aeruginosa* PAO1*lecB*::Tc^r didn't bind to the carbohydrate consistently (Fig. 20H) although fluorescent individual cells were observed after FITC stain (Fig. 20G). However, the repetition of the one-day incubation in Grelet's modified medium did not consistently result in fluorescent signals. These findings suggest that *P. aeruginosa* PAO1/pMRP9-1 is able to bind to α-L-fucose, but the conditions for this binding to take place are many, all of which are critical and must be satisfied.

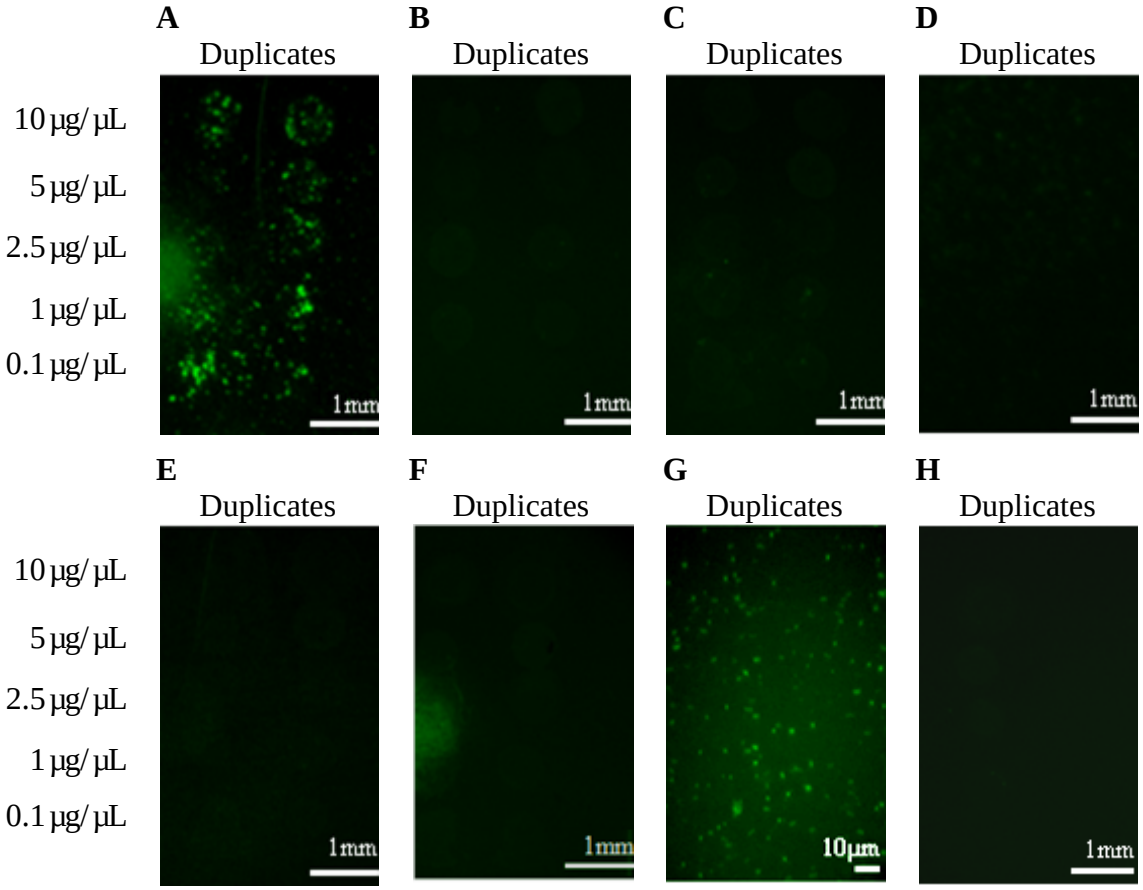

Figure 20: The Binding of *Pseudomonas aeruginosa* PAO1 and *Pseudomonas aeruginosa* PAO1*lecB*::Tc^r to α-L-fucose-PAA on a Whatman FAST slide. The wild type cells were incubated for (A) one day, (B) two days, or (C) three days in GE broth, and incubated for (D) one day, (E) two days, or (F) three days in nutrient broth. The cells of the mutant *P. aeruginosa* PAO1*lecB*::Tc^r were (G) stained with FITC (25 µg/mL) and then (H) hybridized with α-L-fucose-PAA on a Whatman FAST slide. The images were magnified at 25×, except (G), which was magnified at 100×. The carbohydrate concentration of each dot is shown on the left.

4.2 Microcantilever-Based Biosensor

The optimized conditions for the binding of *E. coli* ORN178 to α-D-mannose obtained from the carbohydrate microarrays were applied to a microcantilever-based biosensor. First, carbohydrate immobilization methods were investigated using gold-coated slides and then gold-coated microcantilevers. Finally, the resonance frequencies of these uncoated, carbohydrate functionalized, and bacteria bound gold-coated microcantilevers were measured using a Polytec Micro System Analyzer 400 (MSA-400) [118].

4.2.1 Gold-Coated Slide Functionalization with Carbohydrates

Gold-coated slide surfaces were functionalized for the printing of the monomer mannose, α-D-mannose-PAA-fluor, α-D-mannose-PAA and mannan, which is a polymer of α-D-mannose. No fluorescence was observed after the hybridization of *E. coli* ORN178/pGREEN with mannose or after printing α-D-mannose-PAA-fluor on Whatman FAST slides, although the binding of *E. coli* ORN178/pGREEN to this fluorescent carbohydrate was seen (data not shown). The binding of *E. coli* ORN178/pGREEN to α-D-mannose-PAA is shown in Fig. 21A, while the mutant *E. coli* ORN208/pGREEN did not bind (Fig. 21B). One carbohydrate dot seen in Fig. 21A was enlarged, showing individual cells densely grouped together covering its surface (Fig. 21C). Then, mannan was printed on a functionalized gold-coated slide. The images obtained using an epi-fluorescence microscope showed the binding of *E. coli* ORN178/pGREEN to mannan (Fig. 22A), while the mutant *E. coli* ORN208/pGREEN did not bind (Fig. 22B). These

results suggest that mannose is not applicable on gold surfaces detecting *E. coli* ORN178 and the fluorescence of printed α-D-mannose-PAA-fluor cannot be observed on gold surfaces, while α-D-mannose-PAA and mannan were immobilized and able to serve as receptors for *E. coli* ORN178/pGREEN on the gold-coated slide.

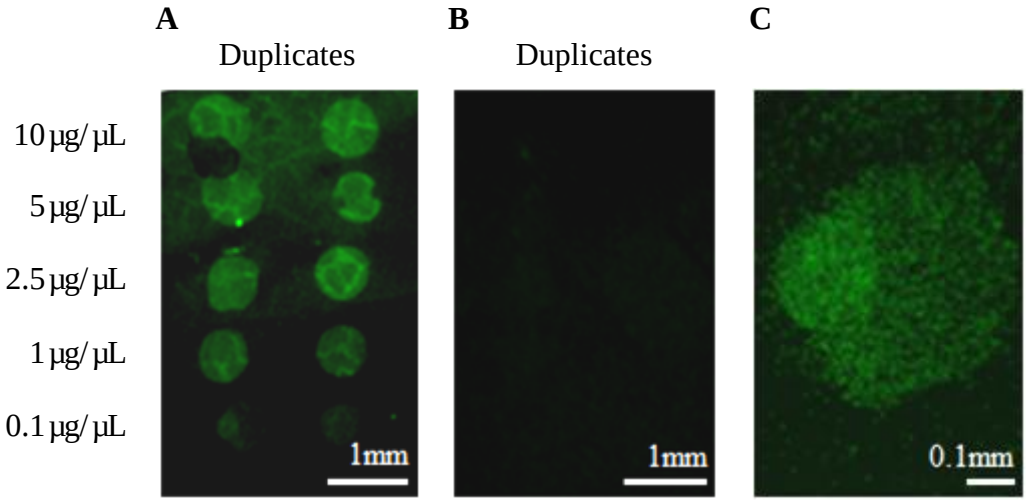

Figure 21: The Binding of *Escherichia coli* ORN178/pGREEN and *Escherichia coli* ORN208/pGREEN to α-D-mannose-PAA Functionalized Gold-Coated Slide. Images obtained using an epi-fluorescence microscope demonstrating the binding of (A) *E. coli* ORN178/pGREEN and (B) *E. coli* ORN208/pGREEN to α-D-mannose-PAA printed on a gold slide magnified at 25×. The carbohydrate concentration of each dot is shown on the left. (C) A single carbohydrate dot in A was magnified at 100× to show individual cells binding densely to the printed mannose.

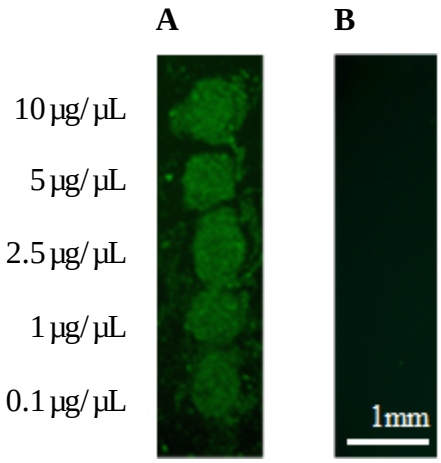

Figure 22: The Binding of *Escherichia coli* ORN178/pGREEN and *Escherichia coli* ORN208/pGREEN to Mannan Functionalized Gold-Coated Slide. Images obtained using an epi-fluorescence microscope demonstrating the binding of (A) *E. coli* ORN178/pGREEN, and (B) *E. coli* ORN208/pGREEN to mannan immobilized on a gold slide. The magnification was 25×. The carbohydrate concentration of each dot is shown on the left.

4.2.2 Microcantilever Functionalization with Carbohydrates

The functionalization method using α-D-mannose-PAA was then applied to microcantilevers coated in gold on one side. A microcantilever has a relatively large base with a tiny beam anchored at one end. The images observed using an epi-fluorescence microscope demonstrated that *E. coli* ORN178/pGREEN (OD_{600}=1) bound to the gold surface of the microcantilever (Fig. 23A), while *E. coli* ORN208/pGREEN (OD_{600}=1) did not (Fig. 23B). The binding of individual *E. coli* ORN178/pGREEN cells to the microcantilever in Fig. 23A could be seen in the enlarged image (Fig. 23C). Based on the

graph in Fig. 10, the population density of the bacterial suspension was approximately 10^9cells/mL, much higher than that seen in field samples. Then, the bacterial suspension concentration was decreased to 10^6cfu/mL (OD_{600}=0.001), the resulting image showing approximately 50 cells bound on the beam (Fig. 23D). However, the coating was not uniform for either bacterial suspension concentration. More cells were on the free end of the microcantilever beam than on the other in Fig. 23C, but more cells were near the microcantilever base in Fig. 23D, indicating the distribution was random rather than uniform. Mannan was also immobilized and hybridized with *E. coli* ORN178/pGREEN (OD_{600}=1 and OD_{600}=0.001), yielding similar results (data not shown). These experiments suggested that *E. coli* ORN178/pGREEN can be detected through gold-coated microcantilevers fabricated with mannose using the protocols for carbohydrate functionalization on gold surfaces and bacteria hybridization on Whatman FAST slides.

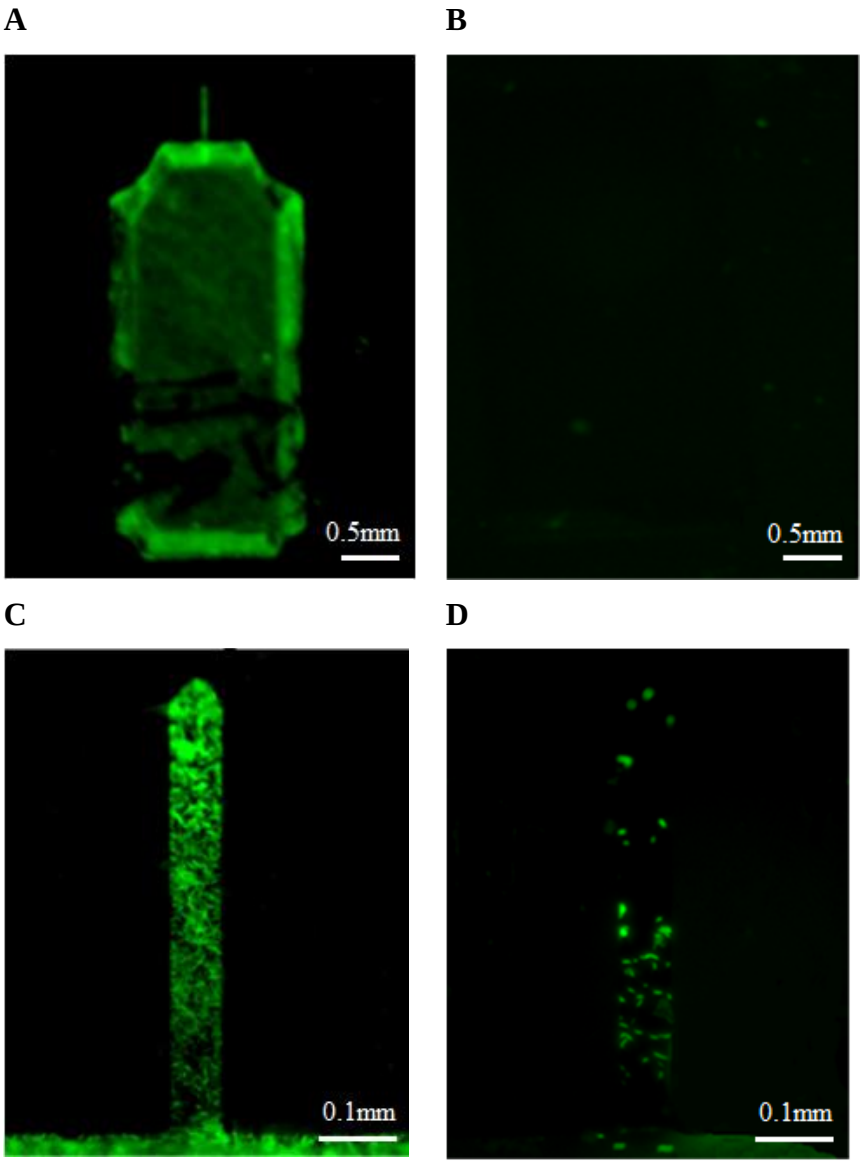

Figure 23: The Binding of *Escherichia coli* ORN178/pGREEN and *Escherichia coli* ORN208/pGREEN to α-D-mannose-PAA on Gold-Coated Microcantilevers. Images obtained using an epi-fluorescence microscope demonstrated the binding of (A) *E. coli* ORN178/pGREEN and (B) *E. coli* ORN208/pGREEN (OD=1) to α-D-mannose-PAA coated gold microcantilevers magnified at 25X, and cantilever beams with *E. coli* ORN178/pGREEN with OD_{600} of (C) 1 and (D) 0.001 (magnification: 100×).

4.2.3 Microcantilever Resonance Frequency Measurements

Observations using a fluorescent microscope require fluorescence-emitting molecules in bacterial cells, but not all strains are intrinsically fluorescent. In addition, fluorescent labeling is laborious and time-consuming. MSA-400 measures the resonance frequency of uncoated, α-D-mannose-PAA functionalized- and *E. coli* ORN178/pGREEN or *E. coli* ORN208/pGREEN bound-microcantilevers without requiring a label. Six microcantilevers were measured for their resonance frequencies before and after carbohydrate functionalization as shown in Fig. 24. For each microcantilever, there was always an increase in frequency after the process. The mean resonance frequency of the microcantilevers after α-D-mannose-PAA functionalization (11.66 ± 0.93 kHz) was 5% higher than that of the uncoated microcantilevers (11.07 ± 0.85 kHz) (paired one-tailed t-test, $p<0.05$, $n=6$), indicating the uniformity of the carbohydrate coating on the microcantilever beams.

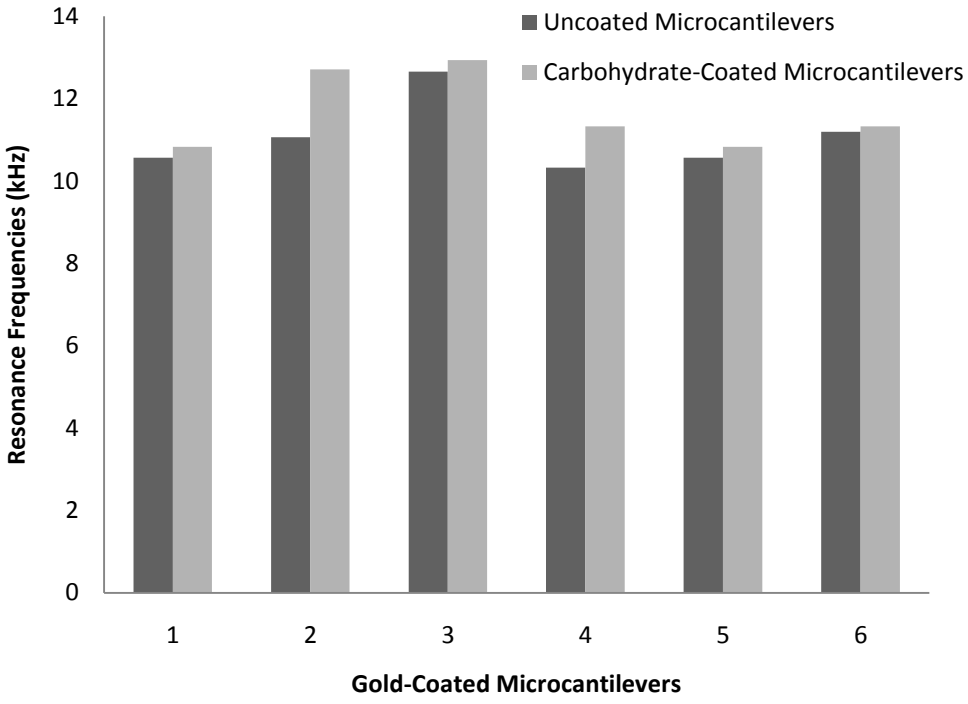

Figure 24: Resonance Frequency Shifts of Gold-Coated Microcantilevers after Carbohydrate Functionalization. Dark and light grey columns represent the resonance frequency values (kHz) of six uncoated microcantilevers and of the same microcantilevers after carbohydrate functionalization, respectively.

Then, six microcantilevers were measured for their resonance frequencies before and after bacteria hybridization as shown in Fig. 25. For microcantilevers hybridized with *E. coli* ORN178/pGREEN (OD=1), the mean resonance frequency shifted from 12.16 ± 1.16 kHz before hybridization to 13.94 ± 5.18 kHz after hybridization. The p-value was 0.30, which was greater than 0.05 (n=3). After the exposure to *E. coli* ORN208/pGREEN (OD=1), the mean resonance frequency shifted from 10.93 ± 1.65 kHz before

hybridization to 10.38 ± 1.77 kHz after hybridization, with a p-value equal to 0.40, which was greater than 0.05 (n=3) (Table 3). These results indicated that *E. coli* ORN208/pGREEN did not bind to microcantilevers as expected, and this phenomenon can also be observed in Fig. 23B. However, although the binding was shown in Fig. 23A, C and D, no evidence based on the statistical analysis concluded that *E. coli* ORN178/pGREEN bound to microcantilevers, a result not expected.

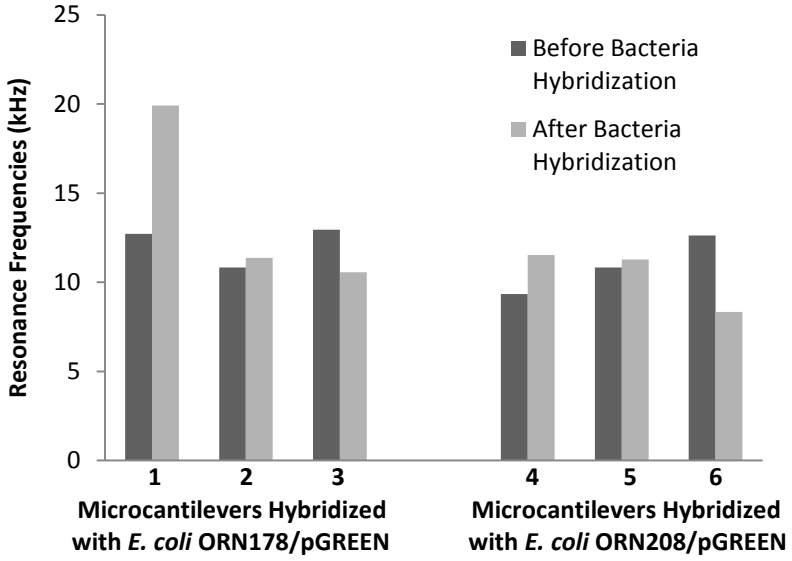

Figure 25: Resonance Frequency Shifts of Gold-Coated Microcantilevers after Bacteria Hybridization. Dark and light grey columns represent the resonance frequency values (kHz) of six carbohydrate functionalized microcantilevers and of the same microcantilevers after bacteria hybridization, respectively. Microcantilevers number 1, 2, and 3 were hybridized with *E. coli* ORN178/pGREEN, while the other three were hybridized with *E. coli* ORN208/pGREEN.

Table 3: Resonance Frequencies (kHz) of Microcantilevers Before and After Bacteria Hybridization.

	M[a] + Man[b] (kHz)	M +Man + Bact[c] (kHz)	Change[d] (kHz)	P-value
E. coli ORN178/pGREEN:				
M1	12.94	10.56	-2.38	
M2	10.83	11.37	0.54	
M3	12.71	19.90	7.19	0.30
Mean	12.16	13.94	1.78	
Standard Deviation	1.16	5.18	4.90	
E. coli ORN208/pGREEN:				
M4	12.63	8.34	-4.29	
M5	10.83	11.27	0.44	
M6	9.33	11.52	2.20	0.40
Mean	10.93	10.38	-0.55	
Standard Deviation	1.65	1.77	3.35	

M[a]: microcantilever
Man[b]: α-D-mannose-PAA
Bact[c]: bacteria, either *E. coli* ORN178/pGREEN or *E. coli* ORN208/pGREEN
Change[d] = (M+Man+bact) – (M+Man)

CHAPTER 5

DISCUSSION

Most of the results reported in Chapter 4 were expected, specifically the design, optimization, evaluation and application of the carbohydrate microarray system, and the functionalization of gold-coated slides and microcantilevers. However, the resonance frequency measurements require further discussion to relate them to previous research.

5.1 Polyacrylamide-Conjugated Carbohydrates

In this research, the use of α-D-mannose-PAA was advantageous over mannose. First, the former with a large molecular weight of 30kD was immobilized on nitrocellulose membranes while the latter with a small molecular weight of 180g/mol was not. This phenomenon was consistent with the findings by Wang *et al.* that large molecules such as dextrans ranging from 20kD to 2,000kD immobilized better than small molecules on nitrocellulose membranes [55]. Second, α-D-mannose-PAA has 20%mol mannose, a multivalent sugar that increases the binding affinity of *E. coli* compared to monosaccharides since bacterial cells have 100 to 400 mannose-binding fimbriae on their cell surfaces [30]. Third, α-D-mannose-PAA has a polyacrylamide backbone which plays an important role by helping it to be absorbed into the nitrocellulose matrix and by serving as a spacer between the membrane and the carbohydrate for better bacterial cell access [62].

The carbohydrate dots immobilized on Whatman FAST slides did not have a uniform size nor a regular shape as seen in Figures 3, 4, 5 and 9 in Chapter 3, a result partially due to the slit at the pin head and the speed at which the pins were lifted up from the sample solution [119]. According to Whatman, GmhB, the more quickly the pins are lifted, the larger the hanging drops on the pin tips are [119]. As a result, this company suggests lifting the pins at a moderate speed from the center of the container and pressing them quickly and firmly on nitrocellulose membranes using a crisp, rapid motion for consistent dot shape [119].

After carbohydrate printing, storing the printed slides overnight at room temperature increased the stability of immobilized proteins, consistent with the protocol of Whatman, GmhB, the manufacturer of Whatman FAST slides [120]. Similar results were obtained by baking slides at 80 ℃; this process also used by Wilkison *et al.* to immobilize nucleic acids on nylon membranes [121].

5.2 Bacteria Hybridization: Time, Temperature, and Cell Viability

The hybridization results of *E. coli* ORN178/pGREEN with immobilized α-D-mannose-PAA on Whatman FAST slides were not affected by hybridization time, temperature, or cell viability. For hybridization time, a three-hour hybridization time was sufficient for this strain to reach binding equilibrium although a shorter hybridization time of one hour was used by Disney and Seeberger [76]. To test cell viability, non-viable cells were generated by mixing with formaldehyde. This result was consistent with those reported by James-Holmquest *et al.* that 3% (vol/vol) formaldehyde killed

gonococci after a 30-minute exposure [122] and those demonstrated by Loshon *et al.* that the incubation of *Bucillus subtilis* spores with 25mg/mL formaldehyde at 30℃ killed approximately 99% of the spores within 40 min [123]. These non-viable cells maintained their binding abilities since formaldehyde is able to preserve protein secondary structure as well as most tertiary structure [124]. However, this result was not supported by the findings of McSweegan and Walker that the adhesion of formaldehyde-treated *Campylobacter jejuni* to epithelial cells was significantly decreased [125]. A possible reason explaining this decrease is that formaldehyde changes cell structure by irreversibly cross-linking primary amino groups in proteins through a $-CH_2-$ linkage [126] or introducing artifacts into cells. For example, mesosome, once considered a bacterial organelle, is actually an artifact caused by cytoplasmic membrane alteration induced by chemical fixatives [127,128]. Given these inconsistent results, the effect of formaldehyde fixation on maintaining the binding abilities of bacterial strains needs to be further studied.

5.3 Bacterial Growth Phase and Expression of Lectins (Adhesins)

The hybridization results were affected by bacterial growth phase. *E. coli* ORN178/pGREEN cells harvested from exponential phase exhibited weaker binding ability than those from stationary phase in this research. Muller *et al.* reported that during fast growth, 3', 5'-cyclic adenosine monophosphate (cAMP) receptor proteins (CPRs) sensing bacterial metabolism repressed the type-1 fimbriae expression, while no repression was found during slow growth [129]. Then, bacterial cells can express type-1

fimbriae to adapt to harsh conditions by forming biofilm or adhering to host cells. A western blot specifically detecting type-1 fimbriae using antibodies could be done to verify the presence of these fimbriae in different growth phases.

5.4 Specificity Test

The mannose-specificity of *E. coli* ORN178/pGREEN was demonstrated in this research by the observation that this strain did not bind to α-D-mannose-PAA after being exposed to 10 μg/μL free α-D-mannose (Fig. 9B). Disney and Seeberger also designed a carbohydrate microarray system on glass slides investigating the inhibitory effects of *p*-nitrophenyl-α-D-mannospyranoside (*p*-NPMan) and a mannose-functionalized polymer on the *E. coli* ORN178-mannose recognition [76]. They found that the chemical derivatives had stronger inhibitory abilities than mannose, with the polymer being the strongest, followed by *p*-NPMan [76]. These chemical derivatives can be used to substitute α-D-mannose as bacterial receptors to increase adherence affinity.

The type-1 fimbriae specificity of mannose was demonstrated by the different binding patterns of mutated *E. coli* ORN208 on Whatman FAST slides as shown in Fig. 9C. These results suggest that the carbohydrate microarray system is able to distinguish mutants from wild-type bacteria based on their affinity to carbohydrates. Since lower affinity for carbohydrate receptors often means lower pathogenicity when the adhesins play a role in host cell adherence, these mutants selected using the microarrays are sources for pathogenesis research and immunization development. In addition, this specificity was demonstrated by the different binding characteristics of *E. coli*

ORN178/pGREEN and *E. coli* O157:H7/pWM1007. While the former bound to α-D-mannose (Fig. 9A), the latter did not (Fig. 9D).

5.5 Sensitivity Test

The detection limit of the carbohydrate microarray system used here for *E. coli* ORN178/pGREEN of 10^4–10^5 cells/membrane was by one order lower than the 10^5-10^6 cells/slide of the system designed by Disney and Seeberger, although they used a fluorescence scanner to quantitatively measure the signal intensity while an epi-fluorescent microscope was used here for qualitative observation [76]. Therefore, the sensitivity of the microarray system designed in this research is acceptable, although it is less sensitive compared to the 10^3–10^4 cells/mL of pre-enriched bacterial suspension of polymerase chain reactions, reported by Malorny *et al.* as a theoretical value [130], and the 10^3–10^4 cells/mL of the ELISA assay developed by Morgan *et al.* detecting *E. coli* cells in lake water [131]. The detection sensitivity increased 10 fold after TSB grown *E. coli* ORN178/pGREEN cells have been washed and suspended in PBS before being used in the sensitivity tests. This may be due to the fact that the adherence of bacterial cells to the immobilized carbohydrate may be affected by other components present in the TSB supernatant.

5.6 Fluorescent Dyes as Visualizing Agents

Intracellular fluorophores such as GFPs in *E. coli* ORN178/pGREEN cells emitted strong fluorescence in the carbohydrate microarrays evaluated in this research as

they are less likely to stereochemically interfere with adhesin-carbohydrate interactions and are less prone to photo-bleaching. However, the observation that these fluorescent cells did not densely cover the carbohydrate dots as seen in Fig. 4 revealed a disadvantage of these intracellular fluorophores: the pGREEN plasmids may be cured during bacteria cultivation, hence, decreasing the fluorescent intensity. Fluorescent dyes were used in this study to address this issue.

The choice of the fluorescent dye is affected by the analyte, the array matrix, and the observation device. In this study, FITC as a protein dye stained bacterial cells on nitrocellulose membrane and its fluorescence was observed with a filter for GFP. Michel and Ravoo also used FITC to label lectins, which are bacterial surface proteins; their binding to carbohydrates on modified glass and silicon wafers was visualized [132]. The staining results of six bacterial strains were shown in Fig. 18 with different signal intensity. Since FITC bound to lysine residues, this phenomenon may be due to the different amount of this amino acid in different bacterial strains [112]. The nucleic acid dye of SYTO 9, however, was not a good choice under this experimental setting. It leaked from the stained cells and bound non-specifically to nitrocellulose membranes according to the manufacturer Invitrogen (Eugene, OR) [133]. A similar dye, SYTO 85, however, was successfully used by Park *et al.* to visualized *E. coli* ORN178 since functionalized glass slides were used instead of nitrocellulose membranes [134].

In this research, both the pre-hybridization and post-hybridization staining resulted in strong fluorescence emitted from bound *E. coli* ORN178 cells on Whatman FAST slides. Although the former has the disadvantage that the pre-incubation of dyes

and cells may alter the structure of the adhesin binding sites [135], it is more economically feasible than the latter since it uses less dye.

A limitation of FITC was revealed by the finding that the fluorescence generated from an area seen in Fig. 13C was darker than the rest, affecting the appearance of several dots, possibly due to the photo-bleaching of this dye. Alexa Fluor 488 exhibiting less photolability than FITC is an effective remedy although it is more expensive. Another method for addressing this issue is to reduce the excitation intensity and at the same time maximize the detecting sensitivity utilizing high numerical aperture objectives, low light detecting devices and/or emission filters with the widest bandpass allowed [72].

5.7 Fluorescent Carbohydrates as Visualizing Agents

The fluorescent carbohydrates hybridized with printed *E. coli* ORN178 and *E. coli* ORN208 cells emitted fluorescence similar in intensity, probably due to the weak affinity exhibited by *E. coli* ORN208 to mannose when the density of mannose was above 5% [136]. Although the affinity of *E. coli* ORN208 for mannose is only 3% of that of *E. coli* ORN178 [136], it is possible that the fluorescence emitted from the small amount of α-D-mannose-PAA-fluor bound to printed *E. coli* ORN208 was similar in intensity to that emitted from the carbohydrate bound to printed *E. coli* ORN178. The *E. coli* dots printed directly on Whatman FAST slides had a donut shape with more intense signals on the outside of the dots than the inside as seen in Fig. 16, a result not observed for the printed carbohydrate dots. According to Walther *et al.*, this phenomenon results because the directly printed bacterial cells flow to the edge of the dot during evaporation

on the nitrocellulose membranes, while carbohydrates result in uniform dots when they are dry [120]. Evaporation control may address this problem though complete elimination is difficult. However, this donut phenomenon usually does not interfere with quantitative analyses because the signal intensity at the edge effectively reflects the amount of bound analyte [120].

5.8 Other Carbohydrates and Bacteria

Past research has not reported the weak binding of *E. coli* ORN178 and *E. coli* O157:H7 to Neu5Ac found here, although this monosaccharide derivative was found to be a component in the carbohydrate receptors of *E. coli* K99, *Haemophilus influenzae*, *H. pylori*, *Neisseria gonorrhea*, *N. meningitidis*, *Streptococcus pneumoniae*, and *S. sanguis* [16]. *E. coli* O157:H7 was also found to bind to α-D-galactose-PAA and β-GalNAc-PAA with weak signals here, probably due to the periplasmic galactose-binding proteins [106]. The monomer of GalNAc has also been found in the carbohydrate receptors of *Actinomyces naeslundii*, *E. coli* S, *E. coli* F1C, and *Helicobacter pylori* [16].

The weak affinity of *Klebsiella pneumonia* to α-D-mannose-PAA found here was supported by Centeno *et al.*, who reported that mannose significantly decreased the attachment of heavily piliated *K. pneumonia* to epithelial cells [137]. This strain also showed weak binding ability to β-GalNAc-PAA, GlcNAcGlcNAc-PAA, β-D-galactose-PAA, and α-L-fucose-PAA in this research. These structures are found in fucosylasialo-GM1 (FucGalGalNAcGalGlcCer), asialo-GM1 (GalGalNAcGalGlcCer), and asialo-GM2 (GalNAcGalGlcCer), which function as carbohydrate receptors of this strain [138].

Salmonella typhimurium bound weakly to α-D-mannose-PAA, β-GalNAc-PAA, and D-galactose-PA, a result supported by the finding of Oyoto *et al*. that mannose and lactose when administered into the drinking water of broiler chickens significantly reduced the colonization of this bacteria [139]. Its binding to α-D-mannose-PAA is mediated by type-1 fimbriae subject to phase variation, a response similar to *E. coli* ORN178 [140].

Pseudomonas aeruginosa PAO1 did not bind to α-D-galactose-PAA and β-D-galactose-PAA, a phenomenon which differs from the finding by Gilboa-Garber that PA-I lectin on cell surfaces of this strain mediated the binding to these two carbohydrates [44]. It is possible that the PA-I lectin was not expressed by this strain or the lectin did not function properly in this experimental setting. However, this strain bound to α-L-fucose-PAA and α-D-mannose-PAA in this research, although the affinity was low, contrary to the unusually high affinity reported by Garber *et al*. [141]. This difference may be explained by two reasons. First, the environmental conditions were critical to the binding of *P. aeruginosa* to α-L-fucose in this study, a complexity addressed by many researchers through the purification of the lectins of PA I and PA II before hybridization [142,143,144,145,146]. Second, the cells used in this research were planktonic cells, with the majority of PA-II lectins located in their cytoplasm as demonstrated by Tielker *et al.*, while in sessile cells isolated from a biofilm the lectins were mainly presented on the outer membranes [43]. Therefore, the detection of *P. aeruginosa* using this carbohydrate microarray system is impractical since it is difficult to provide an incubation and

hybridization environment meeting the requirements for the binding to occur, and it is easy to obtain false negative results when the samples contain planktonic cells.

5.9 Gold-Coated Slide Functionalization with Carbohydrates

The lack of fluorescence emitted from α-D-mannose-PAA-fluor or from *E. coli* ORN178/pGREEN hybridized to mannose monomers printed on functionalized gold-coated slides was probably due to a well-known phenomenon that gold surfaces quench fluorescence [114]. These findings were consistent with the results reported by Zhi *et al.*, who found no fluorescent signals when a fluorescent dye was directly attached to a self-assembled monolayer (SAM) fabricated gold-coated slide while the signals were observed attaching to two or three layers of proteins on top of the SAM [114]. In the research reported here, MHDA with a 16-carbon chain and polysaccharides of α-D-mannose-PAA and mannan served as spacers between the fluorophores and the gold surfaces, effectively reducing this fluorescence-quenching.

Several pitfalls of using gold surfaces were found in this study or have been reported by other researchers. The first issue is the non-specific binding of bacterial cells to the background seen in Fig. 21A and 22A. This phenomenon was also observed by Zhi *et al.*, who found that a mixture of polyethylene glycol aldehyde and bovine serum albumin blocked gold surfaces more effectively than the two reagents working separately [147]. Second, this functionalization process requires a long period of time, approximately 3 days. To save time, MHDA and adipic dihydrazide can be linked in advance [147]. Third, negatively charged carbohydrates such as sulfated sugars

nonspecifically bind to the positively charged hydrazide surfaces while other reducing carbohydrates covalently bind to these surfaces [147].

5.10 Gold-Coated Microcantilever-Based Biosensors

The research reported here makes obvious the advantages and disadvantages of employing gold-coated microcantilevers as biosensors based on resonance frequency measurements. The increase in their resonance frequencies after carbohydrate functionalization was possibly related to the thickness of the absorbates on the beam. The random frequency shift after bacterial hybridization was probably a result of the non-uniformity of the bacterial coating. The specificity and sensitivity of this biosensor are discussed at the end of this section.

5.10.1 Pitfalls and Alternative Methods

One advantage of the functionalization method using gold-coated microcantilevers is that the microcantilever can be sealed in a Petri dish and stored for weeks at 4℃ after carbohydrate immobilization [147]. This relatively long shelf-life enables mass production of carbohydrate functionalized gold-coated microcantilevers, saving time, effort and expense. However, this method has several pitfalls. **First**, it is difficult to pick up the microcantilevers using a pair of forceps since they are small, consisting of a larger base measuring 450nm by 50nm, and a smaller beam anchored at one end measuring 3.4μm by 1.6μm. The dark lines at the bottom of the microcantilever

seen in Fig. 23A were caused by forcep feet sliding over the microcantilever base when it could not be picked up.

Second, the beams are extremely fragile, breaking easily when touched, meaning they are then useless for resonance frequency measurements. Although extra care was taken when these microcantilevers were handled during this research, the beams broke regularly, especially when they were being transferred from one reagent to another during functionalization and hybridization, and when they were being mounted on the stages of the Polytec Microsystem Analyser-400 and of the microscope. As a result, only one of ten microcantilevers on average survived the tedious functionalization process, the multiple hybridization procedures, and the three frequency measurements in this research. This problem was also mentioned in the protocol prepared in 2006 by the Veeco Instruments Company for its Veeco Dimension 3100 Atomic Force Microscope. Unfortunately, no solution addressing this issue was offered by this company. A microcantilever frame protecting the fragile beams or a pair of specially designed forceps is recommended to reduce the number of broken microcantilevers, saving time, expense, and effort.

Third, the cost of this protocol is expensive. Given the price of current microcantilevers ($25-$50 each) and the 1:10 survival ratio, it costs approximately $300 to obtain one setting of frequencies and approximately $10,000 to finish a sensitivity study for both *E. coli* ORN178 and *E. coli* ORN208 when five bacterial concentrations were evaluated, three replications each. The expense of this research is also a result of the

non-regeneracy of the microcantilevers since dried bacterial cells bound to gold surfaces cannot be removed using regeneration protocols [114].

5.10.2 Resonance Frequencies After Carbohydrate Functionalization

The uniformity of the carbohydrate coating on the gold-coated microcantilever beams was important for this research since the resonance frequency shifts represent the amount of absorbates loaded. The resonance frequency was higher after carbohydrate functionalization than that of unbound microcantilevers, a result consistent with the findings of Tamayo *et al.* that resonance frequency increased when the thickness of the SAM was more than 10% of the thickness of the silicon beam it was coated on [148]. The thickness of the microcantilever beam in this research was 2 μm, 10% of which is 0.2 μm. It is probable that the thickness of absorbates here was more than 0.2 μm due to the C16 fatty acid linked to form the SAM and the 30kD polysaccharides covalently attached. According to Ramos *et al.*, the resonance frequency increase is due to layer stiffness instead of added mass which decreases resonance frequencies [149]. Therefore, the effect of layer stiffness dominated after carbohydrate functionalization in this study. Although not as direct as added mass, layer stiffness also indicates the amount of carbohydrate functionalized, a hypothesis supported by the linear increase of resonance frequency in relation to the increase in the thickness of the SAM presented by Tamayo *et al.* [148].

5.10.3 Resonance Frequencies After Bacteria Hybridization

Although uniformity of the carbohydrate coating was achieved, the distribution of bacterial cells on the microcantilever beams was not uniform based on the images from the fluorescent microscope seen in Fig. 23C and D. A similar phenomenon was also observed on carbohydrate functionalized gold-coated slides: the bacterial cells did not uniformly cover the mannose dots (Fig. 21A and C) as they did on the nitrocellulose membranes. This non-uniformity was probably due to surface tension since Gupta *et al.* obtained similar results when *Listeria innocua* antibodies and bacterial cells were air-dried on the beam of surface micromachined thin silicon cantilever resonators [150]. In the future, critical point drying can be used to avoid the surface tension caused by water molecules crossing the phase boundary from liquid to gas [150].

The resonance frequencies measured after bacterial hybridization exhibiting all three kinds of shifts, positive, negative and neutral, confirmed this inconsistency (Table 3). This finding was also reported by Ramos *et al.*, who found under similar conditions, resonance frequency increased based on layer stiffness when cells were near the cantilever base, decreased linearly with loaded mass when the free ends of the cantilevers were loaded with cells, and did not change when the cells attached to the middle of the cantilever beam since the effects of layer stiffness and added mass counteracted each other (Fig. 26) [149]. Therefore, when bacterial cells randomly bind to beams, the direction of the resonance frequency shift is determined by the position of the cells.

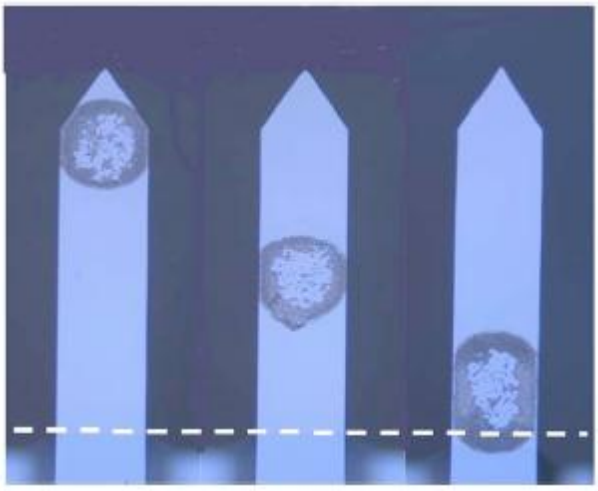

Figure 26: The Positions of Bacteria Droplets on Three Silicon Cantilever Beams Deposited by an Inkjet Printer. An image taken under an optical microscope shows three silicon cantilever beams (500×100×1 μm) on which the bacterial cells have been deposited by an inkjet printer at 73 μm (left), 200 μm (middle), and 390 μm (right) from the clamping position indicated by the dashed line [149].

To address this issue, it is ideal to functionalize only the free end of microcantilever beams with carbohydrates so that bacterial cells are loaded at that location as the decrease of resonance frequency is linear in relation to the number of cells. However, this situation cannot be achieved with dip coating techniques used in this research, which result in beams uniformly coated with carbohydrates, or with the Whatman manual printer used here, which touches and, therefore, breaks the fragile beams as discussed in Section 5.10.1. A possible solution involving an ink jet printing technique was reported by Ramos, *et al.*, who demonstrated that 0.5nL of *E. coli* suspension was deposited at different positions along the beam length [149]. Similarly,

nanoliters of carbohydrate solutions can be dropped at particular positions on beams without contact.

5.10.4 Specificity and Sensitivity

The detection specificity for the type-1 fimbriae expressed by *E. coli* ORN178/pGREEN was demonstrated using an epi-fluorescence microscope as seen in Fig 23. Although the recognition of *P. aeruginosa* to α-L-fucose was studied using carbohydrate microarrays, this interaction was not applied to microcantilever-based biosensors, because first the expression of the PA-II lectin in *P. aeruginosa* needs many cultivation conditions and second the non-uniformity of bacteria distribution on the microcantilever beams affected the data analyses of resonance frequency shifts. The high sensitivity suggested by the observation of fluorescent *E. coli* ORN178/pGREEN cells on a microcantilever beam after the hybridization with a suspension of 10^6cells/mL was comparable to the findings of Ilic *et al.* that silicon-nitride microcantilevers coated with *E. coli* O157:H7 antibodies captured 16 cells from a bacterial suspension of 10^6 cells/mL as seen under a scanning electron microscope [151]. Given that the surface area of the microcantilever bases is 5.44mm^2 (3.4mm×1.6mm), 242 times larger than the 0.0225mm^2 (0.45mm×0.05mm) of the beams, the proportion of cells exposed to the beams is only 1/243 of the total. When the concentration of cell sample is 10^6cells/mL, approximately 2,000 cells could hybridize on the beam per 500 μL bacterial suspension. The capture rate of the beam is only 2.5% given that the approximate cell number seen in Fig. 23D is 50. To further increase the sensitivity, it is ideal to only functionalize carbohydrates on the

beams using materials other than gold. Bradley, *et al.* reported that using a delayed-feedback signal to excite the microcantilever beam enhanced the sensitivity of the sensor [152]. Higher vibration modes such as the fourth bending mode [153] and smaller cantilever size may also improve sensitivity [149].

CHAPTER 6

CONCLUSIONS AND RECOMMENDATIONS

Detection tools based on carbohydrates have currently attracted the attention of researchers. A primary macromolecule in organisms, carbohydrates heavily coat cell surfaces and carry information for specific bacterial adhesin recognition; thus, they can be used as receptors in biosensors to detect the presence of target bacteria. In this present work, a carbohydrate microarray system has been developed on nitrocellulose membranes and evaluated to obtain the profiles of six bacteria bound to eight carbohydrates. Then, the recognition of *Escherichia coli* ORN178/pGREEN to mannose was applied to microcantilever-based biosensors as an initiatory step toward a novel pathogen detection tool. This tool has the potential for a wide impact from disease diagnostics to national security.

The recognition of *E. coli* ORN178/pGREEN to α-D-mannose was confirmed through a yeast agglutination assay. Detailed information about the binding conditions, such as the hybridization time, the hybridization temperature, the growth phase, and the bacteria viability, was used to construct carbohydrate microarrays. First, both three-hour and overnight hybridization resulted in high affinity. Second, the hybridization temperatures of 4 ℃, room temperature, and 37 ℃ were all suitable for the binding. Third, *E. coli* ORN178/pGREEN cells harvested during the stationary phase bound to mannose, but not those from the exponential phase. Fourth, the preservation of the *E. coli* ORN178 adhesins in non-viable cells after formaldehyde treatment suggests bacterial samples may

be inactivated with this chemical before being handled, ensuring the safety of personnel since both target and non-target microorganisms may have potential virulence. For non-fluorescent strains, both fluorescein isothiocyanate (FITC) and Alexa Fluor 488 C_5 maleimide offer promise for visualization. However, for other bacterial strains such as *Pseudomonas aeruginosa*, different conditions may be required for high expression of lectins and recognition affinities to their carbohydrate receptors.

The nitrocellulose membrane coated Whatman FAST slides and the gold-coated slides used in this research can both serve as matrices for carbohydrate microarrays. The use of the Whatman FAST slides bypassed the tedious functionalization of slide surfaces, which was required by the gold-coated slides. Eight polyacrylamide-conjugated carbohydrates were directly purchased from GlycoTech, avoided the carbohydrate microarray production bottle-neck of carbohydrate access. They were printed on the Whatman FAST slides and the adherence profiles of six bacterial strains binding to these carbohydrates were obtained. It is possible to generate a library of carbohydrate receptors for a particular strain using one Whatman slide, given that as many as 768 dots can be printed on it [119]. Because of this number of dots, a precise robotic printer is recommended for easy manipulation, consistent printing and high through-put, key factors for quantitative analyses of carbohydrate microarrays. In addition to a robotic printer, Blixt *et al.* also used a confocal scanner and image analysis software designed for DNA microarrays without modifications to construct a carbohydrate microarray on amino-reactive glass slides printed with 200 amine functionalized carbohydrates [75].

Similarly, a fluorescent microarray scanner and bioinformatics tools may also benefit the understanding of bacterial adherence patterns on host cell surfaces.

The detection for *E. coli* ORN178/pGREEN using the Whatman FAST slide based carbohydrate microarray system printed with α-D-mannose is relatively specific and sensitive. The specificity was exhibited by the ability to distinguish *E. coli* ORN178/pGREEN from *E. coli* ORN208/pGREEN with abnormal type-1 fimbriae and *E. coli* O157:H7 without type-1 fimbriae in this research. However, α-D-mannose is also recognized by other bacteria, such as *Klebsiella pneumonia* [137] and *Salmonella typhimurium* [139]. Using a set of oligosaccharides or polysaccharides specifically recognized by a particular bacterial strain in future research may further increase the specificity. During the specificity test, the inhibitory effect exhibited by free α-D-mannose demonstrates the potential of this system as a suitable platform to screen for carbohydrates which can serve as inhibitors preventing bacterial adherence. These carbohydrates may also be used to treat diseases by saturating the binding sites on bacterial surfaces, a hypothesis exemplified by the observation that fucose added 2 hours after the incubation of PA-II lectins with respiratory tract endoepithelial cell culture restored the beating of cilia [40]. The sensitivity of the system was acceptable at 10^4-10^5 cells/membrane here, comparing with those reported for other carbohydrate microarray systems and other pathogen detection tools. This sensitivity may be further improved by using microarray scanners to evaluate fluorescence and staining the non-fluorescent bacteria with intense fluorophores to increase the fluorescence intensity emitted from bound bacteria.

Another potential matrix for carbohydrate microarrays demonstrated in this research is gold-coated slides since α-D-mannose-PAA and mannan were immobilized on it and bound by *E. coli* ORN178/pGREEN specifically, although this protocol requires more steps than that using Whatman FAST slides. This protocol also uniformly immobilized α-D-mannose-PAA on gold-coated microcantilevers, a result supported by the statistical analysis of the resonance frequencies measured before and after carbohydrate functionalization. *E. coli* ORN178/pGREEN with optical density of both 1 and 0.001 bound to these microcantilever beams with individual cells being observed under an epi-fluorescent microscope. This binding was specific to type-1 fimbriae since *E. coli* ORN208/pGREEN did not bind. However, the statistical analysis of *E. coli* ORN178/pGREEN indicated that there was no evidence to conclude this strain bound to the microcantilever beams, different from the observation using an epi-fluorescent microscope. This difference is probably due to the non-uniform coating of bacterial cells on the microcantilever beams. This situation may be addressed by using an ink-jet printer to drop nanoliters of carbohydrate on the free end of the beam or by coating only that area with gold. However, the handling of the microcantilevers during the process is a problem needing to be resolved. A microcantilever frame protecting the fragile beams or a pair of specially designed forceps is recommended to reduce the number of broken microcantilevers, saving time, expense, and effort. In addition, a reference microcantilever beam without treatment is recommended to be measured along with each resonance frequency measurement to eliminate any possible environmental interference.

This research contributed to the area of bacteria detection by initially designing two tools utilizing the specific interaction between bacterial adhesins and carbohydrate receptors: the slide-based carbohydrate microarray system and the microcantilever-based biosensor. This research showed a simplified method to construct carbohydrate microarrays through immobilizing polyacrylamide-conjugated carbohydrates on nitrocellulose-coated Whatman FAST slides without requiring slide functionalization or carbohydrate modification. In addition, this research also showed for the first time that it is feasible for carbohydrates to serve as sensing molecules capturing target bacterial cells using microcantilever-based biosensors. Although their application in studying bacteria adherence and detecting bacterial cells was demonstrated here, this study represent the first step, opening the door for more research to enhance the understanding of the complex bacteria-carbohydrate interactions and to develop diagnostic tools and biosensors that are more stable, easier to fabricate, and ones that do not require sample pre-enrichment, cell lysis, or cell staining typically required for current antibody- or nucleic acid-based bioassays.

APPENDIX

Appendix A

American Institute of Physics License Terms and Conditions

Nov 21, 2010

This is a License Agreement between Yunyan Cheng ("You") and American Institute of Physics ("AIP") provided by Copyright Clearance Center ("CCC"). The license consists of your order details, the terms and conditions provided by American Institute of Physics , and the payment terms and conditions.

All payments must be made in full to CCC. For payment instructions, please see information listed at the bottom of this form.

License Number	2553821316172
License date	Nov 21, 2010
Licensed content publisher	American Institute of Physics
Licensed content publication	Journal of Applied Physics
Licensed content title	Origin of the response of nanomechanical resonators to bacteria adsorption
Licensed content author	D. Ramos, J. Tamayo, J. Mertens, et al
Licensed content date	Nov 30, 2006
Volume number	100
Issue number	10
Type of Use	Thesis/Dissertation
Requestor type	Author (original article)
Format	Print and electronic
Portion	Figure/Table
Number of figures/tables	1

Title of your thesis / dissertation	DEVELOPMENT OF A CARBOHYDRATE MICROARRAY SYSTEM AND A MICROCANTILEVER-BASED BIOSENSOR FOR DETECTION OF TARGET BACTERIA
Expected completion date	Dec 2010
Estimated size (number of pages)	125
Total	0.00 USD

Terms and Conditions

American Institute of Physics -- Terms and Conditions: Permissions Uses

American Institute of Physics ("AIP") hereby grants to you the non-exclusive right and license to use and/or distribute the Material according to the use specified in your order, on a one-time basis, for the specified term, with a maximum distribution equal to the number that you have ordered. Any links or other content accompanying the Material are not the subject of this license.

1. You agree to include the following copyright and permission notice with the reproduction of the Material: "Reprinted with permission from [FULL CITATION]. Copyright [PUBLICATION YEAR], American Institute of Physics." For an article, the copyright and permission notice must be printed on the first page of the article or book chapter. For photographs, covers, or tables, the copyright and permission notice may appear with the Material, in a footnote, or in the reference list.
2. If you have licensed reuse of a figure, photograph, cover, or table, it is your responsibility to ensure that the material is original to AIP and does not contain the copyright of another entity, and that the copyright notice of the figure, photograph, cover, or table does not indicate that it was reprinted by AIP, with permission, from another source. Under no circumstances does AIP, purport or intend to grant permission to reuse material to which it does not hold copyright.
3. You may not alter or modify the Material in any manner. You may translate the Material into another language only if you have licensed translation rights. You may not use the Material for promotional purposes. AIP reserves all rights not specifically granted herein.
4. The foregoing license shall not take effect unless and until AIP or its agent, Copyright Clearance Center, receives the Payment in accordance with Copyright Clearance Center Billing and Payment Terms and Conditions, which are incorporated herein by reference.
5. AIP or the Copyright Clearance Center may, within two business days of granting this license, revoke the license for any reason whatsoever, with a full refund payable to you. Should you violate the terms of this license at any time,

AIP, American Institute of Physics, or Copyright Clearance Center may revoke the license with no refund to you. Notice of such revocation will be made using the contact information provided by you. Failure to receive such notice will not nullify the revocation.

6. AIP makes no representations or warranties with respect to the Material. You agree to indemnify and hold harmless AIP, American Institute of Physics, and their officers, directors, employees or agents from and against any and all claims arising out of your use of the Material other than as specifically authorized herein.
7. The permission granted herein is personal to you and is not transferable or assignable without the prior written permission of AIP. This license may not be amended except in a writing signed by the party to be charged.
8. If purchase orders, acknowledgments or check endorsements are issued on any forms containing terms and conditions which are inconsistent with these provisions, such inconsistent terms and conditions shall be of no force and effect. This document, including the CCC Billing and Payment Terms and Conditions, shall be the entire agreement between the parties relating to the subject matter hereof.

This Agreement shall be governed by and construed in accordance with the laws of the State of New York. Both parties hereby submit to the jurisdiction of the courts of New York County for purposes of resolving any disputes that may arise hereunder.

Gratis licenses (referencing $0 in the Total field) are free. Please retain this printable license for your reference. No payment is required.

If you would like to pay for this license now, please remit this license along with your payment made payable to "COPYRIGHT CLEARANCE CENTER" otherwise you will be invoiced within 48 hours of the license date. Payment should be in the form of a check or money order referencing your account number and this invoice number RLNK10887559.
Once you receive your invoice for this order, you may pay your invoice by credit card. Please follow instructions provided at that time.

Make Payment To:
Copyright Clearance Center
Dept 001
P.O. Box 843006
Boston, MA 02284-3006

If you find copyrighted material related to this license will not be used and wish to cancel, please contact us referencing this license number 2553821316172 and noting the reason for cancellation.

REFERENCES

1. Food and Drug Administration. Foodborne illness-causing organisms in the U.S. - what you need to know. 2008 [cited 2010 9/24]; Available from: http://www.fda.gov/Food/ResourcesForYou/Consumers/ucm103263.htm.

2. Roberts T (2007) WTP estimates of the societal costs of U.S. food-borne illness. American Journal of Agricultural Economics 89: 1183-1188.

3. James E, Joyce M (2004) Assessment and management of watershed microbial contaminants. Critical Reviews in Environmental Science and Technology 34: 109 - 139.

4. Fratamico PM (2003) Comparison of culture, polymerase chain reaction (PCR), TaqMan *Salmonella*, and transia card *Salmonella* assays for detection of *Salmonella* spp. in naturally-contaminated ground chicken, ground turkey, and ground beef. Molecular and Cellular Probes 17: 215-221.

5. Ashimoto A, Chen C, Bakker I, Slots J (1996) Polymerase chain reaction detection of 8 putative periodontal pathogens in subgingival plaque of gingivitis and advanced periodontitis lesions. Oral Microbiology and Immunology 11: 266-273.

6. Magliulo M, Simoni P, Guardigli M, Michelini E, Luciani M, Lelli R, Roda A (2007) A rapid multiplexed chemiluminescent immunoassay for the detection of *Escherichia coli* O157:H7, *Yersinia enterocolitica*, *Salmonella typhimurium*, and *Listeria monocytogenes* pathogen bacteria. Journal of Agricultural and Food Chemistry 55: 4933-4939.

7. de Paz J, Seeberger P (2006) Recent advances in carbohydrate microarrays. QSAR & Combinatorial Science 25: 1027-1032.

8. Lazcka O, Campo FJD, Munoz FX (2007) Pathogen detection: a perspective of traditional methods and biosensors. Biosensors and Bioelectronics 22: 1205-1217.

9. Apweiler R, Hermjakob H, Sharon N (1999) On the frequency of protein glycosylation, as deduced from analysis of the SWISS-PROT database. Biochimica et Biophysica Acta (BBA) - General Subjects 1473: 4-8.

10. Shriver Z, Raguram S, Sasisekharan R (2004) Glycomics: a pathway to a class of new and improved therapeutics. Nature Reviews Drug Discovery 3: 863-873.

11. Roseman S (2001) Reflections on glycobiology. Journal of Biological Chemistry 276: 41527-41542.

12. Perillo NL, Pace KE, Seilhamer JJ, Baum LG (1995) Apoptosis of T cells mediated by galectin-1. Nature 378: 736-739.

13. Kannagi R (1997) Carbohydrate-mediated cell adhesion involved in hematogenous metastasis of cancer. Glycoconjugate Journal 14: 577-584.

14. Connor RJ, Kawaoka Y, Webster RG, Paulson JC (1994) Receptor specificity in human, avian, and equine H2 and H3 influenza virus isolates. Virology 205: 17-23.

15. Abrami L, Fivaz M, Glauser P-E, Parton RG, van der Goot F (1998) A pore-forming toxin interacts with a GPI-anchored protein and causes vacuolation of the endoplasmic reticulum. The Journal of Cell Biology 140: 525-540.

16. Sharon N, Ofek I (2000) Safe as mother's milk: Carbohydrates as future anti-adhesion drugs for bacterial diseases. Glycoconjugate Journal 17: 659-664.

17. Kuusela P, Moran AP, Vartio T, Kosunen TU (1989) Interaction of *Campylobacter jejuni* with extracellular matrix components. Biochimica et Biophysica Acta (BBA) - General Subjects 993: 297-300.

18. Sylvester F, Philpott D, Gold B, Lastovica A, Forstner J (1996) Adherence to lipids and intestinal mucin by a recently recognized human pathogen, *Campylobacter upsaliensis*. Infection and Immunity 64: 4060-4066.

19. Ofek I, Doyle R (1994) Bacterial adhesion to cells and tissues. Chapman & Hal: 1-578.

20. Henderson IR, Owen P, Nataro JP (1999) Molecular switches--the ON and OFF of bacterial phase variation. Molecular Microbiology: Wiley-Blackwell. pp. 919-932.

21. Ofek I, Hasty D, Doyle R (2003) Bacterial adhesion to animal cells and tissues: ASM Press.

22. Sharon N (2006) Carbohydrates as future anti-adhesion drugs for infectious diseases. Biochimica et Biophysica Acta (BBA) - General Subjects 1760: 527-537.

23. Ohlsen K, Oelschlaeger T, Hacker J, Khan A (2009) Carbohydrate receptors of bacterial adhesins: implications and reflections. Glycoscience and Microbial Adhesion: Springer Berlin / Heidelberg. pp. 1-12.

24. Kyogashima M, Ginsburg V, Krivan HC (1989) *Escherichia coli* K99 binds to N-glycolylsialoparagloboside and N-glycolyl-GM3 found in piglet small intestine. Archives of Biochemistry and Biophysics 270: 391-397.

25. Firon N, Ashkenazi S, Mirelman D, Ofek I, Sharon N (1987) Aromatic alpha-glycosides of mannose are powerful inhibitors of the adherence of type 1 fimbriated *Escherichia coli* to yeast and intestinal epithelial cells. Infection and Immunity 55: 472-476.

26. Simon P, Goode P, Mobasseri A, Zopf D (1997) Inhibition of *Helicobacter pylori* binding to gastrointestinal epithelial cells by sialic acid-containing oligosaccharides. Infection and Immunity 65: 750-757.

27. Bouckaert J, Berglund J, Schembri M, De Genst E, Cools L, Wuhrer M, Hung CS, Pinkner J, Slättegård R, Zavialov A, Choudhury D, Langermann S, Hultgren SJ, Wyns L, Klemm P, Oscarson S, Knight SD, De Greve H (2005) Receptor binding studies disclose a novel class of high-affinity inhibitors of the *Escherichia coli* FimH adhesin. Molecular Microbiology 55: 441-455.

28. Garber N, Guempel U, Gilboa-Garber N, Royle R (1987) Specificity of the fucose-binding lectin of *Pseudomonas aeruginosa*. FEMS Microbiology Letters 48: 331-334.

29. Blattner FR, Plunkett G, III, Bloch CA, Perna NT, Burland V, Riley M, Collado-Vides J, Glasner JD, Rode CK, Mayhew GF, Gregor J, Davis NW, Kirkpatrick HA, Goeden MA, Rose DJ, Mau B, Shao Y (1997) The Complete Genome Sequence of Escherichia coli K-12. Science 277: 1453-1462.

30. Sharon N (1987) Bacterial lectins, cell-cell recognition and infectious disease. FEBS Letters 217: 145-157.

31. Aprikian P, Tchesnokova V, Kidd B, Yakovenko O, Yarov-Yarovoy V, Trinchina E, Vogel V, Thomas W, Sokurenko E (2007) Interdomain interaction in the FimH adhesin of *Escherichia coli* regulates the affinity to mannose. Journal of Biological Chemistry 282: 23437-23446.

32. Russell PW, Orndorff PE (1992) Lesions in two *Escherichia coli* type 1 pilus genes alter pilus number and length without affecting receptor binding. Journal of Bacteriology 174: 5923-5935.

33. Soto GE, Hultgren SJ (1999) Bacterial adhesins: common themes and variations in architecture and assembly. Journal of Bacteriology 181: 1059-1071.

34. Choudhury D, Thompson A, Stojanoff V, Langermann S, Pinkner J, Hultgren SJ, Knight SD (1999) X-ray structure of the FimC-FimH chaperone-adhesin complex from uropathogenic *Escherichia coli*. Science 285: 1061-1066.

35. Hung CS, Bouckaert J, Hung D, Pinkner J, Widberg C, DeFusco A, Auguste CG, Strouse R, Langermann S, Waksman G, Hultgren SJ (2002) Structural basis of tropism of *Escherichia coli* to the bladder during urinary tract infection. Molecular Microbiology 44: 903-915.

36. Nagahori N, Lee RT, Nishimura SI, Pagé D, Roy R, Lee YC (2002) Inhibition of adhesion of type 1 fimbriated *Escherichia coli* to highly mannosylated ligands. ChemBioChem 3: 836-844.

37. Lyczak JB, Cannon CL, Pier GB (2002) Lung infections associated with cystic fibrosis. Clin Microbiol Rev 15: 194-222.

38. Imberty A, M. W, Mitchell EP, Gilboa-Garber N (2004) Structures of the lectins from Pseudomonas aeruginosa: insight into the molecular basis for host glycan recognition. Microbes and Infection 6: 221-228.

39. Chemani C, Imberty A, de Bentzmann S, Pierre M, Wimmerova M, Guery BP, Faure K (2009) Role of LecA and LecB lectins in *Pseudomonas aeruginosa*-induced lung injury and effect of carbohydrate ligands. Infection and Immunity 77: 2065-2075.

40. Adam E, Mitchell B, Schumacher D, Grant G, Schumacher U (1997) *Pseudomonas aeruginosa* II lectin stops human ciliary beating: therapeutic implications of fucose. Am J Respir Crit Care Med 155: 2102-2104.

41. Glick J, Garber N (1983) The intracellular localization of *Pseudomonas aeruginosa* lectins. Journal of Genetical Microbiology 129: 3085-3090.

42. ATCC. *Pseudomonas aeruginosa* ATCC 33347. 2010 [cited 2010 10/7]; Available from: http://www.atcc.org/ATCCAdvancedCatalogSearch/ProductDetails/tabid/452/Default.aspx?ATCCNum=33347&Template=bacteria.

43. Tielker D, Hacker S, Loris R, Strathmann M, Wingender J, Wilhelm S, Rosenau F, Jaeger K-E (2005) *Pseudomonas aeruginosa* lectin LecB is located in the outer membrane and is involved in biofilm formation. Microbiology 151: 1313-1323.

44. Gilboa-Garber N (1982) *Pseudomonas aeruginosa* lectins. Methods in Enzymology 83: 378-385.

45. Winzer K, Falconer C, Garber NC, Diggle SP, Camara M, Williams P (2000) The *Pseudomonas aeruginosa* lectins PA-IL and PA-IIL are controlled by quorum sensing and by RpoS. Journal of Bacteriology 182: 6401-6411.

46. Garber N, Guempel U, Gilboa-Garber N, Doyle RJ (1987) Specificity of the fucose-binding lectin of *Pseudomonas aeruginosa*. FEMS Microbiol Lett 48: 331-334.

47. Mitchell E, Houles C, Sudakevitz D, Wimmerova M, Gautier C, Pérez S, Wu AM, Gilboa-Garber N, Imberty A (2002) Structural basis for oligosaccharide-mediated adhesion of *Pseudomonas aeruginosa* in the lungs of cystic fibrosis patients. Nature Structural Biology 9: 918 - 921.

48. Imberty A, M. W, Mitchell EP, Gilboa-Garber N (2004) Structures of the lectins from *Pseudomonas aeruginosa*: insight into the molecular basis for host glycan recognition. Microbes and Infection 6: 221-228.

49. Leriche V, Sibille P, Carpentier B (2000) Use of an enzyme-linked lectinsorbent assay to monitor the shift in polysaccharide composition in bacterial biofilms. Applied Environmental Microbiology 66: 1851-1856.

50. Dam TK, Brewer CF (2002) Thermodynamic studies of lectin-carbohydrate interactions by isothermal titration calorimetry. Chemical Review 102: 387-430.

51. Duverger E, Frison N, Roche AC, Monsingny M (2003) Carbohydrate-lectin interactions assessed by surface plasmon resonance. Biocheimie 85.

52. Lis H, Sharon N (1972) Lectins: cell-agglutinating and sugar-specific proteins. Science 177: 949-959.

53. Wormald MR, Petrescu AJ, Pao Y-L, Glithero A, Elliott T, Dwek RA (2002) Conformational studies of oligosaccharides and glycopeptides: complementarity of NMR, X-ray crystallography, and molecular modeling. Chem Rev 102: 371-386.

54. Bryan MC, Plettenburg O, Sears P, Rabuka D, Wacowich-Sgarbi S, Wong C-H (2002) Saccharide display on microtiter plates. Chemistry & Biology 9: 713-720.

55. Wang D, Liu S, Trummer BJ, Deng C, Wang A (2002) Carbohydrate microarrays for the recognition of cross-reactive molecular markers of microbes and host cells. Nature Biotechnology 20: 275-281.

56. Willats WGT, Rasmussen SE, Kristensen T, Mikkelsen JD, Knox JP (2002) Sugar-coated microarrays: a novel slide surface for the high-throughput analysis of glycans. Proteomics 2: 1666-1671.

57. Fukui S, Feizi T, Galustian C, Lawson AM, Chai W (2002) Oligosaccharide microarrays for high-throughput detection and specificity assignments of carbohydrate-protein interactions. Nature Biotechnology 20: 1011-1017.

58. Feizi T, Fazio F, Chai W, Wong C-H (2003) Carbohydrate microarrays -- a new set of technologies at the frontiers of glycomics. Current Opinion in Structural Biology 13: 637-645.

59. Zhang Z, Ollmann IR, Ye X-S, Wischnat R, Baasov T, Wong C-H (1999) Programmable one-pot oligosaccharide synthesis. Journal of the American Chemical Society 121: 734-753.

60. Koeller KM, Wong C-H (2001) Enzymes for chemical synthesis. Nature 409: 232-240.

61. Seeberger PH, Haase W-C (2000) Solid-phase oligosaccharide synthesis and combinatorial carbohydrate libraries. Chemical Reviews 100: 4349-4394.

62. Horlacher T, Seeberger PH (2008) Carbohydrate arrays as tools for research and diagnostics. Chemical Society Reviews 37: 1414-1422.

63. Seeberger PH (2008) Automated oligosaccharide synthesis. Chemical Society Reviews 37: 19-28.

64. Plante OJ, Palmacci ER, Seeberger PH (2001) Automated solid-phase synthesis of oligosaccharides. Science 291: 1523-1527.

65. Houseman BT, Mrksich M (2002) Carbohydrate arrays for the evaluation of protein binding and enzymatic modification. Chemistry & Biology 9: 443-454.

66. Park S, Shin I (2002) Fabrication of carbohydrate chips for studying protein–carbohydrate interactions. Angewandte Chemie International Edition 41: 3180-3182.

67. Liu Y, Feizi T, Campanero-Rhodes MA, Childs RA, Zhang Y, Mulloy B, Evans PG, Osborn HMI, Otto D, Crocker PR, Chai W (2007) Neoglycolipid Probes Prepared via Oxime Ligation for Microarray Analysis of Oligosaccharide-Protein Interactions Chemistry & Biology 14: 847-859.

68. Pirrung MC (2002) How to Make a DNA Chip. Angewandte Chemie International Edition 41: 1276-1289.

69. Barbulovic-Nad I, Lucente M, Sun Y, Zhang M, Wheeler AR, Bussmann M (2008) Bio-Microarray Fabrication Techniques- A Review. Critical Reviews in Biotechnology 26: 237-259.

70. Nishioka GM, Markey AA, Holloway CK (2004) Protein damage in drop-on-demand printers. Journal of the American Chemical Society 126: 16320-16321.

71. Song E-H, Pohl NLB (2009) Carbohydrate arrays: recent developments in fabrication and detection methods with applications. Current Opinion in Chemical Biology 13: 626-632.

72. Haugland RG. Molecular Probes The Handbook-Fluorescence Fundamentals. 2010 [cited 2010 7/12]; Available from: http://www.invitrogen.com/site/us/en/home/References/Molecular-Probes-The-Handbook/Introduction-to-Fluorescence-Techniques.html.

73. Disney MD, Seeberger PH (2004) Aminoglycoside microarrays to explore interactions of antibiotics with RNAs and proteins. Chemistry – A European Journal 10: 3308-3314.

74. Parthasarathy N, DeShazer D, England M, Waag DM (2006) Polysaccharide microarray technology for the detection of *Burkholderia pseudomallei* and *Burkholderia mallei* antibodies. Diagnostic Microbiology and Infectious Disease 56: 329-332.

75. Blixt O, Head S, Mondala T, Scanlan C, Huflejt ME, Alvarez R, Bryan MC, Fazio F, Calarese D, Stevens J, Razi N, Stevens DJ, Skehel JJ, van Die I, Burton DR, Wilson IA, Cummings R, Bovin N, Wong C-H, Paulson JC (2004) Printed covalent glycan array for ligand profiling of diverse glycan binding proteins. Proceedings of the National Academy of Sciences of the United States of America 101: 17033-17038.

76. Disney MD, Seeberger PH (2004) The use of carbohydrate microarrays to study carbohydrate-cell interactions and to detect pathogens. Chemistry & Biology 11: 1701-1707.

77. Consortium for Functional Glycomics. Biology of glycan binding proteins: Insights from glycan microarrays; 2006; Universal City, CA. pp. 17.

78. Cavalcanti A, Shirinzadeh B, Zhang M, Kretly L (2008) Nanorobot Hardware Architecture for Medical Defense. Sensors 8: 2932-2958.

79. Hansen KM, Thundat T (2005) Microcantilever biosensors. Methods 37: 57-64.

80. Ko S, Grant SA (2003) Development of a novel FRET method for detection of *Listeria* or *Salmonella*. Sensors and Actuators B: Chemical 96: 372-378.

81. Koubová V, Brynda E, Karasová L, Škvor J, Homola J, Dostálek J, Tobiška P, Rošický J (2001) Detection of foodborne pathogens using surface plasmon resonance biosensors. Sensors and Actuators B: Chemical 74: 100-105.

82. Muhammad-Tahir Z, Alocilja EC (2003) Fabrication of a disposable biosensor for *Escherichia Coli* O157:H7 detection. Sensors Journal, IEEE 3: 345-351.

83. Abdel-Hamid I, Ivnitski D, Atanasov P, Wilkins E (1999) Flow-through immunofiltration assay system for rapid detection of *E. coli* O157:H7. Biosensors and Bioelectronics 14: 309-316.

84. Binnig G, Quate CF, Gerber C (1986) Atomic force microscope. Physical Review Letters 56: 930.

85. McKendry R, Zhang J, Arntz Y, Strunz T, Hegner M, Lang HP, Baller MK, Certa U, Meyer E, Güntherodt H-J, Gerber C (2002) Multiple Label-Free Biodetection and Quantitative DNA-Binding Assays on a Nanomechanical Cantilever Array. Proceedings of the National Academy of Sciences 99: 9783-9788.

86. Marie R, Jensenius H, Thaysen J, Christensen CB, Boisen A (2002) Adsorption kinetics and mechanical properties of thiol-modified DNA-oligos on gold investigated by microcantilever sensors. Ultramicroscopy 91: 29-36.

87. Karyakin AA, Presnova GV, Rubtsova MY, Egorov AM (2000) Oriented immobilization of antibodies onto the gold surfaces via their native thiol groups. Analytical Chemistry 72: 3805-3811.

88. Salehi-Khojin A, Bashash S, Jalili N, Müller M, Berger R (2009) Nanomechanical cantilever active probes for ultrasmall mass detection. Journal of Applied Physics Letters 105: 1-8.

89. Afshari M, Jalili N (2007) Towards nonlinear modeling of molecular interactions arising from adsorbed biological species on the microcantilever surface. International Journal of Non-Linear Mechanics 42: 588-595.

90. Braun T, Ghatkesar MK (2009) Measuring the intrinsic nanomechanics of molecular interactions with microcantilever sensors. European Journal of Nanomedicine 2: 13-15.

91. Jones E, Murphy K, Begley M (2003) Mechanical measurements of adhesion in microcantilevers: Transitions in geometry and cyclic energy changes. Experimental Mechanics 43: 280-288.

92. Florin EL, Radmacher M, Fleck B, Gaub HE (1994) Atomic force microscope with magnetic force modulation. Review of Scientific Instruments 65: 639-643.

93. Hagan MF, Majumdar A, Chakraborty AK (2004) Nanomechanical forces generated by surface grafted DNA. Journal of Physical Chemistry B 106: 10163-10173.

94. Stephan AC, Gaulden T, Brown AD, Smith M, Miller LF, Thundat T (2002) Microcantilever charged-particle flux detector. Review of Scientific Instruments 73: 36-41.

95. Shin S, Kim JP, Sim SJ, Lee J (2008) A multisized piezoelectric microcantilever biosensor array for the quantitative analysis of mass and surface stress. Applied Physics Letters 93: 102902-102903.

96. Campbell GA, Medina MB, Mutharasan R (2007) Detection of *Staphylococcus* enterotoxin B at picogram levels using piezoelectric-excited millimeter-sized cantilever sensors. Sensors and Actuators B: Chemical 126: 354-360.

97. Porter TL, Eastman MP, Pace DL (2001) Sensor Based on Piezoresistive Microcantilever Technology. Sensors and Actuators A 88: 47-51.

98. Britton CL, Jones RL, Oden PI, Hu Z, Warmack RJ, Smith SF, Bryan WL, Rochelle JM (2000) Multiple-Input Microcantilever Sensors. Ultramicroscopy 82: 17-21.

99. Tzeng T-RJCYR, Saeidpourazar R, Aphale SS, Jalili N (2011) Adhesin-specific nanomechanical cantilever biosensors for detection of microorganisms. ASME Transactions Journal of Heat Transfer 133: 1-5.

100. Carrascosa LG, Moreno M, Álvarez M, Lechuga LM (2006) Nanomechanical biosensors: a new sensing tool. TrAC Trends in Analytical Chemistry 25: 196-206.

101. Mahmoodi SN, Afshari M, Jalili N (2008) Nonlinear vibrations of piezoelectric microcantilevers for biologically-induced surface stress sensing. Journal of Communications in Nonlinear Science and Numerical Simulation 13: 1964-1977.

102. Weeks BL, Camarero J, Noy A, Miller AE, De Yoreo JJ, Stanker L (2003) A microcantilever-based pathogen detector. Scanning 25: 297-299.

103. Cha BH, Lee S-M, Park JC, Hwang KS, Kim SK, Lee Y-S, Ju B-K, Kim TS (2009) Detection of Hepatitis B Virus (HBV) DNA at femtomolar concentrations using a

silica nanoparticle-enhanced microcantilever sensor. Biosensors and Bioelectronics 25: 130-135.

104. Lin C-C, Yeh Y-C, Yang C-Y, Chen C-L, Chen G-F, Chen C-C, Wu Y-C (2002) Selective binding of mannose-encapsulated gold nanoparticles to type 1 pili in *Escherichia coli*. Journal of the American Chemical Society 124: 3508-3509.

105. Harris SL, Spears PA, Havell EA, Hamrick TS, Horton JR, Orndorff PE (2001) Characterization of Escherichia coli Type 1 Pilus Mutants with Altered Binding Specificities. J Bacteriol 183: 4099-4102.

106. Luo PG (2006) Carbohydrate biofunctionalized nanomaterials as antiadhesion and detection agents for bacterial pathogens [Dissertation]. Clemson: Clemson University. 122 p.

107. Singh R, Jiang X, Luo F (2010) Thermal inactivation of heat-shocked *Escherichia coli* O157:H7, *Salmonella*, and *Listeria monocytogenes* in dairy compost Journal of Food Protection 73: 1633-1640.

108. Whiteley M, Bangera MG, Bumgarner RE, Parsek MR, Teitzel GM, Lory S, Greenberg EP (2001) Gene expression in *Pseudomonas aeruginosa* biofilms. Nature 413: 860-864.

109. Jacobs MA, Alwood A, Thaipisuttikul I, Spencer D, Haugen E, Ernst S, Will O, Kaul R, Raymond C, Levy R, Chun-Rong L, Guenthner D, Bovee D, Olson MV, Manoil C (2003) Comprehensive transposon mutant library of *Pseudomonas aeruginosa*. Proceedings of the National Academy of Sciences of the United States of America 100: 14339-14344.

110. Muller CM, Aberg A, Straseviciene J, Emody L, Uhlin BE, Balsalobre C (2009) Type 1 fimbriae, a colonization factor of uropathogenic *Escherichia coli*, are controlled by the metabolic sensor CRP-cAMP. PLoS Pathogens 5: e1000303.

111. Owen T, English D, Dowland L, Parker B. MicroCaster™ a tool for building protein microarrays. 2006 [cited 2010 7/26]; Available from: http://www.whatman.com/References/MicroCaster%20Application%20Note.pdf.

112. Haugland RG. Molecular Probes the handbook-introduction to thiol modification and detection. 2010 [cited 2010 11/11]; Available from: http://www.invitrogen.com/site/us/en/home/References/Molecular-Probes-The-Handbook/Thiol-Reactive-Probes/Introduction-to-Thiol-Modification-and-Detection.html#head4.

113. Ziegler C (2004) Cantilever-based biosensors. Analytical and Bioanalytical Chemistry 379: 946-959.

114. Zhi Z-l, Powell AK, Turnbull JE (2006) Fabrication of carbohydrate microarrays on gold surfaces: direct attachment of nonderivatized oligosaccharides to hydrazide-modified self-assembled monolayers. Analytical Chemistry 78: 4786-4793.

115. Budgetsensors. AFM probe model: ContGD. 2007 [cited 2010 10/21]; Available from: http://www.budgetsensors.com/contact_mode_afm_probes_GD.html.

116. Firon N, Ashkenazi S, Mirelman D, Ofek I, Sharon N (1987) Aromatic alpha-glycosides of mannose are powerful inhibitors of the adherence of type 1 fimbriated *Escherichia coli* to yeast and intestinal epithelial cells. Infect Immun 55: 472-476.

117. Enamia M, Nakasonea N, Honmaa Y, Kakinohanaa S, Kudakaa J, Iwanagaa M (2006) Expression of type I pili is abolished in verotoxin-producing *Escherichia coli* O157. FEMS Microbiology Letters 179: 467 - 472.

118. Polytech GmbH. MSA-500 Micro System Analyzer - features. 2010 [cited 2010 7/19]; Available from: http://www.polytec.com/eur/158_6392.asp.

119. Whatman GmbH. MicroCaster™ Microarrayer System. 2007 [cited 2010 7/26]; Available from: http://www.whatman.com/References/MicroCaster%20Protocol.pdf.

120. Walther M, Stillman B, Friße A, Beator J. The FAST Guide to Protein Microarrays. 2007 [cited 2010 7/27]; Available from: http://www.whatman.com/References/FAST%20Guide%20to%20Protein%20Microarrays.pdf.

121. Wilkinson M, Doskow J, Lindsey S (1991) RNA blots: staining procedures and optimization of conditions. Nucl Acids Res 19: 679.

122. James-Holmquest AN, Swanson J, Buchanan TM, Wende RD, Williams RP (1974) Differential attachment by piliated and nonpiliated *Neisseria gonorrhoeae* to human sperm. Infect Immun 9: 897-902.

123. Loshon CA, Genest PC, Setlow B, Setlow P (1999) Formaldehyde kills spores of *Bacillus subtilis* by DNA damage and small, acid-soluble spore proteins of the alpha/beta-type protect spores against this DNA damage. J Appl Microbiol 87: 8-14.

124. Wikipedia. Fixation (Histology). 2010 4/24/2010 [cited 2010 7/09]; Available from: http://en.wikipedia.org/wiki/Fixation_(histology).

125. McSweegan E, Walker RI (1986) Identification and characterization of two *Campylobacter jejuni* adhesins for cellular and mucous substrates. Infection and Immunity 53: 141-148.

126. Fox CH, Johnson FB, Whiting J, Roller PP (1985) Formaldehyde fixation. The Journal of Histochemistry and Cytochemistry 33: 845-853.

127. Friedrich CL, Moyles D, Beveridge TJ, Hancock REW (2000) Antibacterial action of structurally diverse cationic peptides on Gram-positive bacteria. Antimicrob Agents Chemother 44: 2086-2092.

128. Ryter A (1988) Contribution of new cryomethods to a better knowledge of bacterial anatomy. Ann Inst Pasteur Microbiol 139: 33-44.

129. Muller CM, Aberg A, Straseviciene J, Emody L, Uhlin BE, Balsalobre C (2009) Type 1 fimbriae, a colonization factor of uropathogenic *Escherichia coli*, are controlled by the metabolic sensor CRP-cAMP. PLoS Pathog 5: e1000303.

130. Malorny B, Tassios PT, Rådström P, Cook N, Wagner M, Hoorfar J (2003) Standardization of diagnostic PCR for the detection of foodborne pathogens. International Journal of Food Microbiology 83: 39-48.

131. Morgan JA, Winstanley C, Pickup RW, Jones JG, Saunders JR (1989) Direct phenotypic and genotypic detection of a recombinant pseudomonad population released into lake water. Applied Environmental Microbiology 55: 2537-2544.

132. Michel O, Ravoo BJ (2008) Carbohydrate microarrays by microcontact "click" chemistry. Langmuir 24: 12116-12118.

133. Invitrogen (2008) Personal communication: the appropriateness of SYTO 9 as a visualizing dye on nitrocellulose membranes. In: Lewis GS, editor. Eugene.

134. Park S, Lee M-R, Shin I (2007) Fabrication of carbohydrate chips and their use to probe protein-carbohydrate interactions. Nature Protocols 2: 2747-2758.

135. Nimrichter L, Gargir A, Gortler M, Altstock RT, Shtevi A, Weisshaus O, Fire E, Dotan N, Schnaar RL (2004) Intact cell adhesion to glycan microarrays. Glycobiology 14: 197-203.

136. Zhu XY, Holtz B, Wang Y, Wang L-X, Orndorff PE, Guo A (2009) Quantitative glycomics from fluidic glycan microarrays. Journal of the American Chemical Society 131: 13646-13650.

137. Centeno A, DAVIS CP, COHEN MS, WARREN MM (1983) Modulation of *Candida albicans* attachment to human epithelial cells by bacteria and carbohydrates. Infection and immunity 39: 1354-1360.

138. Krivan HC, Roberts DD, Ginsburg V (1988) Many pulmonary pathogenic bacteria bind specifically to the carbohydrate sequence GalNAcβ1-4Gal found in some glycolipids. PNAS 85: 6157-6161.

139. Oyofo BA, DeLoach JR, Corrier DE, Norman JO, Ziprin RL, Mollenhauer HH (1989) Effect of carbohydrates on *Salmonella typhimurium* colonization in broiler chickens. Avian diseases 33: 531-534.

140. Althouse C, Patterson S, Fedorka-Cray P, Isaacson RE (2003) Type 1 fimbriae of *Salmonella enterica* serovar *typhimurium* bind to enterocytes and contribute to colonization of swine *in vivo*. Infection and Immunity 71: 6446-6452.

141. Garber N, Guempel U, Gilboa-Garber N, Doyle RJ (1987) Specificity of the fucose-binding lectin of *Pseudomonas aeruginosa*. FEMS Microbiol Lett 48: 331-334.

142. Lerrer B, Gilboa-Garber N (2001) Interactions of *Pseudomonas aeruginosa* PA-IIL lectin with quail egg white glycoproteins. Can J Microbiol: 1095-1100.

143. Chemani C, Imberty A, de Bentzmann S, Pierre M, Wimmerova M, Guery BP, Faure K (2009) Role of LecA and LecB Lectins in *Pseudomonas aeruginosa*-Induced Lung Injury and Effect of Carbohydrate Ligands. Infect Immun 77: 2065-2075.

144. Gilboa-Garber N, Sudakevitz D (1999) The hemagglutinating activities of *Pseudomonas aeruginosa* lectins PA-IL and PA-IIL exhibit opposite temperature profiles due to different receptor types. FEMS Immunology and Medical Microbiology 25: 365-369.

145. Loris R, Tielker D, Jaeger K-E, Wyns L (2003) Structural basis of carbohydrate recognition by the lectin LecB from *Pseudomonas aeruginosa*. Journal of Molecular Biology 331: 861-870.

146. Kirkeby S, Hansen AK, d'Apice A, Moe D (2006) The galactophilic lectin (PA-IL, gene *LecA*) from *Pseudomonas aeruginosa*. Its binding requirements and the localization of lectin receptors in various mouse tissues. Microbial Pathogenesis 40: 191-197.

147. Zhi Z-l, Powell AK, Turnbull JE (2006) Fabrication of carbohydrate microarrays on gold surfaces: direct attachment of nonderivatized oligosaccharides to hydrazide-modified self-assembled monolayers. Anal Chem 78: 4786-4793.

148. Tamayo J, Ramos D, Mertens J, Calleja M (2006) Effect of the adsorbate stiffness on the resonance response of microcantilever sensors. Applied Physics Letters: American Institute of Physics. pp. 224104.

149. Ramos D, Tamayo J, Mertens J, Calleja M, Zaballos A (2006) Origin of the response of nanomechanical resonators to bacteria adsorption. Journal of Applied Physics 100: 106105-106103.

150. Gupta A, Akin D, Bashir R (2004) Detection of bacterial cells and antibodies using surface micromachined thin silicon cantilever resonators. Journal of Vacuum Science & Technology B: Microelectronics and Nanometer Structures 22: 2785-2791.

151. Ilic B, Czaplewski D, Craighead HG, Neuzil P, Campagnolo C, Batt C (2000) Mechanical resonant immunospecific biological detector. Applied Physics Letters 77: 450-452.

152. Bradley C, Daqaq MF, Bibo A, Jalili N (2010) Sensitivity enhancement of cantilever-based sensors using feedback delays. ASME Journal of Computational and Nonlinear Dynamics 5: 1-9.

153. Dohn S, xf, ren, Sandberg R, Svendsen W, Boisen A (2005) Enhanced functionality of cantilever based mass sensors using higher modes. Applied Physics Letters 86: 233501-233503.